NTNU – Trondheim
Norwegian University of
Science and Technology

Spin- and Charge-Supercurrent and Density of States in Diffusive Spin-Active Josephson Junctions

Ingvild Ruud Gomperud

Master of Science in Physics and Mathematics
Submission date: June 2015
Supervisor: Jacob Rune Wüsthoff Linder, IFY

Norwegian University of Science and Technology
Department of Physics

Problem Description

Using quasiclssical theory, we solve the Usadel equation via a Ricatti-parametrization in a system consisting of a SNS Josephson junction with spin-active interfaces. This is done both analytically and numerically, incorporating spin-dependent phase-shifts and magnetoresistance terms coming from interface scattering. We determine how an exotic form of superconductivity known as odd-frequency pairing is manifested in experimentally accessible quantities such as the supercurrent and density of states.

NTNU
Faculty of Natural Sciences
and Technology
Department of Physics

Spin- and Charge-Supercurrent and Density of States in Diffusive Spin-Active Josephson Junctions

Ingvild Ruud Gomperud

Master thesis, supervisor Jacob Linder.

Trondheim, June 2015

Abstract

In this thesis we investigate theoretically the properties of spin-active Josephson junctions, using a normal metal as the weak link. The system is examined both analytically in the weak proximity effect regime and numerically in the full proximity effect regime. We consider the diffusive limit, and use the quasiclassical Usadel equation to find the Green function representation of the system. We assume that all materials are in equilibrium, i.e. in the absence of applied voltages and temperature gradients, and show that a conserved long-ranged spin-supercurrent flows through the normal metal, driven by both magnetic misalignment and the difference in phase between the two superconductors.

Another result from this thesis is that we find the 0-π transition to be accessible not only through the superconducting phase difference θ, but also by varying the magnetic displacement angle α between the magnetizations of the spin-active interfaces. Moreover, we show analytically that the spin-supercurrent has a term which is independent of the superconducting phase difference, and that the remaining term goes like $\cos\theta$, in contrast to $\sin\theta$ which is found for the charge-supercurrent. The charge-supercurrent can be split into one singlet and one triplet term, where both has an s-wave symmetry and where the triplet term is odd in frequency.

The numerical solutions consider both the situations in absence and in presence of isotropic spin-flipping on magnetic impurities and isotropic spin-orbit coupling. We find that the spin-flip scattering weakens the overall superconductivity, and that the spin-flip strength has monotonic behavior on the supercurrents. Interestingly, we find different behavior for the spin-orbit coupling. Here it seems like the triplet correlations are converted back into singlets, which can be understood by the averaging over spin, due to the isotropic form of the spin-orbit coupling. At last, we briefly discuss how the inverse proximity affects the superconducting correlations.

Sammendrag

I denne masteroppgaven har vi gjennomført en teoretisk analyse av spinn- og ladningssuperstrøm og tilstandstettheter i en nanostuktur bestående av to superledere separert av et normalmetal som svakt bindeledd. Ved begge grensesjiktene mellom superleder og normalmetal er det innsatt tynne spinn-aktive magnetiske isolatorer, og vi kaller denne strukturen en spinn-aktiv Josephson junction. Systemet er undersøkt både analytisk i grensetilfellet hvor superlederen har svak virkning på normalmetallet, og numerisk hvor vi løser likningene fullt ut. Vi betrakter diffuse materialer og bruker den kvasiklassiske Usadel likningen til å finne Greenfunksjonene som representerer systemet vårt. Det er antatt at materialer er i likevekt, som vil si i fravær av tilførte spenninger og temperaturendringer. Vi viser at en bevart langt-rekkende spinnsuperstrøm propagerer igjennom normalmetallet, drevet av både ikke-parallelle magnetiseringesretninger og faseforskjell mellom superlederne.

Fra før av er det kjent at man kan styre fortegnet på ladningsstrømmen gjennom endring av den superledende faseforskjellen θ. Dette er kalt en 0-π overgang. Vi finner at denne overgangen også kan styres via endring i den relative vinkelen α mellom magnetiseringsretningene ved grenseflatene. Videre finner vi analytisk at spinnsuperstrømmen har et ledd som er uavhengig av θ og at det resterende leddet går som $\cos\theta$, i kontrast til $\sin\theta$ som vi finner for ladningsstrømmen. Ladningsstrømmen kan bli delt inn i to ledd, hvor det ene leddet kommer fra spinn-singlet-kopling, mens det andre kommer fra spinn-triplet-kopling. Både singlet- og triplet-superledningen har s-bølge-symmetri i impulsrommet og triplet-leddet er derfor odd i frekvenssymmetri, som følge av Pauli prinsippet.

I den numeriske løsningen ser vi på situasjonene både i fravær av og i tilstedeværelse av isotropisk spinn-flipping ved å introdusere magnetiske urenheter, og spinn-orbital-kopling. Det blir vist at tilstedeværelsen av magnetiske urenheter svekker den overordnede superledningen på en strengt avtagende måte. Vi finner det interessant at spinn-orbital-koplingen er av annen karakter. Her virker det som om triplet-korrelasjonene blir konvertert tilbake til singlet-kopling. Vi begrunner dette ved midlingen over spinn, som følge av at orbital-koplingen er isotrop. Helt til slutt er det inkludert en kort diskusjon om hvordan kontakten med normalmetallet kan kan i gjengjeld påvirke superlederen.

Preface

This master thesis was conducted during the spring of 2015, and marks the end of the master program "Physics and Mathematics" at NTNU. It was written within theoretical physics, at the Department of Physics and Faculty of Natural Science. The work has resulted in a research article available on arXiv:1503.08229 that is currently undergoing review in Physical Review B. The theory is building upon a project that was written by me in the fall of 2014, which again partly is based on the master thesis of Jan Petter Morten of 2003 [1], with corrections of 2005. To get the most out of this thesis the reader should be well acquainted with the Green function representation used in many particle quantum mechanics. As an example of a sources on this topic, we have the text book by Mahan [2]. For a general introduction to superconductivity, the reading of the book [3] is one of many useful ways to acquire better insight into this field.

The chapters are organized as follows: Chapter 1 gives a qualitative introduction to the field of superconducting spintronics. In chapter 2 we present the theory of our theoretical framework. And in both chapter 3 and 4 we present results and discuss each result subsequently. The last chapter is a summary of the thesis along with a section that proposes further work. In addition to the main chapters, we also have four appendices where the first one summarizes the Pauli matrices used throughout the thesis, the second appendix provides some insight regarding the underlying Green function representation and the quasiclassical approximation, while the third appendix is an attachment of selected MATLAB-scripts used in the numerical calculations. The the last appendix we have inclosed a preprint of the research article.

Conventions

We have defined the electron charge as $e = -|e|$, and denoted $\theta = \theta_R - \theta_L$ as the superconducting phase difference. When going from the Cartesian coordinate system (x, y, z) to the Polar coordinates, we use α as the polar angle from the z-axis and ϕ as the azimuth angle in the xy-plane measured relative the x-axis with positive angle towards the y-axis. We define $\beta = 1/k_{\mathrm{B}}T$ as the inverse temperature with k_{B} as the Boltzmann constant, and use natural units, meaning that the reduced Planck constant is defined $\hbar = 1$ and the speed of light $c = 1$.

The commutator notation $[A, B]$ means $AB - BA$ and the anti-commutator is defined as $\{A, B\} = AB + BA$. To save space, we introduce the common derivative symbol $\partial_x \equiv \partial/\partial x$. The superconducting coupling strength λ is a negative constant $\lambda = -|\lambda|$, due to the attraction between electrons.

To avoid confusion, we use L and R as notation for the left and right side of the normal metal, and l and r as the left and right side of a magnetic interface. The

Latin R for right should not be mistaken for the upright R for "retarded", used for the retarded Green function. Many articles write "Green's function" while we chose to use the correct English term "Green function".

Acknowledgments

I would like to thank my exceptionally proficient supervisor, Jacob Linder, for his dedication to his research and to the work of his students. Your talent and capacity inspires me, and I am grateful for the opportunity to participate at the international workshop conference SUPERSPIN15 on superconducting spintronics. I would also like to thank Jabir Ali Ouassou for cheerful discussions on the topic of inverse proximity, and for generally being a great classmate. And at last I will greatly thank my best friend and life partner Olja Pehilj for all the travels he made to Trondheim this last year. I look forward to living with you again, my love.

Contents

Chapter 1

Introduction

The field of superconducting spintronics has been a very active research field over the past decades [4, 5]. The work has mostly been evolving around the theoretical description of hybrid nanostructures [6, 7], but there has also been some upswing in the experimental field [8]. Superconducting spintronics has created a promising area for observing novel quantum phenomena such as spin-polarized supercurrents [9], and showed that the interplay between superconductivity and magnetism still exhibits many unexplored features [10, 11].

The word spintronics originates from spin-electronics and the basic idea is to utilize spin-polarization to represent information transfer [12], instead of charge-currents as in conventional electronics. This technique has already been taken into use in most computer hard-drives, where the giant magneto resistance effect [13] is responsible for the reading-writing process. A huge challenge within spintronics today, is the overflow of heating from such devices. However, by introducing superconducting components in spintronic devices, the possibility to strongly reduce heating appears due to the zero resistance property of superconductors. Idealistically, this will also lessen the energy requirement.

For a physicist, the main motivation for working with superconducting spintronics is the promising opportunities of learning about new and interesting quantum phenomena, which in itself creates an alluring effect on the curious individual. At the moment, experimental scientists are facing challenges when trying to observe some of the theoretical predictions. To examine systems at the nanoscale, the quality of the available equipment becomes extremely important. In addition, the development of broader and more accurate theory will contribute to improving our understanding of nanophysics and be of great advantage when engineering the components in laboratories.

1.1 Conventional Superconductivity

The zero resistance property of superconductivity was experimentally discovered as early as in 1911 by Heike Kamerlingh Onnes, but it took more than 40 years before a successful theoretical explanation was introduced. It were the scientists Bardeen, Cooper and Schrieffer (BCS) that published a paper [14] in 1957, explaining the emergence of superconductivity by an effectively attractive potential between electrons. The attraction can be illustrated by imagining an electron traveling through a lattice, disturbing the ions. Shortly after, another electron enters the area and gets influenced attractively by the phonon caused by the first one. We call this a phonon-mediated interaction, and when it becomes stronger than the repelling Coulomb potential, we get a total attractive interaction between electrons. This coupling causes electrons to behave in an orderly manner, known as Cooper pairing [15]. Due to this pairing, superconductors are phase coherent and have zero DC resistance. The most likely scenario for this attraction to occur is when the electrons involved are of opposite momentum and opposite spin. In BCS theory a superconductor is described by an order parameter Δ that is isotropic. By use of BCS theory, we can describe an s-wave spin singlet superconductor, or a conventional BCS superconductor, if you will.

In 1933, long before the BCS theory was developed, it was discovered that when trying to apply a magnetic field to a superconducting sample the field would not penetrate the superconductor. This phenomenon is called the Meissner effect [16] and appears as if the superconductor was a perfect diamagnet. It was later shown that the diamagnetism originates from currents running at the surface of the superconductor. Thus, it seemed like magnetism was not compatible with superconductivity. However, as we know today, this is not the case. When considering hybrid structures at the nanoscale unconventional superconductivity may arise, leading to the possibility of creating polarized spin-supercurrents.

1.2 Symmetries and Odd-Frequency Pairing

Due to the fact that electrons are spin-1/2 particles, they have to obey the laws for fermions. The Pauli exclusion principle states that the fermionic wave function has to change sign when interchanging two particles in time, space and spin, at equal times. In table 1.1 the possible symmetry combinations are listed. There are strong indications that there exists intrinsic triplet p-wave symmetry in the ferromagnet UGe2 [17] when exposed to pressure, and that also URhGe and UCoGe [18] exhibit p-wave symmetry. A p-wave has negative parity causing the wave function to change sign when inverted in momentum space.

For a dirty material we need to have an s-wave symmetry to get a net propa-

Table 1.1: Symmetry combinations of the wave function

	Momentum	Spin	Time
Even-frequency singlet	even	odd	even
Even-frequency triplet	odd	even	even
Odd-frequency singlet	odd	odd	odd
Odd-frequency triplet	even	even	odd

gation of particles, due to impurity scattering [19]. This means that the only two options in Table 1.1, are the conventional spin-singlet even-frequency pairing and the unconventional spin-triplet odd-frequency pairing. When a superconductor of opposite spin-pairing is in contact with a collinear ferromagnet the supercurrent decays rapidly inside the ferromagnet, since the magnetism breaks the pairing. This is the case for the singlet $\sqrt{1/2}(|\uparrow\downarrow\rangle - |\downarrow\uparrow\rangle)$ and the opposite pairing triplet $\sqrt{1/2}(|\uparrow\downarrow\rangle + |\downarrow\uparrow\rangle)$. However, if the superconducting pairing is of equal spins, it does not have to fight the magnetic exchange field, and experiments have shown that a supercurrent can flow a long distance inside a ferromagnet [20, 21, 22]. To obtain this effect we need to have misaligned magnetizations, which will produce the equal spin triplet pairings $|\uparrow\uparrow\rangle$ and $|\downarrow\downarrow\rangle$, due to spin rotation.

The first to initiate the odd-frequency superconductivity was Berezinskii back in 1974 [23]. His idea was to create a wave function that was odd in time by transforming the function into a Matsubara sum. This would provide the opportunity for the total sum to be zero, while having odd-frequency in the components of the sum. This way, we avoid breaking the Pauli principle at equal times, since changing the sign of something zero remains zero. A review on odd-frequency superconductivity is given in Ref. [24].

It has been shown experimentally that textured ferromagnets like Ho [25] and compositions with layers of non-collinear ferromagnets [26], can in contact with an s-wave superconductor give rise to triplet currents. It is known that triplet pairing can be generated from a conventional s-wave superconductor when connected to a spin-dependent interface [27]. This effect is due to the fact that spin-$\uparrow$ and spin-$\downarrow$ electrons reflected from such an interface picks up different phases, leading to a mixture of singlet and triplet pairing. Experimentally, the triplet pairing is manifested as a low energy peak in the density of states [28]. However, such a peak may also occur from other effects that we call dirt effects, for instance found in some cuprates [29] and topological insulators [30]. When we calculate observables in a system, it is a good idea to analyze both the density of states and the transport of spin and charge to obtain a more comprehensive understanding of the properties.

1.3 Spin-Active Josephson Junctions

Already in 1960, experiments by H. Meissner [31] suggested that the superconductivity from a superconductor could leak into a normal metal contact. This has been known as the proximity effect [32, 33] and causes many interesting quantum phenomena. A few years later, B. D. Josephson published a paper on the possibility of tunneling currents in a bilayer of two superconductors separated by an insulating layer. This phenomenon has been called the Josephson effect [34, 35]. Intuitively, we also expect the normal metal to affect the superconducting correlation at the superconducting side of the interface. This is the inverse proximity effect, and it is known that for low interface transparencies this effect can be neglected when using large superconducting reservoirs.

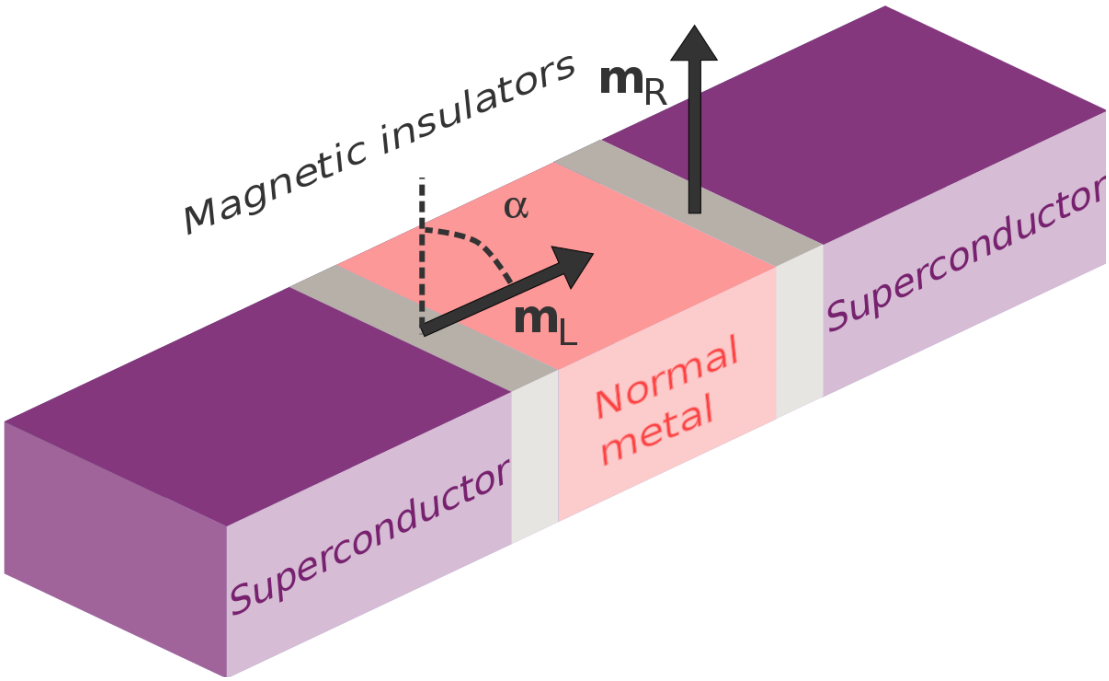

Figure 1.1: Illustration of a spin-active Josephson junction. The junction is called spin-active when the interfaces are complimented by spin-active components, in this case thin layers of magnetic insulators. Such interfaces give rise to spin-dependent effects, which cause spin-imbalance.

The main goal of this thesis is to investigate the charge- and spin-supercurrent occurring in spin-active Josephson junctions, and to understand how to control these quantities and how to manipulate their behavior. The setup for the junction that we will analyze is illustrated in Figure 1.1, where the two very thin magnetic insulators (MI's) at the interfaces give rise to spin-dependent interfacial phase

shifts and spin polarization. These layers are just a few nanometers in thickness, and will be accounted for by boundary conditions, whereas the length of the normal metal is much larger than the Fermi wavelength and is described by the Usadel equation, which we will come back to.

A long-ranged supercurrent has been theoretically reported as a second harmonic feature [36] when using only two ferromagnets. However, it would be of great desire to have a long-ranged spin-current in the first harmonic, since it generally is quantitatively much larger than the second harmonic and does not need any fine-tuning in order to be observed. We therefore want to explore systems that have as few ferromagnetic elements as possible and still generate long-ranged spin-supercurrents. This is why we have chosen to use a normal metal as the weak link, illustrated in Fig. 1.1.

The spin-active SNS junction proposed in this thesis has so far not been explored in the literature. However, a spin-active junction that has been experimentally examined is that of only a single magnetic insulator as the weak link between two superconductors [37]. Here the authors use the s-wave superconductor NbN and the magnetic insulator GdN. It is shown that the second harmonic in the current-phase-relation is insensitive to the change in barrier thickness, in contrast to earlier predictions for a ferromagnetic junction. In ref. [38] it is argued that the second harmonic can dominant when the first harmonic is suppressed, which can be near the 0-π transition. Due to band splitting the 0-π transition is again controllable by the length of the ferromagnet, which means that this cannot explain the second harmonics found in the junction with a single magnetic insulator.

To experimentally control the superconducting phase difference, the superconducting reservoirs can be connected in a loop geometry that uses a flux minute, as demonstrated in Ref. [39] on a conventional SNS junction. To map the density of state we can use scanning tunneling microscope (STM), and to trace the sample spatially we can use atomic force microscopy (AFM). In addition, the magnetic interface directions can be altered via an applied weak magnetic field. To do this, we need one spin-active interface to be more resistant to external magnetization than the other. One way to obtain this effect is to use a different thickness of each magnetic insulator, demonstrated in Ref. [40]. Alternatively, we could use different materials for the two magnetic insulators, where one of them has a higher magnetic anisotropy than the other. This means that the experimental techniques needed to test our results are in fact available, making it highly relevant to examine a Josephson junction with spin-active interfaces.

Chapter 2

Theory

In this chapter we will provide the theory essential to perform the calculations presented in the two subsequent chapters. We will start from the kinetic equation called the Usadel equation, and its belonging boundary conditions. From quasiclassical theory [41, 42, 43], we have the 8×8 Green function in the Nambu-Keldysh space constructed as

$$\check{g} = \begin{pmatrix} \hat{g}^{\mathrm{R}} & \hat{g}^{\mathrm{K}} \\ 0 & \hat{g}^{\mathrm{A}} \end{pmatrix}. \tag{2.1}$$

Here we find the 4×4 advanced Green function $\hat{g}^{\mathrm{A}}$ and the Keldysh Green function $\hat{g}^{\mathrm{K}}$ from the retarded Green function $\hat{g}^{\mathrm{R}}$ via the relations

$$\hat{g}^{\mathrm{A}} = -\left[\hat{\rho}_3 \hat{g}^{\mathrm{R}} \hat{\rho}_3\right]^{\dagger}, \quad \hat{g}^{\mathrm{K}} = \left(\hat{g}^{\mathrm{R}} - \hat{g}^{\mathrm{A}}\right) \tanh\left(\frac{\beta E}{2}\right), \tag{2.2}$$

where E is the quasiparticle energy and β is the inverse temperature. The last relation is valid since we consider materials in equilibrium.

Conventional Green functions are represented by annihilation and creation operations from the second quantization representation of many particle quantum mechanics (see Appendix B). These functions are interpreted as matrices of probability amplitudes describing different fermionic actions in the material, whereas the quasiclassical Green function (2.1) is an approximation where we have integrated out the relative oscillations at the atomic level, and averaged over the momentum value. The quasiclassical description of hybrid structures has proven to fit experimental results in a very satisfactory manner [44, 45] and is considered as a highly realistic approximation for metals.

2.1 The Usadel Equation

The Usadel equation is the dirty material description from the quasiclassical Eilenberger equation [46, 47], which again is based on kinetic equations developed by L. P. Gor'kov. We can derive the Usadel equation from the Eilenberger equation by approximating the Green function to only include the first and second harmonic, and average over the momentum direction [48]. This is valid since we consider dirty materials where electrons behave in a diffusive manner. This gives us

$$D\left[\hat{\boldsymbol{\partial}} \circ \check{g} \circ \left[\hat{\boldsymbol{\partial}} \circ \check{g}\right]\right] + i\left[E\hat{\rho}_3 - \check{\Sigma} + \hat{\Delta} \circ \check{g}\right] = 0, \tag{2.3}$$

which is the Usadel equation and only depends on the first harmonic Green function. Here we have that $D = \frac{1}{3}\tau v_{\mathrm{F}}^2$ is the diffusion constant in the material, τ is the elastic scattering relaxation time, and v_{F} is the Fermi velocity. We have also used the third Pauli matrix in particle hole-space $\hat{\rho}_3 = \mathrm{diag}(1, 1, -1, -1)$, and defined $[\hat{\boldsymbol{\partial}} \circ \check{g}] = \nabla_{\boldsymbol{R}}\check{g} - ie[\boldsymbol{A}\hat{\rho}_3 \circ \check{g}]$, where $\boldsymbol{A}$ is the magnetic vector potential. The matrix $\check{\Sigma}$ contains the possible contribution from self-energy terms due to scattering events, and the superconducting gap matrix is defined as:

$$\hat{\Delta} = \begin{pmatrix} 0 & i\sigma_y\Delta \\ i\sigma_y\Delta^* & 0 \end{pmatrix}, \tag{2.4}$$

where Δ is the scalar energy gap and $\sigma_y = \mathrm{offdiag}(i, -i)$ is the third Pauli matrix in spin-space.

The self-energy term from isotropic spin-flip scattering [10] is given by

$$\check{\Sigma}_{\mathrm{sf}} = -\frac{i}{8\tau_{\mathrm{sf}}}\hat{\boldsymbol{\tau}}\check{g}\hat{\boldsymbol{\tau}} \tag{2.5}$$

and when including isotropic spin-orbit coupling [49] we get the similar self-energy term

$$\check{\Sigma}_{\mathrm{so}} = -\frac{i}{8\tau_{\mathrm{so}}}\hat{\boldsymbol{\tau}}\hat{\rho}_3\check{g}\hat{\rho}_3\hat{\boldsymbol{\tau}}. \tag{2.6}$$

We have introduced the vector matrix $\hat{\boldsymbol{\tau}} = (\hat{\tau}_x, \hat{\tau}_y, \hat{\tau}_z)$, where the components are defined as the matrices

$$\hat{\tau}_\nu = \begin{pmatrix} \sigma_\nu & 0 \\ 0 & (\sigma_\nu)^* \end{pmatrix} \tag{2.7}$$

constructed from the Pauli spin matrices (see Appendix A equation (A.1)). We now define the normalized scattering strengths $g_{\mathrm{so,sf}} = 1/8\Delta_0\tau_{\mathrm{so,sf}}$, for future use. The scattering lifetime reflects the average time between two scattering events, and we see from equations (2.5) and (2.6) that when the scattering lifetimes $\tau_{\mathrm{sf,so}}$ goes to infinity, these terms vanish as expected.

In the absence of applied field, when $\boldsymbol{A} = 0$, and when only considering the retarded part of the Green function in the x-direction, we write the Usadel equation like

$$D\partial_x \hat{g}^{\mathrm{R}}(\partial_x \hat{g}^{\mathrm{R}}) + i\left[E\hat{\rho}_3 - \hat{\Sigma} + \hat{\Delta}, \hat{g}^{\mathrm{R}}\right] = 0, \tag{2.8}$$

where $\hat{\Sigma}$ is the same as in (2.5) and (2.6) only with $\hat{g}^{\mathrm{R}}$ instead of $\check{g}$. To solve this equation we also need to know the boundary conditions, which we will come back to in section 2.2. After we have found the solution of the retarded Green function, we can easily get the advanced and Keldysh Green functions via the aforementioned relations (2.2). When we are solving the Usadel equation in the normal metal we set $\hat{\Delta} = 0$ in the Usadel equation, and when excluding spin-dependent scattering we also set $\hat{\Sigma} = 0$.

The symmetry of the retarded Green function is such that we may write

$$\hat{g}^{\mathrm{R}} = \begin{pmatrix} g & f \\ -\tilde{f} & -\tilde{g} \end{pmatrix}, \tag{2.9}$$

where g is the normal 2×2 Green function describing transport of particles, and f is the anomalous Green function describing pairing of particles. We have defined the tilde operator $\tilde{}$ that equals changing the sign of the quasiparticle energy and complex conjugate, such that $\tilde{F}(E) = (F(-E))^*$. The 2×2 anomalous Green function can again be parameterized as

$$f = \begin{pmatrix} f_\uparrow & f_t + f_s \\ f_t - f_s & f_\downarrow \end{pmatrix}, \tag{2.10}$$

where f_s and f_t respectively describe the singlet and triplet pairing correlations of opposite spins, and $f_\uparrow, f_\downarrow$ are the correlations of equal spins.

Riccati Parameterization

To our convenience, we apply the Riccati parameterization [50, 51] to support numerical calculations. This way we ensure the correct symmetry properties and normalization of the Green function, and provide an environment for simplifications to a 2×2-matrix representation via the Riccati matrices $(\gamma, \tilde{\gamma})$,

$$\hat{g}^{\mathrm{R}} = \begin{pmatrix} N(1+\gamma\tilde{\gamma}) & 2N\gamma \\ -2\tilde{N}\tilde{\gamma} & -\tilde{N}(1+\tilde{\gamma}\gamma) \end{pmatrix}. \tag{2.11}$$

Following from the Riccati parameterization and our choice of normalization $(\hat{g}^{\mathrm{R}})^2 = 1$, we have the relations

$$\begin{aligned} &N = (1-\gamma\tilde{\gamma})^{-1}, \quad N\gamma = \gamma\tilde{N}, \quad \partial_x N = N\mathfrak{D}N, \quad \mathfrak{D} = \partial_x(\gamma\tilde{\gamma}), \\ &\tilde{N} = (1-\tilde{\gamma}\gamma)^{-1}, \quad \tilde{N}\tilde{\gamma} = \tilde{\gamma}N, \quad \partial_x\tilde{N} = \tilde{N}\tilde{\mathfrak{D}}\tilde{N}, \quad \tilde{\mathfrak{D}} = \partial_x(\tilde{\gamma}\gamma). \end{aligned} \tag{2.12}$$

In an earlier project [52], we have shown that when employing the Riccati parameterization to the Usadel equation and using the relations in (2.12), it gives us the two parameterized equations

$$\begin{aligned} D[2(\partial_x\gamma)\tilde{\gamma}N(\partial_x\gamma) + (\partial_x^2\gamma)] + i[a\gamma - \gamma d + \gamma c\gamma - b] = 0, \\ D[2(\partial_x\tilde{\gamma})\gamma\tilde{N}(\partial_x\tilde{\gamma}) + (\partial_x^2\tilde{\gamma})] - i[d\tilde{\gamma} - \tilde{\gamma}a + \tilde{\gamma}b\tilde{\gamma} - c] = 0. \end{aligned} \tag{2.13}$$

Here we have defined the 2×2 a, b, c, d matrices as follows:

$$\begin{pmatrix} a & b \\ c & d \end{pmatrix} = E\hat{\rho}_3 - \hat{\Sigma} + \hat{\Delta}, \tag{2.14}$$

which gives us

$$\begin{aligned} a &= E + i(g_{\text{sf}} + g_{\text{so}})(\sigma_x g\sigma_x + \sigma_y g\sigma_y + \sigma_z g\sigma_z), \\ b &= i\sigma_y\Delta + i(g_{\text{sf}} - g_{\text{so}})(\sigma_x f\sigma_x - \sigma_y f\sigma_y + \sigma_z f\sigma_z), \\ c &= i\sigma_y\Delta^* - i(g_{\text{sf}} - g_{\text{so}})(\sigma_x \tilde{f}\sigma_x - \sigma_y \tilde{f}\sigma_y + \sigma_z \tilde{f}\sigma_z), \\ d &= -E - i(g_{\text{sf}} + g_{\text{so}})(\sigma_x \tilde{g}\sigma_x + \sigma_y \tilde{g}\sigma_y + \sigma_z \tilde{g}\sigma_z). \end{aligned} \tag{2.15}$$

We now see that the two equations in (2.13) are exactly the tilded versions of each other.

BCS Solution

The solution of the conventional s-wave superconductors at the left and right side is given by

$$\hat{g}^{\text{R}}_{L(R)} = \begin{pmatrix} \cosh\Theta & i\sigma_y \sinh\Theta \mathrm{e}^{i\theta_{L(R)}} \\ i\sigma_y \sinh\Theta \mathrm{e}^{-i\theta_{L(R)}} & -\cosh\Theta \end{pmatrix}, \tag{2.16}$$

where we have defined $\Theta = \tanh^{-1}(|\Delta|/E)$. The superconducting phases θ_L and θ_R are constant inside each bulk superconductor, and the physics will eventually only depend on the phase difference $\theta = \theta_R - \theta_L$.

By comparing equation (2.11) with (2.16), we get the BCS solution written with Riccati matrices

$$\gamma_{L(R)} = \frac{i\sigma_y \sinh\Theta}{[1 + \cosh\Theta]}\mathrm{e}^{i\theta_{L(R)}}, \tag{2.17}$$

$$\tilde{\gamma}_{L(R)} = -\frac{i\sigma_y \sinh\Theta}{[1 + \cosh\Theta]}\mathrm{e}^{-i\theta_{L(R)}}, \tag{2.18}$$

which can be useful in numerical calculations.

2.2 Spin-Active Boundary Conditions

When solving a second order coupled differential equation like the Usadel equation, we need to know the boundary conditions in order to get an unambiguous solution. The boundary conditions for a spin-active interface in the tunneling limit [53] are given by

$$\begin{aligned} 2\ell_l\zeta_l\check{g}_l(\partial_x\check{g}_l) &= [\check{g}_l,\check{g}_r] + G_{\mathrm{MR}}\left[\check{g}_l,\{\hat{A},\check{g}_r\}\right] + iG_\varphi^l\left[\check{g}_l,\hat{A}\right], \\ 2\ell_r\zeta_r\check{g}_r(\partial_x\check{g}_r) &= [\check{g}_l,\check{g}_r] - G_{\mathrm{MR}}\left[\check{g}_r,\{\hat{A},\check{g}_l\}\right] - iG_\varphi^r\left[\check{g}_r,\hat{A}\right]. \end{aligned} \tag{2.19}$$

Here the $[\check{g}_l,\check{g}_r]$ terms are the usual Kupriyanov-Lukichev (KL) boundary conditions [54], valid for interfaces with low transparency, and the last two are the spin-dependent terms. To extend the KL boundary conditions we could employ the Nazarov boundary conditions instead, which allows us to have higher transparency at the interfaces [55]. However, this migth affect the spin-dependent boundary conditions, since they are derived in the tunneling limit. The subscripts l and j stand for the solution of the left and right side of the interface. We use $\ell_{l(r)}$ as the length of the material on the left (right) side, and have $\zeta_{l(r)} = R_B/R_{l(r)}$, where R_B is the normal state resistance of the interface, and $R_{l(r)}$ is the bulk resistance on the left (right) side of the interface.

We have defined the interface parameters $G_{\mathrm{MR}} = \sum_n T_nP_n/\sum_n 2T_n$ and $G_\varphi^{l(r)} = -\sum_n \mathrm{d}\phi_n^{l(r)}/\sum_n T_n$, where the T_n is the transmission probability for channel n, P_n is the spin polarization of the transmission probability, and $\mathrm{d}\phi_n^{l(r)}$ is the spin-mixing angle describing the spin-dependent interfacial phase shift at the left (right) side of the interface. We have that the parameter $G_\varphi^{l(r)}$ could be both larger and smaller than one, but that $G_{\mathrm{MR}} \ll 1$, due to the assumption that $P_n \ll 1$ in the derivation in Ref. [53]. Finally we have used the interface matrix

$$\hat{A} = \begin{pmatrix} \boldsymbol{m}\cdot\boldsymbol{\sigma} & 0 \\ 0 & \boldsymbol{m}\cdot\boldsymbol{\sigma}^* \end{pmatrix}, \tag{2.20}$$

where $\boldsymbol{m}$ is the magnetization direction of the interface, and $\boldsymbol{\sigma}$ is the 2×2 Pauli matrix vector in spin space. When only considering the retarded Green function, we insert equation (2.1) into (2.19) and get the boundary conditions

$$\begin{aligned} 2\ell_l\zeta_l\hat{g}_l^{\mathrm{R}}(\partial_x\hat{g}_l^{\mathrm{R}}) &= \left[\hat{g}_l^{\mathrm{R}},\hat{g}_r^{\mathrm{R}}\right] + G_{\mathrm{MR}}\left[\hat{g}_l^{\mathrm{R}},\{\hat{A},\hat{g}_r^{\mathrm{R}}\}\right] + iG_\varphi^l\left[\hat{g}_l^{\mathrm{R}},\hat{A}\right], \\ 2\ell_r\zeta_r\hat{g}_r^{\mathrm{R}}(\partial_x\hat{g}_r^{\mathrm{R}}) &= \left[\hat{g}_l^{\mathrm{R}},\hat{g}_r^{\mathrm{R}}\right] - G_{\mathrm{MR}}\left[\hat{g}_r^{\mathrm{R}},\{\hat{A},\hat{g}_l^{\mathrm{R}}\}\right] - iG_\varphi^r\left[\hat{g}_r^{\mathrm{R}},\hat{A}\right], \end{aligned} \tag{2.21}$$

which are similar to the equations in (2.19), only as 4×4-matrices.

Riccati Parameterization

When employing the Riccati parameterization (2.11) to the boundary conditions (2.21), we get the following expressions after some extensive derivations using the properties given in equation (2.12)

$$\begin{aligned}
4\ell_l\zeta_l\partial_x\gamma_l &= \Gamma_l + 2iG^l_\varphi[\gamma_l(\boldsymbol{m}\cdot\boldsymbol{\sigma}^*) - (\boldsymbol{m}\cdot\boldsymbol{\sigma})\gamma_l] - 2G_{\mathrm{MR}}[a_r\gamma_l - \gamma_l d_r + \gamma_l c_r\gamma_l - b_r],\\
4\ell_r\zeta_r\partial_x\gamma_r &= \Gamma_r - 2iG^r_\varphi[\gamma_r(\boldsymbol{m}\cdot\boldsymbol{\sigma}^*) - (\boldsymbol{m}\cdot\boldsymbol{\sigma})\gamma_r] + 2G_{\mathrm{MR}}[a_l\gamma_r - \gamma_r d_l + \gamma_r c_l\gamma_r - b_l],\\
4\ell_l\zeta_l\partial_x\tilde{\gamma}_l &= \tilde{\Gamma}_l - 2iG^l_\varphi[\tilde{\gamma}_l(\boldsymbol{m}\cdot\boldsymbol{\sigma}) - (\boldsymbol{m}\cdot\boldsymbol{\sigma}^*)\tilde{\gamma}_l] + 2G_{\mathrm{MR}}[d_r\tilde{\gamma}_l - \tilde{\gamma}_l a_r + \tilde{\gamma}_l b_r\tilde{\gamma}_l - c_r],\\
4\ell_r\zeta_r\partial_x\tilde{\gamma}_r &= \tilde{\Gamma}_r + 2iG^r_\varphi[\tilde{\gamma}_r(\boldsymbol{m}\cdot\boldsymbol{\sigma}) - (\boldsymbol{m}\cdot\boldsymbol{\sigma}^*)\tilde{\gamma}_r] - 2G_{\mathrm{MR}}[d_l\tilde{\gamma}_r - \tilde{\gamma}_r a_l + \tilde{\gamma}_r b_l\tilde{\gamma}_r - c_l].
\end{aligned} \tag{2.22}$$

The detailed derivation was performed in the project [52]. All of these four conditions only belong to one interface, so that in the most general case, we get 8 boundary conditions for a spin-active SNS junction. In (2.22) we have the symmetry relations $\tilde{d}_j = -a_j$ and $\tilde{c}_j = -b_j$, where the matrices are defined as

$$\begin{pmatrix} a_{l(r)} & b_{l(r)} \\ c_{l(r)} & d_{l(r)} \end{pmatrix} = \left\{\hat{A}, \hat{g}^{\mathrm{R}}_{l(r)}\right\}, \tag{2.23}$$

which means that we only need to know the two elements

$$\begin{aligned}
a_j &= N_j(1+\gamma_j\tilde{\gamma}_j)(\boldsymbol{m}\cdot\boldsymbol{\sigma}) + (\boldsymbol{m}\cdot\boldsymbol{\sigma})N_j(1+\gamma_j\tilde{\gamma}_j),\\
b_j &= 2N_j\gamma_j(\boldsymbol{m}\cdot\boldsymbol{\sigma}^*) + (\boldsymbol{m}\cdot\boldsymbol{\sigma})2\tilde{N}_j\tilde{\gamma}_j,
\end{aligned} \tag{2.24}$$

with $j = l, r$.

We have also defined the KL term given by

$$\Gamma_j = N_j^{-1}\left[\left[\hat{g}^{\mathrm{R}}_l, \hat{g}^{\mathrm{R}}_r\right]_{12} - \left[\hat{g}^{\mathrm{R}}_l, \hat{g}^{\mathrm{R}}_r\right]_{11}\gamma_j\right], \tag{2.25}$$

with the matrices

$$\begin{aligned}
\left[\hat{g}^{\mathrm{R}}_l, \hat{g}^{\mathrm{R}}_r\right]_{11} &= N_l(1+\gamma_l\tilde{\gamma}_l)(1+\gamma_r\tilde{\gamma}_r)N_r - 4N_l\gamma_l\tilde{\gamma}_r N_r\\
&\quad - N_r(1+\gamma_r\tilde{\gamma}_r)(1+\gamma_l\tilde{\gamma}_l)N_l + 4N_r\gamma_r\tilde{\gamma}_l N_l,\\
\left[\hat{g}^{\mathrm{R}}_l, \hat{g}^{\mathrm{R}}_r\right]_{12} &= 2N_l(1+\gamma_l\tilde{\gamma}_l)\gamma_r\tilde{N}_r - 2N_l\gamma_l(1+\tilde{\gamma}_r\gamma_r)\tilde{N}_r\\
&\quad - 2N_r(1+\gamma_r\tilde{\gamma}_r)\gamma_l\tilde{N}_l + 2N_r\gamma_r(1+\tilde{\gamma}_l\gamma_l)\tilde{N}_l,
\end{aligned} \tag{2.26}$$

where we recognize $N(1+\gamma\tilde{\gamma}) = g$ and $2N\gamma = f$.

2.3 Physical Observables

To couple our theoretical work to experimentally accessible observables, we will calculate the spin- and charge-supercurrent and the density of states. These observables can be measured with existing techniques, which makes the calculations highly relevant.

Supercurrents

The charge-supercurrent is given by the expression

$$I_Q = \frac{N_0 e D A}{4} \int_{-\infty}^{\infty} \mathrm{d}E \mathrm{Tr}\left\{\hat{\rho}_3 \left[\check{g}(\partial_x \check{g})\right]_{\mathrm{K}}\right\}, \tag{2.27}$$

and the spin-supercurrents are given by

$$I_S^{\nu} = \frac{N_0 \hbar D A}{8} \int_{-\infty}^{\infty} \mathrm{d}E \mathrm{Tr}\left\{\hat{\rho}_3 \hat{\tau}_\nu \left[\check{g}(\partial_x \check{g})\right]_{\mathrm{K}}\right\}, \tag{2.28}$$

where $\nu = x, y, z$. In equation (2.28) we have included the reduced Planck constant $\hbar$, even though we have defined it equal to one. We have that N_0 is the density of states at the Fermi level in the normal state, and that A is the cross section area, whereas $\mathrm{Tr}\{\cdots\}$ means the sum over all elements on the diagonal. For further reference we define the constant I_0 equal to $N_0 e D A/4$ for the charge-supercurrent and $N_0 \hbar D A/8$ for the spin-supercurrents.

By use of (2.1), (2.2) and (2.9) we can show that

$$\left[\check{g}(\partial_x \check{g})\right]_{\mathrm{K}} = \begin{pmatrix} A & B \\ \tilde{B} & \tilde{A} \end{pmatrix} \tanh\left(\frac{\beta E}{2}\right), \tag{2.29}$$

where we have the 2×2-matrix

$$A = \begin{pmatrix} A_{11} & A_{12} \\ A_{21} & A_{22} \end{pmatrix} = \left[g(\partial_x g) - g^{\dagger}(\partial_x g^{\dagger})\right] - \left[f(\partial_x \tilde{f}) - \tilde{f}^{\dagger}(\partial_x f^{\dagger})\right]. \tag{2.30}$$

The B-matrix will not be relevant to the following calculations, and is therefore not written out. Moreover, we now write for the supercurrents:

$$\begin{aligned}
I_Q =& I_0 \int_{-\infty}^{\infty} \mathrm{d}E \tanh\left(\frac{\beta E}{2}\right) \left[A_{11} + A_{22} - \tilde{A}_{11} - \tilde{A}_{22}\right], \\
I_S^x =& I_0 \int_{-\infty}^{\infty} \mathrm{d}E \tanh\left(\frac{\beta E}{2}\right) \left[A_{12} + A_{21} - \tilde{A}_{12} - \tilde{A}_{21}\right], \\
I_S^y =& I_0 \int_{-\infty}^{\infty} \mathrm{d}E \tanh\left(\frac{\beta E}{2}\right) i\left[A_{21} - A_{12} + \tilde{A}_{21} - \tilde{A}_{12}\right], \\
I_S^z =& I_0 \int_{-\infty}^{\infty} \mathrm{d}E \tanh\left(\frac{\beta E}{2}\right) \left[A_{11} - A_{22} - \tilde{A}_{11} + \tilde{A}_{22}\right].
\end{aligned} \tag{2.31}$$

By using the definition $\tilde{F} = F^*(-E)$ we can write the energy integral as follows:

$$\begin{aligned}
&\int_{-\infty}^{\infty} \mathrm{d}E \tanh\left(\frac{\beta E}{2}\right) \left[F(E) - F^*(-E)\right] \\
&= \int_{-\infty}^{\infty} \mathrm{d}E \tanh\left(\frac{\beta E}{2}\right) F(E) - \int_{-\infty}^{\infty} \mathrm{d}E \tanh\left(\frac{\beta E}{2}\right) F^*(-E) \\
&= \int_{-\infty}^{\infty} \mathrm{d}E \tanh\left(\frac{\beta E}{2}\right) F(E) - \int_{+\infty}^{-\infty} (-1)\mathrm{d}E(-1) \tanh\left(\frac{\beta E}{2}\right) F^*(E) \\
&= \int_{-\infty}^{\infty} \mathrm{d}E \tanh\left(\frac{\beta E}{2}\right) 2\Re\mathrm{e}\big\{F(E)\big\}, \qquad (2.32)
\end{aligned}$$

and similarly we get

$$\int_{-\infty}^{\infty} \mathrm{d}E \tanh\left(\frac{\beta E}{2}\right) \left[F(E) + F^*(-E)\right] = \int_{-\infty}^{\infty} \mathrm{d}E \tanh\left(\frac{\beta E}{2}\right) 2i\Im\mathrm{m}\big\{F(E)\big\}. \qquad (2.33)$$

Next, we use the last two relations to simplify the equations for the supercurrents in (2.31) and obtain

$$\begin{aligned}
I_Q =& I_0 \int_{-\infty}^{\infty} \mathrm{d}E \tanh\left(\frac{\beta E}{2}\right) 2\Re\mathrm{e}\{A_{11} + A_{22}\}, \\
I_S^x =& I_0 \int_{-\infty}^{\infty} \mathrm{d}E \tanh\left(\frac{\beta E}{2}\right) 2\Re\mathrm{e}\{A_{12} + A_{21}\}, \\
I_S^y =& I_0 \int_{-\infty}^{\infty} \mathrm{d}E \tanh\left(\frac{\beta E}{2}\right) 2\Im\mathrm{m}\{A_{21} - A_{12}\}, \\
I_S^z =& I_0 \int_{-\infty}^{\infty} \mathrm{d}E \tanh\left(\frac{\beta E}{2}\right) 2\Re\mathrm{e}\{A_{11} - A_{22}\},
\end{aligned} \qquad (2.34)$$

where we see that all supercurrents are purely real quantities, as they should be since they are physical observables.

The Energy Gap Function

The gap equation is given by

$$\Delta = -\frac{1}{8}N_0\lambda \mathrm{Tr}\Big\{\frac{\hat{\rho}_1 - \hat{\rho}_2}{2}\sigma_z \int \mathrm{d}E\hat{g}^{\mathrm{K}}\Big\}, \tag{2.35}$$

where the coupling strength λ is a negative constant in the superconductor, and zero elsewhere. By employing the definitions from (A.2) and (B.7) from the appendices into equation (2.35), we end up with

$$\Delta(x) = \frac{1}{4}|\lambda|N_0 \int_{\infty}^{-\infty} \mathrm{d}E(f_s - \tilde{f}_s^*)\tanh\Big(\frac{\beta E}{2}\Big). \tag{2.36}$$

First of all, the integrand is symmetric with respect to energy, meaning that it is sufficient to solve it for positive energies. Secondly, this integral diverges as it approaches infinity, and we have to change the boundaries of the integral. This gives us the resulting gap equation

$$\Delta(x) = \frac{1}{2}|\lambda|N_0 \int_{0}^{\omega_c} \mathrm{d}E(f_s - \tilde{f}_s^*)\tanh\Big(\frac{\beta E}{2}\Big), \tag{2.37}$$

where we have the cutoff frequency $\omega_c = \Delta_0 \tanh(1/|\lambda|N_0)$. This limit is found by solving the gap equation for the BCS solution, where $f_s = |\Delta|\mathrm{sign}(E)/\sqrt{E^2 - |\Delta|^2}$ after inserting Θ. Later we will use the convention that all energies are measured in unites of Δ_0, which equals $\Delta_0 = 1$.

Density of States

The density of states expresses the number of quantum states at a given energy, and can easily be found from the Green function as

$$N(E) = \Re\mathrm{e}\left(\frac{g_\uparrow + g_\downarrow}{2}\right) = \frac{1}{2}\mathrm{Tr}\Big\{\Re\mathrm{e}(g)\Big\}, \tag{2.38}$$

where $g = N(1 + \gamma\tilde{\gamma})$. We also define the spin-resolved density of states for spin-$\uparrow$ and spin-$\downarrow$, since it is of interest to see how the spin-active interfaces affect the different spin species.

$$N_\uparrow(E) = \Re\mathrm{e}\left(\frac{g_\uparrow}{2}\right) = \frac{1}{4}\mathrm{Tr}\Big\{(1 + \sigma_z)\Re\mathrm{e}(g)\Big\}, \tag{2.39}$$

$$N\downarrow(E) = \Re\mathrm{e}\left(\frac{g_\downarrow}{2}\right) = \frac{1}{4}\mathrm{Tr}\Big\{(1 - \sigma_z)\Re\mathrm{e}(g)\Big\}. \tag{2.40}$$

When defining the spin-resolved densities of states in this way, we have that $N(E) = N_\uparrow(E) + N_\downarrow(E)$, which is useful to keep in mind when we look at the numerical solutions later in chapter 4.

Chapter 3

Analytical Solution

Before we get to the numerical calculations, we will derive analytical solutions in the weak proximity limit. This gives us guidelines to what we should expect from the full solutions. The main result from this chapter is the derivation of the expressions for the spin- and charge-current.

3.1 The Weak Proximity Effect Regime

In a normal metal bulk, we have the Green function solution

$$\hat{g}^{\mathrm{R}}_{\mathrm{Normal}} = \begin{pmatrix} 1 & 0 \\ 0 & -1 \end{pmatrix}., \tag{3.1}$$

where the anomalous Green function is set to zero, and hence we have no Cooper pairing. In the weak proximity effect, the superconducting correlations in the normal metal are small and the Green function will be close to the solution for the normal metal bulk. We now assume that $\gamma \ll 1$ which means that $f = 2\gamma$, $g = 1$, and $N = 1$. This gives us the weak proximity retarded Green function

$$\hat{g}^{\mathrm{R}} \approx \begin{pmatrix} 1 & 2\gamma \\ -2\tilde{\gamma} & -1 \end{pmatrix} = \begin{pmatrix} 1 & f \\ -\tilde{f} & -1 \end{pmatrix}. \tag{3.2}$$

Usadel

Furthermore, the parameterized Usadel equation (2.13) reduces to the simple uncoupled differential equation

$$\partial_x^2 \gamma + \frac{2iE}{D}\gamma = 0 \quad \Rightarrow \quad \partial_x^2 f + \frac{2iE}{D} f = 0, \tag{3.3}$$

with exactly the same equation for $\tilde{\gamma}$. This gives us the general scalar solutions of the elements of f

$$f_n = A_n \mathrm{e}^{ikx} + B_n \mathrm{e}^{-ikx}, \tag{3.4}$$
$$\tilde{f}_n = \tilde{A}_n \mathrm{e}^{-ikx} + \tilde{B}_n \mathrm{e}^{ikx}, \tag{3.5}$$

where $k = \sqrt{2iE/D}$ and $n = \uparrow, \downarrow, s, t$ denotes the electron pairing.

Boundary Conditions

When we use the bulk BCS solution as the solution at the superconducting side of the interface, the boundary conditions can be written

$$\begin{aligned} 2\ell\zeta_R \hat{g}^{\mathrm{R}}(\partial_x \hat{g}^{\mathrm{R}}) &= \left[\hat{g}^{\mathrm{R}}, \hat{g}^{\mathrm{R}}_R\right] + G^R_{\mathrm{MR}} \left[\hat{g}^{\mathrm{R}}, \{\hat{A}, \hat{g}^{\mathrm{R}}_R\}\right] + iG^R_{\varphi} \left[\hat{g}^{\mathrm{R}}, \hat{A}\right], \\ 2\ell\zeta_L \hat{g}^{\mathrm{R}}(\partial_x \hat{g}^{\mathrm{R}}) &= \left[\hat{g}^{\mathrm{R}}_L, \hat{g}^{\mathrm{R}}\right] - G^L_{\mathrm{MR}} \left[\hat{g}^{\mathrm{R}}, \{\hat{A}, \hat{g}^{\mathrm{R}}_L\}\right] - iG^L_{\varphi} \left[\hat{g}^{\mathrm{R}}, \hat{A}\right], \end{aligned} \tag{3.6}$$

where L and R refers to the left and right superconductor and interface, and not the left and right side of the one magnetic interface as before with the lower case letters l and r. Both equations in (3.6) are the ones for the surfaces facing towards the normal metal, and it is implied that $\hat{g}^{\mathrm{R}}$ in the first and second equation should be taken at $x = l^-$ and $x = 0^+$ respectively. We use l as the length of the normal metal.

Next, we will express the different terms of the boundary conditions, first in 2×2-matrices and then in scalars. This will lead to a solution by use of linear algebra. We only need to solve for the non-tilded versions of the boundary conditions, and find the equivalent expressions from symmetry considerations.

Inserting the BCS solution in the Kupriyanov-Lukichev condition for the left interface we get

$$\begin{aligned} \left[\hat{g}^{\mathrm{R}}_L, \hat{g}^{\mathrm{R}}\right] &= \begin{pmatrix} \cosh\Theta & i\sigma_y \sinh\Theta \mathrm{e}^{i\theta_L} \\ i\sigma_y \sinh\Theta \mathrm{e}^{-i\theta_L} & -\cosh\Theta \end{pmatrix} \begin{pmatrix} 1 & f \\ -\tilde{f} & -1 \end{pmatrix} \\ &- \begin{pmatrix} 1 & f \\ -\tilde{f} & -1 \end{pmatrix} \begin{pmatrix} \cosh\Theta & i\sigma_y \sinh\Theta \mathrm{e}^{i\theta_L} \\ i\sigma_y \sinh\Theta \mathrm{e}^{-i\theta_L} & -\cosh\Theta \end{pmatrix}, \end{aligned} \tag{3.7}$$

with the 2×2-components

$$\left[\hat{g}^{\mathrm{R}}_L, \hat{g}^{\mathrm{R}}\right]_{11} = -i\sigma_y \sinh\Theta \mathrm{e}^{i\theta_L} \tilde{f} - f i\sigma_y \sinh\Theta \mathrm{e}^{-i\theta_L}, \tag{3.8}$$
$$\left[\hat{g}^{\mathrm{R}}_L, \hat{g}^{\mathrm{R}}\right]_{12} = 2f\cosh\Theta - 2i\sigma_y \sinh\Theta \mathrm{e}^{i\theta_L}, \tag{3.9}$$
$$\left[\hat{g}^{\mathrm{R}}_L, \hat{g}^{\mathrm{R}}\right]_{21} = 2i\sigma_y \sinh\Theta \mathrm{e}^{-i\theta_L} + 2\tilde{f}\cosh\Theta, \tag{3.10}$$
$$\left[\hat{g}^{\mathrm{R}}_L, \hat{g}^{\mathrm{R}}\right]_{22} = i\sigma_y \sinh\Theta \mathrm{e}^{-i\theta_L} f + \tilde{f} i\sigma_y \sinh\Theta \mathrm{e}^{i\theta_L}. \tag{3.11}$$

Keeping in mind that $f = 2\gamma$, we see that $\left[\hat{g}_L^{\mathrm{R}}, \hat{g}^{\mathrm{R}}\right]_{11}$ is already proportional to γ, which means that this part will be neglected when put together with the additional γ from equation (2.25). After this, we are left with the expression

$$\Gamma_L = 2f\cosh\Theta - 2i\sigma_y \sinh\Theta \mathrm{e}^{i\theta_L}. \tag{3.12}$$

Assuming that $\gamma << \sinh\Theta$, we neglect the first term relative to the second and after generalizing to the right side as well, we get

$$\Gamma_{L(R)} = \mp 2i\sigma_y \sinh\Theta \mathrm{e}^{i\theta_{L(R)}}. \tag{3.13}$$

The G_φ term is already as simplified as possible, so next we handle the G_{MR} term. When inserting the BCS solution, the expressions in (2.24) becomes

$$\begin{aligned} a_{L(R)} &= 2(\boldsymbol{m}\cdot\boldsymbol{\sigma})\cosh\Theta \\ b_{L(R)} &= i\sigma_y \sinh\Theta \mathrm{e}^{i\theta_{L(R)}}(\boldsymbol{m}\cdot\boldsymbol{\sigma}^*) + (\boldsymbol{m}\cdot\boldsymbol{\sigma})i\sigma_y\sinh\Theta\mathrm{e}^{i\theta_{L(R)}} = 0 \end{aligned} \tag{3.14}$$

where we also find $d_{L(R)}$ from $d_{L(R)} = -\tilde{a}_{L(R)} = -2(\boldsymbol{m}\cdot\boldsymbol{\sigma}^*)\cosh\Theta$. To show that $b_{L(R)} = 0$ we can use the anti-commutator relations $\{\sigma_\nu, \sigma_\mu\} = 2\delta_{\nu\mu}$, where $\delta_{\nu\mu}$ is the Kronecker delta. We then get

$$\sigma_y(\boldsymbol{m}\cdot\boldsymbol{\sigma}^*) + (\boldsymbol{m}\cdot\boldsymbol{\sigma})\sigma_y = \sigma_y(\boldsymbol{m}\cdot\boldsymbol{\sigma}^*) - \sigma_y(\boldsymbol{m}\cdot\boldsymbol{\sigma}^*) = 0. \tag{3.15}$$

This relation is easily verified by writing out the full matrices as well.

Finally, we arrive at the simplified 2×2 boundary conditions for weak proximity effect. At the left interface ($x = 0$) we have

$$\begin{aligned} 2\ell\zeta_L(\partial_x f) = &-2i\sigma_y\sinh\Theta\mathrm{e}^{i\theta_L} - iG_\varphi^L[f(\boldsymbol{m_L}\cdot\boldsymbol{\sigma}^*) - (\boldsymbol{m_L}\cdot\boldsymbol{\sigma})f] \\ &+ 2\cosh\Theta G_{\mathrm{MR}}^L[(\boldsymbol{m_L}\cdot\boldsymbol{\sigma})f + f(\boldsymbol{m_L}\cdot\boldsymbol{\sigma}^*)], \end{aligned} \tag{3.16}$$

$$\begin{aligned} 2\ell\zeta_L(\partial_x \tilde{f}) = &\ 2i\sigma_y\sinh\Theta\mathrm{e}^{-i\theta_L} + iG_\varphi^L[\tilde{f}(\boldsymbol{m_L}\cdot\boldsymbol{\sigma}) - (\boldsymbol{m_L}\cdot\boldsymbol{\sigma}^*)\tilde{f}] \\ &+ 2\cosh\Theta G_{\mathrm{MR}}^L[(\boldsymbol{m_L}\cdot\boldsymbol{\sigma}^*)\tilde{f} + \tilde{f}(\boldsymbol{m_L}\cdot\boldsymbol{\sigma})], \end{aligned} \tag{3.17}$$

and at the right interface ($x = \ell$) we have

$$\begin{aligned} 2\ell\zeta_R(\partial_x f) = &\ 2i\sigma_y\sinh\Theta\mathrm{e}^{i\theta_R} + iG_\varphi^R[f(\boldsymbol{m_R}\cdot\boldsymbol{\sigma}^*) - (\boldsymbol{m_R}\cdot\boldsymbol{\sigma})f] \\ &- 2\cosh\Theta G_{\mathrm{MR}}^R[(\boldsymbol{m_R}\cdot\boldsymbol{\sigma})f + f(\boldsymbol{m_R}\cdot\boldsymbol{\sigma}^*)] \end{aligned} \tag{3.18}$$

$$\begin{aligned} 2\ell\zeta_R(\partial_x \tilde{f}) = &-2i\sigma_y\sinh\Theta\mathrm{e}^{-i\theta_R} - iG_\varphi^R[\tilde{f}(\boldsymbol{m_R}\cdot\boldsymbol{\sigma}) - (\boldsymbol{m_R}\cdot\boldsymbol{\sigma}^*)\tilde{f}] \\ &- 2\cosh\Theta G_{\mathrm{MR}}^R[(\boldsymbol{m_R}\cdot\boldsymbol{\sigma}^*)\tilde{f} + \tilde{f}(\boldsymbol{m_R}\cdot\boldsymbol{\sigma})] \end{aligned} \tag{3.19}$$

To make the calculations easier to read, we will from this point avoid using the left (right) notation of the magnetization until the very last set of equations. However, it is fairly easy to find out which interface the magnetization originates from, since the equations for the left and the right side are fully separated.

At this point we only proceed with the non-tilded version of the equations, since the procedure to solve for $\tilde{f}$ is exactly the same. We continue to simplify the expressions by writing out the matrices in scalars via the relation (2.10). From the left side of the equations (3.16) and (3.18) we get

$$2\ell\zeta_{L(R)}(\partial_x f) = 2\ell\zeta_{L(R)} \begin{pmatrix} \partial_x f_\uparrow & \partial_x(f_t + f_s) \\ \partial_x(f_t - f_s) & \partial_x f_\downarrow \end{pmatrix}, \tag{3.20}$$

while the first term on the right side gives us

$$2i\sigma_y \sinh\Theta \mathrm{e}^{i\theta_{L(R)}} = 2 \begin{pmatrix} 0 & \sinh\Theta \\ -\sinh\Theta & 0 \end{pmatrix} \mathrm{e}^{i\theta_{L(R)}}. \tag{3.21}$$

The spin-mixing term may be expressed as:

$$\begin{pmatrix} \Phi_\uparrow & \Phi_{t+s} \\ \Phi_{t-s} & \Phi_\downarrow \end{pmatrix} \tag{3.22}$$

$$\equiv iG_\varphi[f(\boldsymbol{m_1}\cdot\boldsymbol{\sigma}^*) - (\boldsymbol{m_1}\cdot\boldsymbol{\sigma})f] \tag{3.23}$$

$$= iG_\varphi \begin{pmatrix} f_\uparrow & f_t + f_s \\ f_t - f_s & f_\downarrow \end{pmatrix} \begin{pmatrix} m_z & m_x + im_y \\ m_x - im_y & -m_z \end{pmatrix} \tag{3.24}$$

$$- iG_\varphi \begin{pmatrix} m_z & m_x - im_y \\ m_x + im_y & -m_z \end{pmatrix} \begin{pmatrix} f_\uparrow & f_t + f_s \\ f_t - f_s & f_\downarrow \end{pmatrix}, \tag{3.25}$$

with the components

$$\Phi_\uparrow = iG_\varphi\left[2(m_x - im_y)f_s\right], \tag{3.26}$$

$$\Phi_{t+s} = iG_\varphi\left[(m_x + im_y)f_\uparrow - 2m_z(f_t + f_s) - (m_x - im_y)f_\downarrow\right], \tag{3.27}$$

$$\Phi_{t-s} = iG_\varphi\left[-(m_x + im_y)f_\uparrow + 2m_z(f_t - f_s) + (m_x - im_y)f_\downarrow\right], \tag{3.28}$$

$$\Phi_\downarrow = iG_\varphi\left[-2(m_x + im_y)f_s\right], \tag{3.29}$$

whereas the polarization term gives:

$$\begin{pmatrix} M_\uparrow & M_{t+s} \\ M_{t-s} & M_\downarrow \end{pmatrix} \tag{3.30}$$

$$\equiv 2\cosh\Theta G_{\mathrm{MR}}[f(\boldsymbol{m_1}\cdot\boldsymbol{\sigma}^*) + (\boldsymbol{m_1}\cdot\boldsymbol{\sigma})f] \tag{3.31}$$

$$= 2\cosh\Theta G_{\mathrm{MR}} \begin{pmatrix} f_\uparrow & f_t + f_s \\ f_t - f_s & f_\downarrow \end{pmatrix} \begin{pmatrix} m_z & m_x + im_y \\ m_x - im_y & -m_z \end{pmatrix} \tag{3.32}$$

$$+ 2\cosh\Theta G_{\mathrm{MR}} \begin{pmatrix} m_z & m_x - im_y \\ m_x + im_y & -m_z \end{pmatrix} \begin{pmatrix} f_\uparrow & f_t + f_s \\ f_t - f_s & f_\downarrow \end{pmatrix}, \tag{3.33}$$

with the components

$$M_\uparrow = 2\cosh(\Theta_j) G_{\mathrm{MR}} \left[2m_z f_\uparrow + 2(m_x - im_y) f_t\right], \tag{3.34}$$
$$M_{t+s} = 2\cosh(\Theta_j) G_{\mathrm{MR}} \left[(m_x + im_y) f_\uparrow + (m_x - im_y) f_\downarrow\right], \tag{3.35}$$
$$M_{t-s} = 2\cosh(\Theta_j) G_{\mathrm{MR}} \left[(m_x + im_y) f_\uparrow + (m_x - im_y) f_\downarrow\right], \tag{3.36}$$
$$M_\downarrow = 2\cosh(\Theta_j) G_{\mathrm{MR}} \left[-2(m_x + im_y) f_t - 2m_z f_\downarrow\right]. \tag{3.37}$$

At last, we write out the scalar equations. Notice that we have separated the singlet and triplet anomalous Green function in the following. At the left interface we have:

$$\ell\zeta_L \partial_x f_\uparrow = iG^L_\varphi \big[(m_x - im_y) f_s\big] + 2\cosh\Theta G^L_{\mathrm{MR}} \big[m_z f_\uparrow + (m_x - im_y) f_t\big], \tag{3.38}$$
$$\ell\zeta_L \partial_x f_t = -iG^L_\varphi m_z f_s + \cosh\Theta G^L_{\mathrm{MR}} \big[(m_x + im_y) f_\uparrow + (m_x - im_y) f_\downarrow\big], \tag{3.39}$$
$$\ell\zeta_L \partial_x f_s = -\sinh\Theta \mathrm{e}^{i\theta_L} - \frac{i}{2} G^L_\varphi \big[(m_x + im_y) f_\uparrow - 2m_z f_t - (m_x - im_y) f_\downarrow\big], \tag{3.40}$$
$$\ell\zeta_L \partial_x f_\downarrow = -iG^L_\varphi \big[(m_x + im_y) f_s\big] - 2\cosh\Theta G^L_{\mathrm{MR}} \big[(m_x + im_y) f_t + m_z f_\downarrow\big]. \tag{3.41}$$

And similarly, at the right interface:

$$\ell\zeta_R \partial_x f_\uparrow = -iG^R_\varphi \big[(m_x - im_y) f_s\big] - 2\cosh\Theta G^R_{\mathrm{MR}} \big[m_z f_\uparrow + (m_x - im_y) f_t\big], \tag{3.42}$$
$$\ell\zeta_R \partial_x f_t = iG^R_\varphi m_z f_s - \cosh\Theta G^R_{\mathrm{MR}} \big[(m_x + im_y) f_\uparrow + (m_x - im_y) f_\downarrow\big], \tag{3.43}$$
$$\ell\zeta_R \partial_x f_s = \sinh\Theta \mathrm{e}^{i\theta_R} + \frac{i}{2} G^R_\varphi \big[(m_x + im_y) f_\uparrow - 2m_z f_t - (m_x - im_y) f_\downarrow\big], \tag{3.44}$$
$$\ell\zeta_R \partial_x f_\downarrow = iG^R_\varphi \big[(m_x + im_y) f_s\big] + 2\cosh\Theta G^R_{\mathrm{MR}} \big[(m_x + im_y) f_t + m_z f_\downarrow\big]. \tag{3.45}$$

After employing the solution for f_n, we wind up with the following equations

$$\begin{aligned}
\ell\zeta_L ik(A_\uparrow - B_\uparrow) &= iG_\varphi^L\big[(m_L^x - im_L^y)(A_s + B_s)\big] \\
&\quad + 2\cosh\Theta G_{\mathrm{MR}}^L\big[m_L^z(A_\uparrow + B_\uparrow) + (m_L^x - im_L^y)(A_t + B_t)\big], \qquad (3.46)\\
\ell\zeta_L ik(A_t - B_t) &= -iG_\varphi^L m_L^z(A_s + B_s) + \cosh\Theta G_{\mathrm{MR}}^L\big[(m_L^x + im_L^y)(A_\uparrow + B_\uparrow) \\
&\quad + (m_L^x - im_L^y)(A_\downarrow + B_\downarrow)\big] \qquad (3.47)\\
\ell\zeta_L ik(A_s - B_s) &= -\sinh\Theta e^{i\theta_L} - \frac{i}{2}G_\varphi^L\big[(m_L^x + im_L^y)(A_\uparrow + B_\uparrow) \\
&\quad - 2m_L^z(A_t + B_t) - (m_L^x - im_L^y)(A_\downarrow + B_\downarrow)\big], \qquad (3.48)\\
\ell\zeta_L ik(A_\downarrow - B_\downarrow) &= -iG_\varphi^L\big[(m_L^x + im_L^y)(A_s + B_s)\big] \\
&\quad - 2\cosh\Theta G_{\mathrm{MR}}^L\big[(m_L^x + im_L^y)(A_t + B_t) + m_L^z(A_\downarrow + B_\downarrow)\big], \qquad (3.49)\\
\ell\zeta_R ik(A_\uparrow - B_\uparrow) &= -iG_\varphi^R\big[(m_R^x - im_R^y)(A_s + B_s)\big] \\
&\quad - 2\cosh\Theta G_{\mathrm{MR}}^R\big[m_z(A_\uparrow + B_\uparrow) + (m_R^x - im_R^y)(A_t + B_t)\big], \qquad (3.50)\\
\ell\zeta_R ik(A_t - B_t) &= iG_\varphi^R m_R^z(A_s + B_s) - \cosh\Theta G_{\mathrm{MR}}^R\big[(m_R^x + im_R^y)(A_\uparrow + B_\uparrow) \\
&\quad + (m_R^x - im_R^y)(A_\downarrow + B_\downarrow)\big], \qquad (3.51)\\
\ell\zeta_R ik(A_s - B_s) &= \sinh\Theta e^{i\theta_R} + \frac{i}{2}G_\varphi^R\big[(m_R^x + im_R^y)(A_\uparrow + B_\uparrow) \\
&\quad - 2m_R^z(A_t + B_t) - (m_R^x - im_R^y)(A_\downarrow + B_\downarrow)\big], \qquad (3.52)\\
\ell\zeta_R ik(A_\downarrow - B_\downarrow) &= iG_\varphi^R\big[(m_R^x + im_R^y)(A_s + B_s)\big] \\
&\quad + 2\cosh\Theta G_{\mathrm{MR}}^R\big[(m_R^x + im_R^y)(A_t + B_t) + m_R^z(A_\downarrow + B_\downarrow)\big], \qquad (3.53)
\end{aligned}$$

where we have clarified which side the respective magnetization directions belong to and moved the x, y, z notation to be a superscript like in the spin-current notation.

A good reality check is to see that when using equal interface parameters at the left and right side of the normal metal, we obtain that the boundary conditions are equal at both interfaces except from an overall minus sign at the left side of the equations above. This means that if we define the x-direction in the opposite way and rename left to right and vice versa, the total collection of equations is the same, which it should be since this corresponds to being an observer at the opposite side of a symmetric junction.

To solve these equations we organize them on the form $\check{A}\boldsymbol{x} = \boldsymbol{b}$, known from linear algebra. $\check{A}$ is a matrix of parameters, while $\boldsymbol{x}$ as a column vector, containing the unknown coefficients $\boldsymbol{x} = (A_\uparrow, B_\uparrow, A_t, B_t, A_s, B_s, A_\downarrow, B_\downarrow)^{\mathrm{T}}$ and $\boldsymbol{b}$ is a column vector of the remaining constant terms. We have used the computer program Maple to solve this equation for the case of zero G_{MR} effect, since the effect of G_φ is the prominent one.

We see that the singlet equations (3.48) and (3.52) are independent on G_{MR}, and that when we set $G_\varphi = 0$ the constants A_s and B_s for the singlet component is solved solely from these two equations. The solutions are independent on the triplet components, and we would expect that the singlet correlations would be modified when triplets was made from it. This indicates that we need G_φ to create triplet pairing, and we notice that the singlet terms always enters the triplet equations proportional to G_φ. Since we know that the triplet pairing is made from the singlet there cannot be any triplet pairing when the singlet terms are zero. We have also verified in Maple that for the case of zero G_φ, the analytical solution is independent of G_{MR}. This could be due to the assumption of weak polarization in the derivation of the boundary conditions in Ref. [53], and if we had extended the boundary conditions to include strongly polarized interfaces, we might get another result. If we uses different superconductors on the left and right side, the Θ in the equations above should be dependent on which side it originates from.

When we have the magnetizations at both interfaces in the z-direction, we see that we do not generate $f_\uparrow$ and $f_\downarrow$, only f_s og f_t, which is in accordance with the requirement of misalignment magnetizations to produce long-ranged currents in a ferromagnet since a ferromagnet favors equal spin pairing.

3.2 Spin- and Charge-Supercurrent

In the weak proximity limit, the first part of (2.30) goes to zero since g is regarded as a constant, and we are left with

$$A = -\left[f(\partial_x \tilde{f}) - \tilde{f}^\dagger(\partial_x f^\dagger)\right]. \tag{3.54}$$

Nevertheless, the contribution to the charge-supercurrent I_Q from the removed term is zero regardless of the approximation of weak proximity effect. This can be shown by writing out the matrices in scalars and using (3.61). When employing (2.10), the components of (3.54) can be expressed as:

$$\begin{aligned}
A_{11} &= -f_\uparrow \partial_x \tilde{f}_\uparrow - (f_t + f_s)\partial_x(\tilde{f}_t - \tilde{f}_s) + \tilde{f}_\uparrow^* \partial_x f_\uparrow^* + (\tilde{f}_t^* - \tilde{f}_s^*)\partial_x(f_t^* + f_s^*) \\
A_{12} &= -f_\uparrow \partial_x(\tilde{f}_t + \tilde{f}_s) - (f_t + f_s)\partial_x \tilde{f}_\downarrow + \tilde{f}_\uparrow^* \partial_x(f_t^* - f_s^*) + (\tilde{f}_t^* - \tilde{f}_s^*)\partial_x f_\downarrow^* \\
A_{21} &= -(f_t - f_s)\partial_x \tilde{f}_\uparrow - f_\downarrow \partial_x(\tilde{f}_t - \tilde{f}_s) + (\tilde{f}_t^* + \tilde{f}_s^*)\partial_x f_\uparrow^* + \tilde{f}_\downarrow^* \partial_x(f_t^* + f_s^*) \\
A_{22} &= -(f_t - f_s)\partial_x(\tilde{f}_t + \tilde{f}_s) - f_\downarrow \partial_x \tilde{f}_\downarrow + (\tilde{f}_t^* + \tilde{f}_s^*)\partial_x(f_t^* - f_s^*) + \tilde{f}_\downarrow^* \partial_x f_\downarrow^*
\end{aligned} \tag{3.55}$$

To find the supercurrents, we calculate the following terms in consistence with the

expressions in (2.34)

$$\begin{aligned}\Re\mathrm{e}\{A_{11}+A_{22}\} =&\Re\mathrm{e}\{-(f_\uparrow\partial_x\tilde{f}_\uparrow-\tilde{f}_\uparrow\partial_x f_\uparrow)-2(f_t\partial_x\tilde{f}_t-\tilde{f}_t\partial_x f_t)\\&+2(f_s\partial_x\tilde{f}_s-\tilde{f}_s\partial_x f_s)-(f_\downarrow\partial_x\tilde{f}_\downarrow-\tilde{f}_\downarrow\partial_x f_\downarrow)\},\end{aligned}\tag{3.56}$$

$$\begin{aligned}\Re\mathrm{e}\{A_{12}+A_{21}\} =&\Re\mathrm{e}\{-(f_\uparrow+f_\downarrow)\partial_x\tilde{f}_t+(\tilde{f}_\uparrow+\tilde{f}_\downarrow)\partial_x f_t\\&-f_t\partial_x(\tilde{f}_\uparrow+\tilde{f}_\downarrow)+\tilde{f}_t\partial_x(f_\uparrow+f_\downarrow)\\&-(f_\uparrow-f_\downarrow)\partial_x\tilde{f}_s-(\tilde{f}_\uparrow-\tilde{f}_\downarrow)\partial_x f_s\\&+f_s\partial_x(\tilde{f}_\uparrow-\tilde{f}_\downarrow)+\tilde{f}_s\partial_x(f_\uparrow-f_\downarrow)\},\end{aligned}\tag{3.57}$$

$$\begin{aligned}\Im\mathrm{m}\{A_{21}-A_{12}\} =&\Im\mathrm{m}\{(f_\uparrow-f_\downarrow)\partial_x\tilde{f}_t+(\tilde{f}_\uparrow-\tilde{f}_\downarrow)\partial_x f_t\\&-f_t\partial_x(\tilde{f}_\uparrow-\tilde{f}_\downarrow)-\tilde{f}_t\partial_x(f_\uparrow-f_\downarrow)\\&+(f_\uparrow+f_\downarrow)\partial_x\tilde{f}_s-(\tilde{f}_\uparrow+\tilde{f}_\downarrow)\partial_x f_s\\&+f_s\partial_x(\tilde{f}_\uparrow+\tilde{f}_\uparrow)-\tilde{f}_s\partial_x(f_\uparrow+f_\uparrow)\},\end{aligned}\tag{3.58}$$

$$\begin{aligned}\Re\mathrm{e}\{A_{11}-A_{22}\} =&\Re\mathrm{e}\{-(f_\uparrow\partial_x\tilde{f}_\uparrow-\tilde{f}_\uparrow\partial_x f_\uparrow)+(f_\downarrow\partial_x\tilde{f}_\downarrow-\tilde{f}_\downarrow\partial_x f_\downarrow)\\&-2(f_s\partial_x\tilde{f}_t+\tilde{f}_s\partial_x f_t)+2(f_t\partial_x\tilde{f}_s+\tilde{f}_t\partial_x f_s)\},\end{aligned}\tag{3.59}$$

where we have used that $\Re\mathrm{e}\{\mathbb{Z}^*\}=\Re\mathrm{e}\{\mathbb{Z}\}$, and that $\Im\mathrm{m}\{\mathbb{Z}^*\}=\Im\mathrm{m}\{-\mathbb{Z}\}$, where $\mathbb{Z}$ is just a complex number. From these equations we use the following relations to simplify the current integrals in (2.34).

$$\int_{-\infty}^{\infty}\mathrm{d}E\tanh\left(\frac{\beta E}{2}\right)\Re\mathrm{e}\big\{F(E)-F^*(-E)\big\}=2\int_{0}^{\infty}\mathrm{d}E\tanh\left(\frac{\beta E}{2}\right)\Re\mathrm{e}\big\{F(E)\big\},\tag{3.60}$$

$$\int_{-\infty}^{\infty}\mathrm{d}E\tanh\left(\frac{\beta E}{2}\right)\Re\mathrm{e}\big\{F(E)+F^*(-E)\big\}=0,\tag{3.61}$$

$$\int_{-\infty}^{\infty}\mathrm{d}E\tanh\left(\frac{\beta E}{2}\right)\Im\mathrm{m}\big\{F(E)+F^*(-E)\big\}=2\int_{0}^{\infty}\mathrm{d}E\tanh\left(\frac{\beta E}{2}\right)\Im\mathrm{m}\big\{F(E)\big\},\tag{3.62}$$

$$\int_{-\infty}^{\infty}\mathrm{d}E\tanh\left(\frac{\beta E}{2}\right)\Im\mathrm{m}\big\{F(E)-F^*(-E)\big\}=0.\tag{3.63}$$

After removing terms that are anti-symmetric in quasiparticle energy E, we are

left with only terms that are symmetric in energy, and our supercurrents become:

$$
\begin{aligned}
I_Q &= I_0 \int_0^\infty \mathrm{d}E \tanh\left(\frac{\beta E}{2}\right) 4\Re\mathrm{e}\{-(f_\uparrow \partial_x \tilde{f}_\uparrow - \tilde{f}_\uparrow \partial_x f_\uparrow) - 2(f_t \partial_x \tilde{f}_t - \tilde{f}_t \partial_x f_t) \\
&\qquad + 2(f_s \partial_x \tilde{f}_s - \tilde{f}_s \partial_x f_s) - (f_\downarrow \partial_x \tilde{f}_\downarrow - \tilde{f}_\downarrow \partial_x f_\downarrow)\}, \\
I_S^x &= I_0 \int_0^\infty \mathrm{d}E \tanh\left(\frac{\beta E}{2}\right) 4\Re\mathrm{e}\{-(f_\uparrow + f_\downarrow)\partial_x \tilde{f}_t + (\tilde{f}_\uparrow + \tilde{f}_\downarrow)\partial_x f_t \\
&\qquad - f_t \partial_x (\tilde{f}_\uparrow + \tilde{f}_\downarrow) + \tilde{f}_t \partial_x (f_\uparrow + f_\downarrow)\}, \\
I_S^y &= I_0 \int_0^\infty \mathrm{d}E \tanh\left(\frac{\beta E}{2}\right) 4\Im\mathrm{m}\{(f_\uparrow - f_\downarrow)\partial_x \tilde{f}_t + (\tilde{f}_\uparrow - \tilde{f}_\downarrow)\partial_x f_t \\
&\qquad - f_t \partial_x (\tilde{f}_\uparrow - \tilde{f}_\downarrow) - \tilde{f}_t \partial_x (f_\uparrow - f_\downarrow)\}\}, \\
I_S^z &= I_0 \int_0^\infty \mathrm{d}E \tanh\left(\frac{\beta E}{2}\right) 4\Re\mathrm{e}\{-(f_\uparrow \partial_x \tilde{f}_\uparrow - \tilde{f}_\uparrow \partial_x f_\uparrow) + (f_\downarrow \partial_x \tilde{f}_\downarrow - \tilde{f}_\downarrow \partial_x f_\downarrow)\}.
\end{aligned}
\tag{3.64}
$$

Here I_0 is different for spin- and charge-supercurrent, as mentioned earlier. Furthermore, we insert the weak proximity solution of the Usadel equation, $f_n = A_n \mathrm{e}^{ikx} + B_n \mathrm{e}^{-ikx}$ and $\tilde{f}_n = \tilde{A}_n \mathrm{e}^{-ikx} + \tilde{B}_n \mathrm{e}^{ikx}$ into the supercurrent expressions (3.64), which gives us

$$
\begin{aligned}
I_Q &= I_0 \int_0^\infty \mathrm{d}E \tanh\left(\frac{\beta E}{2}\right) 8\Re\mathrm{e}\{ik[(A_\uparrow \tilde{A}_\uparrow - B_\uparrow \tilde{B}_\uparrow) + 2(A_t \tilde{A}_t - B_t \tilde{B}_t) \\
&\qquad - 2(A_s \tilde{A}_s - B_s \tilde{B}_s) + (A_\downarrow \tilde{A}_\downarrow - B_\downarrow \tilde{B}_\downarrow)]\}, \\
I_S^x &= I_0 \int_0^\infty \mathrm{d}E \tanh\left(\frac{\beta E}{2}\right) 8\Re\mathrm{e}\{ik[(A_\uparrow + A_\downarrow)\tilde{A}_t - (B_\uparrow + B_\downarrow)\tilde{B}_t \\
&\qquad + (\tilde{A}_\uparrow + \tilde{A}_\downarrow)A_t - (\tilde{B}_\uparrow + \tilde{B}_\downarrow)B_t]\}, \\
I_S^y &= I_0 \int_0^\infty \mathrm{d}E \tanh\left(\frac{\beta E}{2}\right) 8\Re\mathrm{e}\{k(-(A_\uparrow - A_\downarrow)\tilde{A}_t + (B_\uparrow - B_\downarrow)\tilde{B}_t \\
&\qquad + (\tilde{A}_\uparrow - \tilde{A}_\downarrow)A_t - (\tilde{B}_\uparrow - \tilde{B}_\downarrow)B_t)\}, \\
I_S^z &= I_0 \int_0^\infty \mathrm{d}E \tanh\left(\frac{\beta E}{2}\right) 8\Re\mathrm{e}\{ik[(A_\uparrow \tilde{A}_\uparrow - B_\uparrow \tilde{B}_\uparrow) - (A_\downarrow \tilde{A}_\downarrow - B_\downarrow \tilde{B}_\downarrow)]\}.
\end{aligned}
\tag{3.65}
$$

The last step in the analytical derivation is to use the expressions for the constants obtained from Maple when we solved the linear algebra problem $\check{A}\boldsymbol{x} = \boldsymbol{b}$. We also do the explicit calculations in Maple, since these are lengthy expressions. When having arbitrary magnetization direction at both interfaces the charge-supercurrent is given by

$$I_Q = I_0 \int_0^\infty \mathrm{d}E \tanh\left(\frac{\beta E}{2}\right) \frac{16ik \sinh^2\Theta \sin\theta \sin(k\ell)\left(k^2\ell^2\zeta_L\zeta_R + \boldsymbol{m}_L \cdot \boldsymbol{m}_R G_\varphi^L G_\varphi^R\right)}{\Lambda_{\text{full}}}, \tag{3.66}$$

where we have defined Λ_{full} as

$$\Lambda_{\text{full}} = \left(h_L(G_\varphi^L)^2 + k^2\ell^2\zeta_L^2\right)\left(h_R(G_\varphi^R)^2 + \ell^2k^2\zeta_R^2\right)\cos^2(k\ell) - \left(wG_\varphi^L G_\varphi^R + k^2\ell^2\zeta_L\zeta_R\right)^2, \tag{3.67}$$

and $h_{L(R)}$ and w as

$$\begin{aligned} h_{L(R)} &= (m_{L(R)}^z)^2 - (m_{L(R)}^x)^2 - (m_{L(R)}^y)^2, \\ w &= m_L^x m_R^x + m_L^y m_R^y - m_L^z m_R^z. \end{aligned} \tag{3.68}$$

We also get that the absolute value of the spin-supercurrent is given by

$$\begin{aligned} |I_S| &= \sqrt{(I_S^x)^2 + (I_S^y)^2 + (I_S^z)^2} \\ &= I_0 \int_0^\infty \mathrm{d}E \tanh\left(\frac{\beta E}{2}\right) 16ikG_\varphi^L G_\varphi^R \sinh^2\Theta \sin(k\ell)|\boldsymbol{m}_L \times \boldsymbol{m}_R|\Lambda_{\text{Full}}^{-2} \\ &\Big(\cos\theta\Big[\{h_L(G_\varphi^L)^2 + k^2\ell^2\zeta_L^2\}\{h_R(G_\varphi^R)^2 + k^2\ell^2\zeta_R^2\}\cos^2(k\ell) + (wG_\varphi^L G_\varphi^R + k^2\ell^2\zeta_L\zeta_R)^2\Big] \\ &+ \Big[\{h_L(G_\varphi^L)^2 + h_R(G_\varphi^R)^2 + k^2\ell^2(\zeta_L^2 + \zeta_R^2)\}\{wG_\varphi^L G_\varphi^R + k^2\ell^2\zeta_L\zeta_R\}\cos(k\ell)\Big]\Big) \end{aligned} \tag{3.69}$$

Here both (3.66) and (3.69) only depend on the relative magnetization angle, such that without loss of generality, we lock the right interface in the z-direction so that $\boldsymbol{m}_R = (0, 0, 1)$, while leaving the left side with the arbitrary magnetization direction $\boldsymbol{m}_L = (\sin\alpha\cos\phi, \sin\alpha\sin\phi, \cos\alpha)$, where we use α as the polar angle and ϕ as the azimuth angle. At last, the spin- and charge-supercurrent is finally

given by

$$
\begin{aligned}
I_Q &= I_0 \sin\theta \int_0^\infty \mathrm{d}E \tanh\left(\frac{\beta E}{2}\right) 16\Re\mathrm{e}\Big\{\Lambda^{-1} ik \sin(k\ell)\sinh^2(\Theta)[k^2\ell^2\zeta_L\zeta_R + \cos\alpha G_\varphi^L G_\varphi^R]\Big\},\\
I_S^x &= I_0 \sin\alpha \sin\phi G_\varphi^L G_\varphi^R \int_0^\infty \mathrm{d}E \tanh\Big(\frac{\beta E}{2}\Big) 16\Re\mathrm{e}\Big\{\Lambda^{-2}\sin(k\ell)\sinh^2(\Theta) ik(a_1 + a_2\cos\theta)\Big\},\\
I_S^y &= -\frac{\cos\phi}{\sin\phi} I_S^x,\\
I_S^z &= 0,
\end{aligned}
\tag{3.70}
$$

where we have defined the expressions

$$
\begin{aligned}
\Lambda &= [k^2\ell^2\zeta_L^2 + 2(G_\varphi^L)^2\cos^2\alpha - (G_\varphi^L)^2][k^2\ell^2\zeta_R^2 + (G_\varphi^R)^2]\cos^2(k\ell) - [k^2\ell^2\zeta_L\zeta_R - G_\varphi^L G_\varphi^R\cos\alpha]^2,\\
a_1 &= [2(G_\varphi^L)^2\cos^2\alpha - (G_\varphi^L)^2 + k^2\ell^2(\zeta_L^2 + \zeta_R^2) + (G_\varphi^R)^2][k^2\ell^2\zeta_L\zeta_R - G_\varphi^L G_\varphi^R\cos\alpha]\cos(k\ell),\\
a_2 &= [k^2\ell^2\zeta_L^2 + 2(G_\varphi^L)^2\cos^2\alpha - (G_\varphi^L)^2][k^2\ell^2\zeta_R^2 + (G_\varphi^R)^2]\cos^2(k\ell) + [k^2\ell^2\zeta_L\zeta_R - G_\varphi^L G_\varphi^R\cos\alpha]^2.
\end{aligned}
\tag{3.71}
$$

From the charge-current in (3.70) we can extract the following relation:

$$
\boxed{I_Q = \sin\theta(I_{Q,0} + \cos\alpha G_\varphi^L G_\varphi^R I_{Q,1})}, \tag{3.72}
$$

where the expressions of $I_{Q,0}$ and $I_{Q,1}$ can be found from the expressions in (3.70). This is one of the main results of this thesis. Here the first term is the current contribution from singlet pairing and second term is the contribution from the total triplet pairing. According to this equation we need to have a non-zero value for the spin-active parameter G_φ on both interfaces in order to have a triplet contribution to the charge-supercurrent. Interestingly we also see that for the special case of

$$
I_{Q,0} = -\cos\alpha G_\varphi^L G_\varphi^R I_{Q,1}, \tag{3.73}
$$

the current goes to zero, which means that we get a 0-π transition that is controllable via the relative misalignment angle of the magnetizations of the magnetic interfaces, a feature that also that was reported in the ballistic regime [56]. The fact that the charge-supercurrent goes as $\sin\theta$ is a known result called the first Josephson equation, and that the current changes sign when going from a positive to a negative superconducting phase difference, is easily understood by observing the same symmetric junction from the opposite side, since physics should be independent of our choice of coordinate system.

When considering the spin-supercurrent we find that

$$\boxed{I_S^x = \sin\alpha G_\varphi^L G_\varphi^R (I_{S,0}^x + \cos\theta I_{S,1})}, \tag{3.74}$$

which is another of the main results. This shows that the spin-current has a term that is independent on the superconducting phase difference, whereas the other term goes as $\cos\theta$, and not $\sin\theta$ as for the charge-supercurrent. This is consistent with the fact that a spin-current is invariant under time-reversal symmetry, in contrast to a charge-current. A spin-↑- particle traveling to the right, will be the same as a spin-↓ going left when reversing the time, both carrying the same spin-current. While we find that the magnitude of the spin-current only depends on the relative misalignment angle, logically, we get that the x, y and z components depend on the spatial orientation. The spin-supercurrent appear in the direction $\boldsymbol{m}_L \times \boldsymbol{m}_R$, which means that as long as we only consider magnetizations perpendicular to the tunneling direction, where $\phi = \pi/2$, both I_S^y and I_S^z will always be zero. Very recently, similar dependencies on α and θ was found in a theoretical study of multiband superconductors coexisting with a spin-density wave state [57], although the system considered is quite different from ours.

The triplet part of the charge-supercurrent derived here is in the first harmonic ($\sin\theta$), in contrast to the second harmonic ($\sin 2\theta$) long-ranged supercurrent found in Ref. [36]. This is an important difference, since we do not need any special fine-tuning in order to suppress the first harmonic in favor of the second. In addition, our system has no ferromagnetic elements that could disturb the spin-current conservation, unlike previous proposals.

Special-Case Solutions

To prove the consistency to earlier reported results we set the spin-dependent phase shift parameters $G_\varphi^L = G_\varphi^R = G_\varphi$ to zero and the interface transparencies equal $\zeta_L = \zeta_R = \zeta$, and regain the result of a normal non-spin-active SNS Josephson junction. We easily see that all the spin-currents go to zero in this case, and we get for the charge-supercurrent:

$$I_Q^0 = \frac{N_0 e D A}{4\ell\zeta^2} 8\sin\theta \int_{-\infty}^{\infty} \mathrm{d}E \tanh\left(\frac{\beta E}{2}\right) \Re\mathrm{e}\left\{\frac{i\sinh^2(\Theta)}{k\ell\sin(k\ell)}\right\}, \tag{3.75}$$

where we have extended the limits. Some places in the literature the normal conductance G_N is used instead of the constant I_0, and we can use the relation $G_N = 2e^2 N_0 D A/\ell$ to compare results. This solution can be rewritten into a sum by taking the real part operator outside the integral and using the residue integration

method. It is known that if the function goes to zero in the infinity of the complex plane [58], we can use the equation

$$\int_{-\infty}^{\infty} \mathrm{d}E\ F(E) = 2\pi i \sum \mathrm{Res}\ F(z), \tag{3.76}$$

where $F(E)$ is a function of real energies and $F(z)$ is the same function, only including complex energies $z = E + i\omega$. In (3.76) we have to sum over the residue of all poles in the upper half plane, and the specific residue formula we are going to use is given by

$$\operatorname*{Res}_{z=z_0} \frac{F_{\mathrm{n}}(z)}{F_{\mathrm{d}}(z)} = \frac{F_{\mathrm{n}}(z_0)}{\partial_z F_{\mathrm{d}}(z)}, \tag{3.77}$$

where the subscripts n and d stand for numerator and denominator. We divide the integrand as

$$F_{\mathrm{n}}(z) = \sinh\left(\frac{\beta z}{2}\right) \Re\mathrm{e}\left\{\frac{i\sinh^2(\Theta)}{k\ell\sin(k\ell)}\right\}, \text{ and } F_{\mathrm{d}}(z) = \cosh\left(\frac{\beta z}{2}\right). \tag{3.78}$$

This means that we have poles for all $z = i\omega_n$, where $\omega_n = \pi(1+2n)/\beta$ and n is all positive integers. Since the $\sinh(\beta z/2)$ in the numerator and the $\sinh(\beta z/2)$ coming from the denominator $\partial_z \cosh(\beta z/2)$ cancels, we are only left with a factor $2/\beta$ from these functions. In reference [59] the authors have included spin-flip scattering to a normal SNS junction and obtained an additional term in the dimensionless product $k\ell = \sqrt{2(iz-\delta)/E_{\mathrm{T}}}$. The addition from δ-energy ships the pole into the lower complex plane, and we will assume that we have an infinitesimal such term to avoid dealing with poles at the real axis. If this is not the case our solution will still be correct, only with possible additional current-terms due to the sum over residues. If so, it is normal to take half the residue of poles that are situated on the counter path.

The total sum from this calculation becomes

$$I_Q^0 = \frac{N_0 e D A}{\ell\zeta^2\beta} 8\pi\sin\theta \sum_{\omega_n} \frac{\frac{|\Delta|^2}{|\Delta|^2+\omega_n^2}}{\sqrt{2\omega_n/E_{\mathrm{T}}}\sinh(\sqrt{2\omega_n/E_{\mathrm{T}}})}, \tag{3.79}$$

and we recognize ω_n as the Matsubara frequency. We have used $\sin^2\theta = |\Delta|^2/(|\Delta|^2 - E^2)$, which comes from $\Theta = \tanh^{-1}(|\Delta|/E)$

If we now instead assume that $k\ell\zeta_{L(R)} \gg G_\varphi^{L(R)}$ and again choose equal interface-parameters, we still get

$$\Lambda = (k\ell\zeta)^4 \sin^2(k\ell) \tag{3.80}$$

which gives us the approximated charge-supercurrent:

$$I_Q = I_Q^0 + I_Q^{\text{triplet}}. \tag{3.81}$$

The dominating first term I_Q^0 is the normal non-spin-active SNS-solution, but the last term is a triplet term expressed as

$$I_Q^{\text{triplet}} = \frac{N_0 eDA}{4\ell} \sin\theta \cos\alpha G_\varphi^L G_\varphi^R \int_{-\infty}^{\infty} \mathrm{d}E \tanh\left(\frac{\beta E}{2}\right) 8\Re\mathrm{e}\left\{\frac{i\sinh^2(\Theta)}{\zeta^4 (k\ell)^3 \sin(k\ell)}\right\}. \tag{3.82}$$

The triplet term can now be expressed as a sum in a very similar way as for the singlet term

$$I_Q^{\text{triplet}} = -\frac{N_0 eDA}{\ell\zeta^4\beta} 8\pi \sin\theta\cos\alpha G_\varphi^L G_\varphi^R \sum_{\omega_n} \frac{\frac{|\Delta|^2}{|\Delta|^2+\omega_n^2}}{(2\omega_n/E_{\mathrm{T}})^{\frac{3}{2}} \sinh(\sqrt{2\omega_n/E_{\mathrm{T}}})}. \tag{3.83}$$

We see that the triplet term is negative compared to the singlet term, which means that the two charge-current contributions add to a maximum value at $\alpha = \pi$.

Chapter 4

Numerical Solution

We will now look further than the assumption of weak proximity and turn back to the full equations from the theory chapter. For selected MATLAB scripts, see Appendix C. In sections 4.2 and 4.3 we will neglect the inverse proximity and assume that we can use the BCS solution at the superconducting side of the interfaces. In reality, the superconducting correlations decline when approaching the interface, where this correction will be briefly discussed in section 4.4. We emphasis that in all forthcoming figures, we have chosen the magnetization of the right magnetic interface in the z-direction so that α and ϕ is related to magnetization of the left magnetic insulator, as in the analytical expressions.

4.1 Dimensionless Quantities

To support numerical calculations we write all equations in terms of dimensionless quantities. We choose to represent the x-coordinate by the dimensionless length $u = x/\ell$, and the energy with the dimensionless energy $\epsilon = E/\Delta_0$. Here we use Δ_0 as the magnitude of the superconducting energy gap for the bulk solution in the superconductors. We also introduce the Thouless energy $E_T = D/\ell^2$ and its dimensionless partner $\epsilon_{\mathrm{T}} = E_{\mathrm{T}}/\Delta_0$. By using that the superconducting coherence length is given by $\xi_S = \sqrt{D/\Delta_0}$, we can write $\epsilon_{\mathrm{T}} = (\xi_S/\ell)^2$. In many published papers the Thouless energy is written with an additional $\hbar$, but then the Usadel

equation also has an extra $\hbar$. The Usadel equation will now transform as follows:

$$\begin{aligned}
& D\partial_x\left(\hat{g}^{\mathrm{R}}(\partial_x\hat{g}^{\mathrm{R}})\right) + i\left[E\hat{\rho}_3 - \hat{\Sigma} + \hat{\Delta}, \hat{g}^{\mathrm{R}}\right] = 0 \\
\rightarrow \quad & \frac{D}{\ell^2}\frac{\partial}{\partial u}\left(\hat{g}^{\mathrm{R}}\left(\frac{\partial}{\partial u}\hat{g}^{\mathrm{R}}\right)\right) + i\left[E\hat{\rho}_3 - \hat{\Sigma} + \hat{\Delta}, \hat{g}^{\mathrm{R}}\right] = 0 \\
\rightarrow \quad & \frac{\partial}{\partial u}\left(\hat{g}^{\mathrm{R}}\left(\frac{\partial}{\partial u}\hat{g}^{\mathrm{R}}\right)\right) + \frac{i}{E_T}\left[E\hat{\rho}_3 - \hat{\Sigma} + \hat{\Delta}, \hat{g}^{\mathrm{R}}\right] = 0 \\
\rightarrow \quad & \partial_u\left(\hat{g}^{\mathrm{R}}(\partial_u\hat{g}^{\mathrm{R}})\right) + \frac{i}{\epsilon_T}\left[\epsilon\hat{\rho}_3 - \frac{\hat{\Sigma}}{\Delta_0} + \frac{\hat{\Delta}}{\Delta_0}, \hat{g}^{\mathrm{R}}\right] = 0. \qquad (4.1)
\end{aligned}$$

This equals changing $x \rightarrow u$ and $D \rightarrow E_T$, and dividing by E_T in the original Usadel equation while measuring all energies relative to Δ_0.

When making the boundary conditions dimensionless, we only need to change the left side of the equations, so that ($\ell\partial_x = \partial_u$), which equals setting the normal metal length equal to one in the original conditions. From this we get

$$\begin{aligned}
& 2\ell\zeta_l\check{g}_l(\partial_x\check{g}_l) = [\check{g}_l, \check{g}_r] + G_{\mathrm{MR}}\left[\check{g}_l, \{\check{A}, \check{g}_r\}\right] + iG^l_\varphi\left[\check{g}_l, \check{A}\right] \\
\rightarrow \quad & 2\zeta_l\check{g}_l(\partial_u\check{g}_l) = [\check{g}_l, \check{g}_r] + G_{\mathrm{MR}}\left[\check{g}_l, \{\check{A}, \check{g}_r\}\right] + iG^l_\varphi\left[\check{g}_l, \check{A}\right] \qquad (4.2)
\end{aligned}$$

and equivalently for the other condition in (2.19)

To make the Riccati parameterized version dimensionless, we just follow the same recipe and set

$$x \rightarrow u, \quad D \rightarrow E_{\mathrm{T}}, \quad \ell \rightarrow 1, \text{ and } \Delta_0 = 1. \qquad (4.3)$$

When we have solved the Usadel equation for many energies and want to integrate over these energies, we have to determine the value of βE. For this we use the known relation $\Delta = 1.76k_{\mathrm{B}}T_c$, which is valid as long as $T << T_c$, and we write $\beta E = \epsilon\Delta/k_{\mathrm{B}}T = 1.76\epsilon T_c/T$.

In all equations the normal metal length only enters relative to the superconducting coherence length, which means that the result will be valid for other choices of these parameters as long as the relative ratio is the same, leading to unchanged Thouless energy. However, it is important to stay inside the scope of the quasiclassical theory. In the computer script, we have added a small imaginary energy term $\delta \ll \Delta_0$ to the quasiparticle energy. This imaginary energy represents a finite inelastic scattering relaxation time in the normal metal and will provide more realistic results, in addition to making the calculations faster.

4.2 Solving the Usadel Equation in the Normal Metal

In this section we neglect the spin-flip and spin-orbit scattering, and the parameterized Usadel equations from (2.13) reduce to

$$\begin{aligned}[2(\partial_x\gamma)\tilde{\gamma}N(\partial_x\gamma)+(\partial_x^2\gamma)]+\frac{2i\epsilon}{\epsilon_{\mathrm{T}}}\gamma=0,\\ [2(\partial_x\tilde{\gamma})\gamma\tilde{N}(\partial_x\tilde{\gamma})+(\partial_x^2\tilde{\gamma})]+\frac{2i\epsilon}{\epsilon_{\mathrm{T}}}\tilde{\gamma}=0.\end{aligned} \tag{4.4}$$

For the boundary conditions (2.22), the results from (3.14) still hold when assigning $L\to l$ and $R\to r$. This is because we still use the BCS bulk solution at the interface for the superconducting side. This gives us the conditions:

$$\begin{aligned}4\ell_l\zeta_l\partial_x\gamma_l&=\Gamma_l+2iG_\varphi^l[\gamma_l(\boldsymbol{m}\cdot\boldsymbol{\sigma}^*)-(\boldsymbol{m}\cdot\boldsymbol{\sigma})\gamma_l]-4\cosh\Theta G_{\mathrm{MR}}[(\boldsymbol{m}\cdot\boldsymbol{\sigma})\gamma_l+\gamma_l(\boldsymbol{m}\cdot\boldsymbol{\sigma}^*)],\\ 4\ell_r\zeta_r\partial_x\gamma_r&=\Gamma_r-2iG_\varphi^r[\gamma_r(\boldsymbol{m}\cdot\boldsymbol{\sigma}^*)-(\boldsymbol{m}\cdot\boldsymbol{\sigma})\gamma_r]+4\cosh\Theta G_{\mathrm{MR}}[(\boldsymbol{m}\cdot\boldsymbol{\sigma})\gamma_r+\gamma_r(\boldsymbol{m}\cdot\boldsymbol{\sigma}^*)],\\ 4\ell_l\zeta_l\partial_x\tilde{\gamma}_l&=\tilde{\Gamma}_l-2iG_\varphi^l[\tilde{\gamma}_l(\boldsymbol{m}\cdot\boldsymbol{\sigma})-(\boldsymbol{m}\cdot\boldsymbol{\sigma}^*)\tilde{\gamma}_l]-4\cosh\Theta G_{\mathrm{MR}}[(\boldsymbol{m}\cdot\boldsymbol{\sigma}^*)\tilde{\gamma}_l+\tilde{\gamma}_l(\boldsymbol{m}\cdot\boldsymbol{\sigma})],\\ 4\ell_r\zeta_r\partial_x\tilde{\gamma}_r&=\tilde{\Gamma}_r+2iG_\varphi^r[\tilde{\gamma}_r(\boldsymbol{m}\cdot\boldsymbol{\sigma})-(\boldsymbol{m}\cdot\boldsymbol{\sigma}^*)\tilde{\gamma}_r]+4\cosh\Theta G_{\mathrm{MR}}[(\boldsymbol{m}\cdot\boldsymbol{\sigma}^*)\tilde{\gamma}_r+\tilde{\gamma}_r(\boldsymbol{m}\cdot\boldsymbol{\sigma})],\end{aligned} \tag{4.5}$$

which will remain the same when we include spin-flip and spin-orbit scattering in the normal metal in section 4.3. We have that

$$\Gamma_{l(r)}=\pm N_{l(r)}^{-1}\left[\left[\hat{g}_{l(r)}^{\mathrm{R}},\hat{g}_{R(L)}^{\mathrm{R}}\right]_{12}-\left[\hat{g}_{l(r)}^{\mathrm{R}},\hat{g}_{R(L)}^{\mathrm{R}}\right]_{11}\gamma_{l(r)}\right], \tag{4.6}$$

with

$$\begin{aligned}\left[\hat{g}_{l(r)}^{\mathrm{R}},\hat{g}_{R(L)}^{\mathrm{R}}\right]_{12}&=i\sinh\Theta\mathrm{e}^{i\theta_{R(L)}}(g\sigma_y+\sigma_y\tilde{g})-2f\cosh\Theta,\\ \left[\hat{g}_{l(r)}^{\mathrm{R}},\hat{g}_{R(L)}^{\mathrm{R}}\right]_{11}&=i\sinh\Theta(f\sigma_y\mathrm{e}^{-i\theta_{R(L)}}+\sigma_y\tilde{f}\mathrm{e}^{i\theta_{R(L)}}),\end{aligned} \tag{4.7}$$

where we recall that $\hat{g}_R^{\mathrm{R}}$ is the BCS solution in the right superconductor, while $\hat{g}_r^{\mathrm{R}}$ is the solution on the right side of the left interface. When we in the following leave out the L,R notation of the interface parameters, we use the same values at both interfaces, except from the phase difference that was defined $\theta=\theta_R-\theta_L$. Notice that in the literature the phase difference sometimes is defined as $\theta=\theta_L-\theta_R$, and $e=|e|$, which both is the negative of the convention used here. However, the charge-supercurrent will still appear in the same way in both conventions since these signs cancel each other out. The spin-supercurrent will also appear in the same way, due to its independency of both the e and the sign of θ.

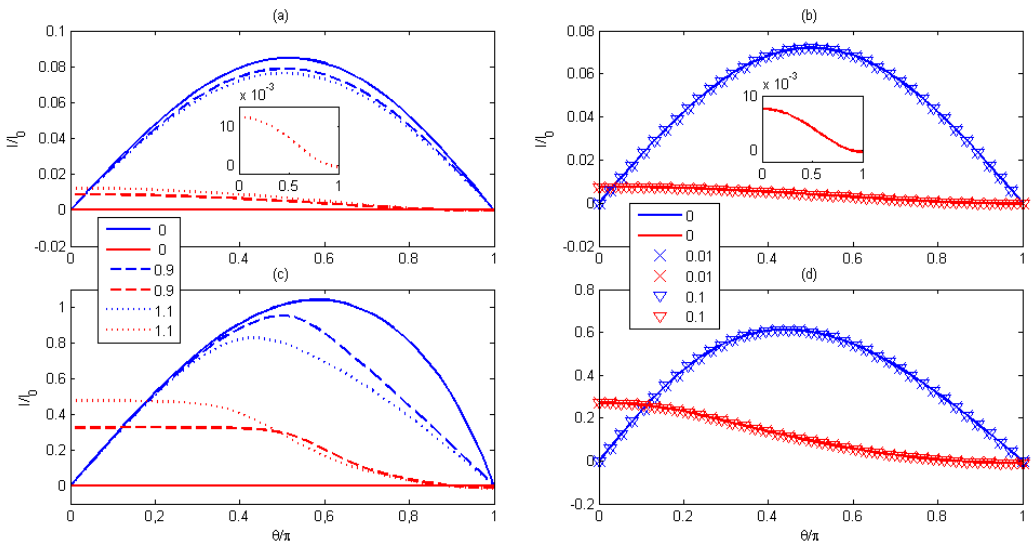

Figure 4.1: Spin- and charge-supercurrent (red and blue) as a function of the superconducting phase difference θ. In the first row we have $\ell = 60$ nm and $\zeta = 8$, while in the second row we have $\ell = 20$ nm and $\zeta = 5$. In (a) and (c) $\alpha = \pi/2$, $G_{\mathrm{MR}} = 0$, and G_φ varies with the values in the respective legend, whereas in (b) and (d) $\alpha = \pi/4$, $G_\varphi = 1.1$, and G_{MR} varies. The other parameters are $\xi_S = 30$ nm, $T/T_c = 0.02$ and $\phi = \pi/2$.

Spin- and Charge-Supercurrent

In Figure 4.1 we demonstrate how the spin- and charge-supercurrent behave as functions of the superconducting phase difference θ for various values of G_φ and G_{MR}. We have in Figure 4.1 (a) and (b) used large normal metal length $\ell = 2\xi_S$ and low interface transparencies, which we get from large values of ζ. This should bring us close to the weak proximity limit, and we see that the charge-current indeed goes as $\cos\theta$ and that the spin-current goes as $\sin\theta$ in addition to a constant term. This is the same as the dependencies we found from the analytical expressions (3.72) and (3.74) However, to go further than the weak proximity limit we also plot the solution for a shorter normal metal length $\ell = (2/3)\xi_S$ and $\zeta = 5$ in Figure 4.1 (c) and (d). Firstly, we find that the solutions resemble to the weak proximity limit but with distinct deviations. The θ-dependence of the charge-current looks more like a deformed sine function, and the spin-supercurrent is almost constant for small phase differences. When we derived the analytical solution in the weak proximity limit, we neglected a $\cosh\theta$ term that might explain these deviations. Secondly, we see that in spite of the fact that we have used a nonzero value for G_φ effect and chosen a nontrivial α, the G_{MR} parameters have very little impact on the currents. For this reason we set the G_{MR} parameters equal to zero for

the rest of this thesis. The effect from G_{MR} could change for strongly polarized insulators, and very recently new boundary conditions have been developed [60]. These general conditions can describe strongly polarized interfaces.

We notice in Figure 4.1 (a) and (c) that the spin-supercurrent increases when we increase the G_φ parameters. The analytical expression for the spin-current is proportional to $G_\varphi^L G_\varphi^R$ which makes it reasonable that the spin-current should increase for higher values. In the case of $G_\varphi = 0$ we find that the spin-current is zero, as expected since we then have a conventoinal SNS-junction. At $\theta = 0$ we demonstrate that there can exist a spin-current in absence of charge-current.

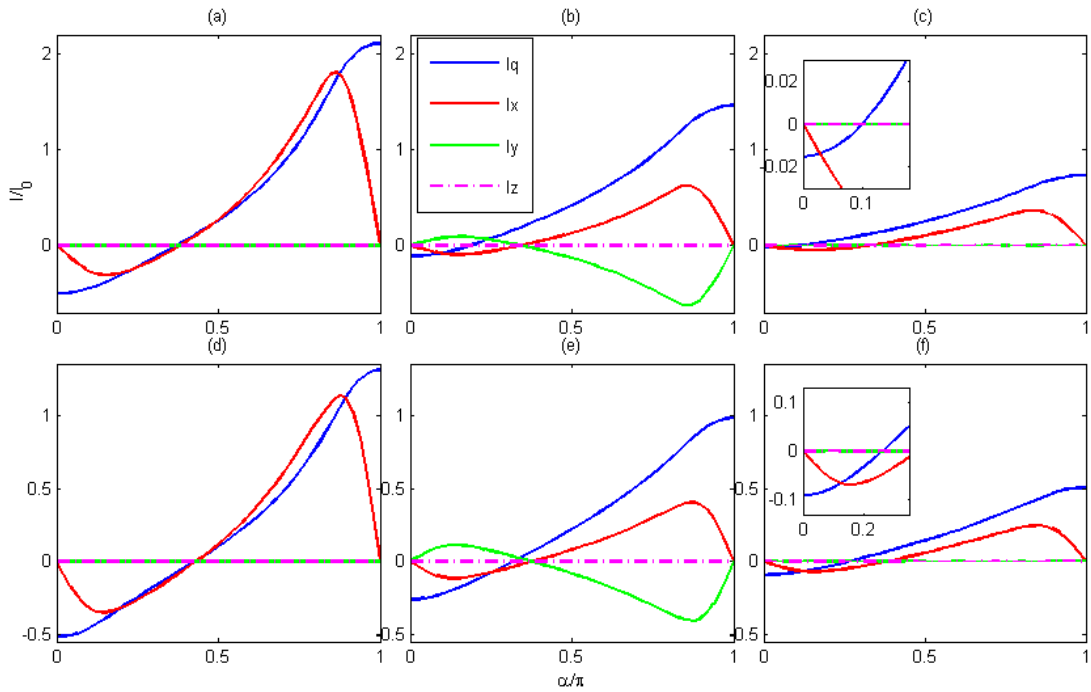

Figure 4.2: Spin- and charge-supercurrent as function of the magnetization displacement angle α. In the first row $G_\varphi = 3$, while in the second row we have used $G_\varphi = 4$. In (a) and (d) $\ell = 5$ nm and $\phi = \pi/2$, in (b) and (e) $\ell = 20$ nm and $\phi = \pi/4$, and in (c) and (f) $\ell = 40$ nm and $\phi = \pi/2$. We have used $\zeta = 5$, $\xi_S = 30$ nm, $\theta = \pi/2$, $T/T_c = 0.02$, and $G_{\mathrm{MR}} = 0$.

When plotting the spin- and charge-supercurrent as functions of α, we see from Figure 4.2 that a new way of controlling the 0-π transition occurs, as expected from the analytical expression (3.72). We can now change the sign of the current, simply by altering the relative magnetization angle. The transition point is dependent on the interface parameters, and to move the point further towards the antiparallel configuration, we have to shorten the length ℓ, lower the parameter ζ, or increase

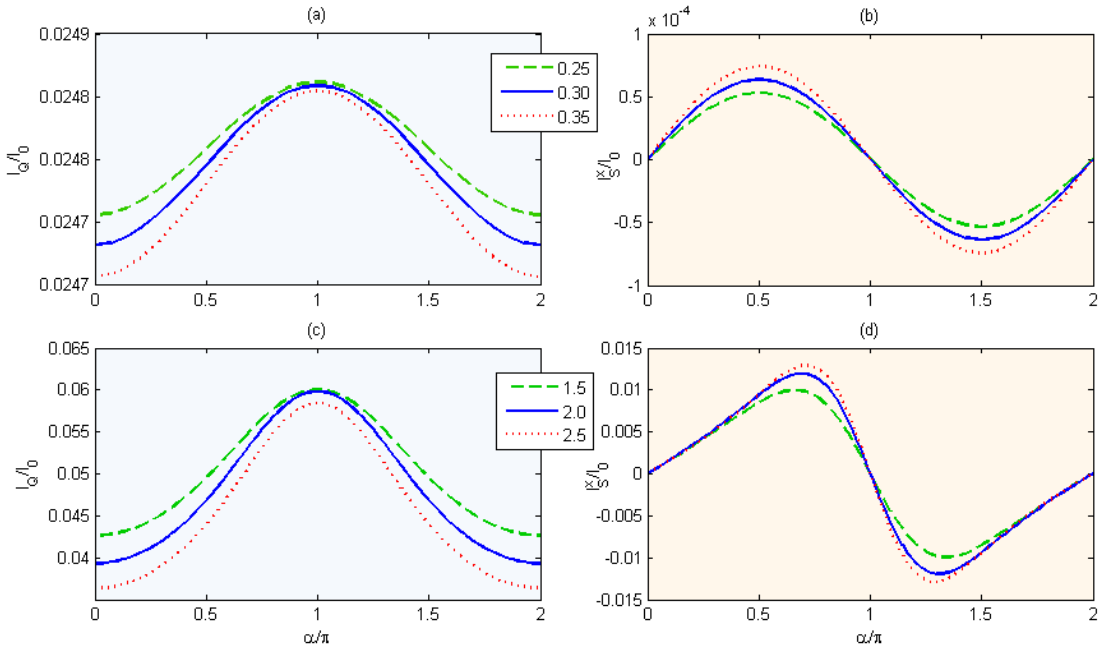

Figure 4.3: Spin- and charge-supercurrent as function of the magnetization displacement angle α. In (a) and (b) $\ell = 90$ nm, $G_\varphi^R = 0.3$ while G_φ^L varies with the values given in the upper legend. In (c) and (d) $\ell = 60$ nm, $G_\varphi^R = 2$ while G_φ^L varies with the values given in the lower legend. The other parameters are $\zeta = 10$, $\xi_S = 30$ nm, $\phi = \pi/2$, $\theta = \pi/2$, $T/T_c = 0.02$, and $G_{\mathrm{MR}} = 0$.

G_φ. We illustrate the Figure 4.2 (b) and (e) that then $\phi = \pi/4$, the spin-current components I_S^x and I_S^y are of equal size with opposite signs as found in (3.70).

We show in Figure 4.3 (a) and (b) that for parameters close to the weak proximity limit, the spin-current behaves as a pure $\sin\alpha$ and that the charge-current goes as $\cos\alpha$ with a constant term, as in the analytical expressions from (3.72) and (3.74). Since the nominator Λ (3.71) in the current expressions also depend on α we have chosen G_φ to be small, which causes the spin-current to be weak. However, when we increase the value of G_φ, still having quite long normal metal length and low transparency, we show in Figure 4.3 (c) and (d) that the spin-current is almost linear for values close $\alpha = 0$, and that the charge-current also has some change in the curvature. This means that we cannot neglect the additional α dependence for large values of G_φ.

Motivated by the fact that it is likely that the two parameters of G_φ are unequal in real samples, we also show in Figure 4.3 how the currents changes when we keep G_φ^R constant while G_φ^L changes weakly. We see that the overall behavior is the same for the currents only with small deviations, which we also would have obtained

when changing both interface parameters.

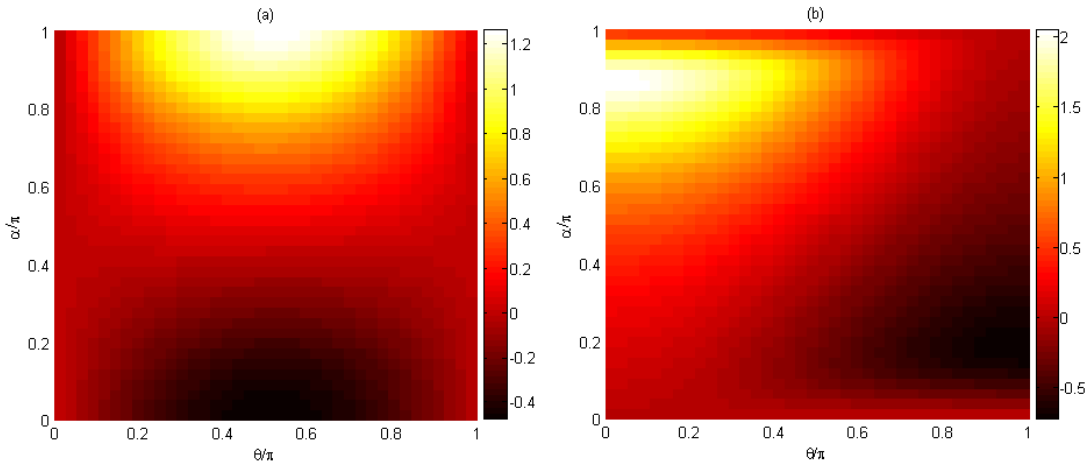

Figure 4.4: Spin- and charge-supercurrent in the plane of superconducting phase difference θ and magnetization displacement angle α. The values in (a) are given in I_Q/I_0 and values in (b) are given in I_S/I_0. We have used the parameters $\zeta = 2$, $G_\varphi = 4$, $\ell = 10$, $\xi_S = 30$ nm, $\phi = \pi/2$, $G_{\mathrm{MR}} = 0$, and $T/T_c = 0.02$.

To get a more complete picture of the α,θ-dependencies we include Figure 4.4 displaying surface-plots of spin- and charge-supercurrent. Here we keep the magnetizations in the x, y-plane and have therefore only spin-current values for I_S^x. The charge-current is given in Figure 4.4 (a) and we see that the 0-π transition occurs for small values of α, and is the most prominent around $\theta = \pi/2$. In Figure 4.4 (b) we show that the spin-current for this case has one area that is mostly positive and one that is mostly negative. These areas are separated by the α=θ-line. This gives us the opportunity to reverse the spin-current, which could be useful in spintronic devices.

Density of States

All forthcoming figures of density of states are normalized to its normal-state value. A collection of density of states surface-plots, given in the plane of E and θ, is shown in Figure 4.5. Firstly, we realize that when the interface magnetizations points in opposite directions as for Figure 4.5 (g), (h) and (i), the low energy enhancement we see for the other plots, vanish and we get solely a minigap in the density of states. The low energy enhancement indicates triplet pairing [61], and the minigap is the singlet signature. That we get a minigap at $\alpha = \pi$, can be understood as spin polarization filtering. This is not much different from the

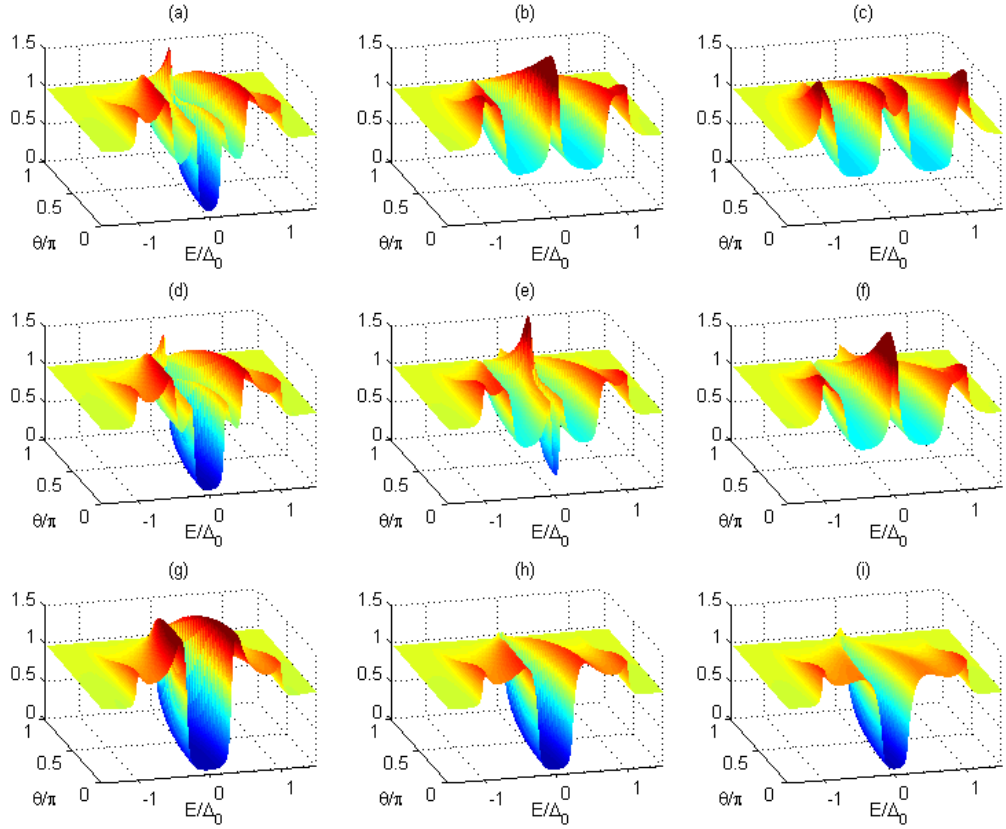

Figure 4.5: Density of states in the the plane of quasiparticle energy E and superconducting phase difference θ. The first, second, and third row has the α values 0, $\pi/2$, and π respectivily, while the first, second, and third column have the G_φ values 0.5, 1.1 and 1.5. The other parameters used are $\ell = 20$ nm, $\xi_S = 30$ nm, $\zeta = 4$, and $G_{\mathrm{MR}} = 0$.

effect we get from applying two linear polarization filters to an optical light source, where we know that when the relative angle between the filters is $\pi/2$, no light will get through. Secondly, we see that for several other cases, we can access both the singlet and triplet nature of the superconductivity, simply by varying the phase, starting with a minigap for small phases and going towards a low energy enhancement before flatting out at $\theta = \pi$. This is the case in Figure 4.5 (a), (d), and (e). That the density of states should be equal to its normal state value at $\theta = \pi$, can be justified by the fact that we measure the density of states in the middle of the junction. A difference of π equals a shift of sign for the superconducting order parameter. If the wave function is $+\Psi$ at left side and $-\Psi$ at the right side, it changes smoothly and has to be zero in the middle of

a symmetric structure. Hence, we get the normal metal value for the density of states here.

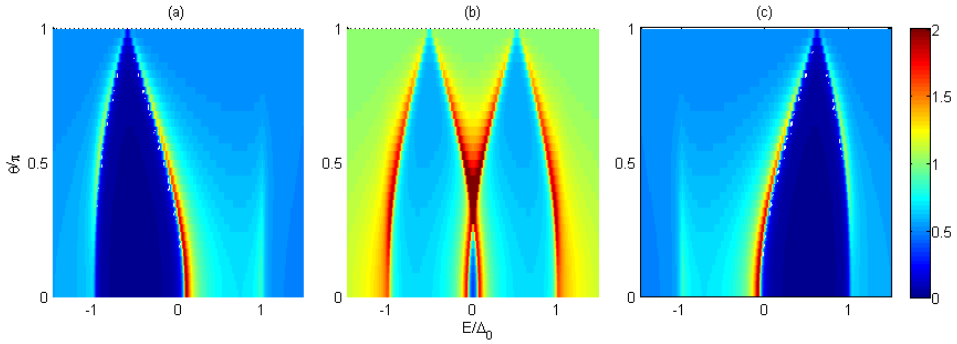

Figure 4.6: Spin-resolved density of states in the plane of quasiparticle energy E and superconducting phase difference θ. In (b) we have the total density of states, while in the (a) and (c), respectively, we have extracted the contributions from spin-↓ and spin-↑. The parameters used are $\zeta = 5$, G_φ=0.9, $G_{\mathrm{MR}} = 0$, $\ell = 10$ nm, $\xi_S = 30$ nm, $\alpha = 0$, and $\phi = \pi/2$.

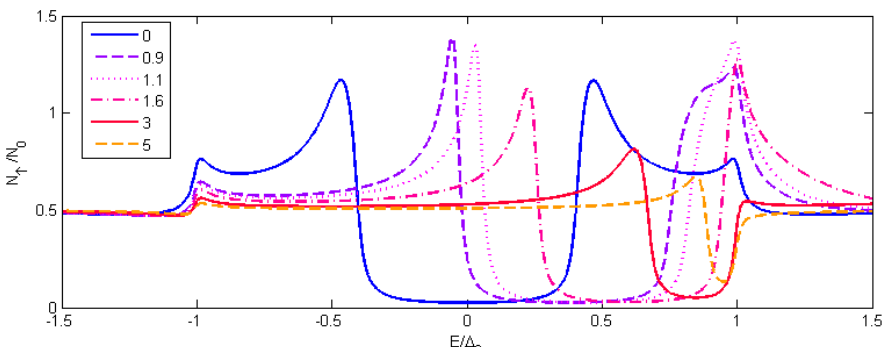

Figure 4.7: Spin-resolved density of states for spin-↑, as function of quasiparticle energy E. The values of G_φ are given in the legend. We have used the parameters $\zeta = 3$, $\phi = \pi/2$, $G_{\mathrm{MR}} = 0$, $\ell = 20$ nm, $\xi_S = 30$ nm, $\alpha = 0$ and $\theta = 0$.

We show in Figure 4.6 that the spin-resolved density of states for spin-↑ has a gap mostly for positive energies while spin-↓ has the mirrored image for negative energies. For a normal SNS junction, without spin-active interfaces, the density of states for spin-↑ and spin-↓ are equal, and we have no total spin transport in the system. When the energy states split up, we can get a net spin-current. In figure 4.7 we have given only the density of spin-↑ particles, but for various strengths of the spin-active interface parameter G_φ, as we know that the spin-↓ is exactly the same only inverted around $E = 0$. We see that by increasing the strength of

spin-mixing, the gap moves further and further away from zero energy and at the same time the width is reduced.

The enhancement in the density of states can be traced to the sum of the split densities. When the splitting is so large that the gap for spin-↑ and spin-↓ are fully separated, the weak enhancement in each spin-resolved density of states add to a clear enhancement. If the strength of the G_φ's becomes even stronger, we can use the same arguments to explain the folding of the low energy peak. The low energy enhancement should appear in the case of $G_\varphi \approx 1$, and this value distinguishes between the appearance of a minigap and a folded low energy peak. This specific value was examined in [62], and showed that a system undergo a transition from singlet to triplet nature at $G_\varphi = 1$.

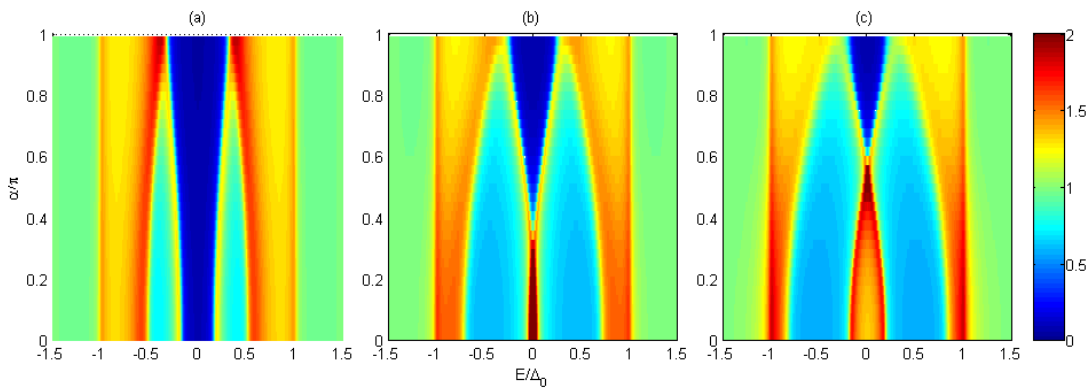

Figure 4.8: Density of states in the plane of quasiparticle energy E and the magnetization displacement angle α. The parameters are $\zeta = 3$, G_φ=0.9, $G_{\mathrm{MR}} = 0$, $\ell = 20$ nm, $\xi_S = 30$ nm, $\theta = 0$, and $\phi = \pi/2$.

In Figure 4.8 (b) and (c) we show that we can change the nature of the superconductivity by changing the relative misalignment angle, which also was indicated in Figure 4.5. To be able to change the nature of the proximity effect, we need the junction to exhibit clear triplet pairing in the parallel configuration, otherwise we only get a gap in the density of states for all values of α as in Figure 4.8 (a). We notice that when α goes from zero to π the energy gap on in Figure 4.8 (a) expands, which suggests that the gaps are weakly split at sharper angles of α.

The magnetic interfaces can be tweaked when the interfaces are made with different thicknesses. The thinnest layer will be easily influenced by an applied field. We estimate that appropriate thicknesses will be about 1-2 nm. This will naturally lead to a difference in the two G_φ values, since they are dependent on the tunneling resistance. The thicker layer will have higher resistance, meaning that the value of G_φ and possibly G_{MR} could be weaker at this interface. However, an enhancement in polarization for thicker interfaces could change G_{MR} differently.

Another way to access the relative magnetization angle is to use different materials at each interface, where one of them is more sensitive to applied magnetic fields, giving us more options to engineer the junction.

4.3 Including Spin-Dependent Scattering

To create a more realistic model of our junction, we include scattering on magnetic impurities and spin-orbit coupling. Since the magnetic insulators are very thin layers, we expect that spin-orbit coupling is present at the magnetic interfaces [63, 64]. Up to this day, no boundary conditions have been developed that take this effect into account. However, the physics should not be essentially different from the one where we include spin-dependent scattering at the interface, since both mechanisms create triplet paring. This means that we will use the boundary condition from (4.5), together with the parameterized Usadel equation (2.13) where we still have $\hat{\Delta} = 0$.

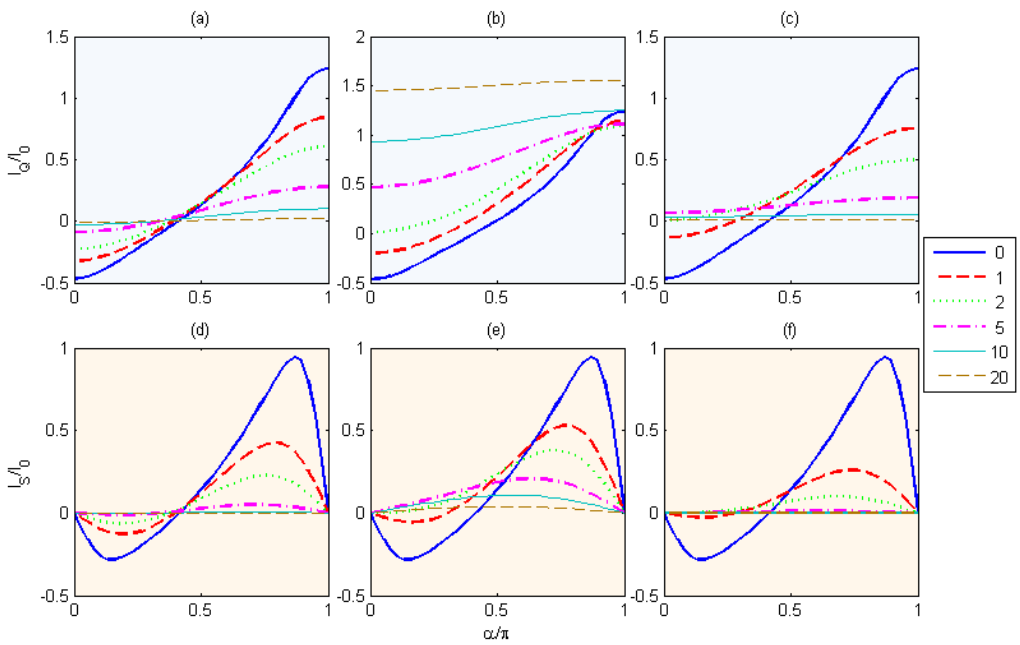

Figure 4.9: Spin- and charge-supercurrent as function of the magnetization displacement angle α, with varying contribution of spin-flip and spin-orbit scattering. In (a) and (d), $g_{\text{so}} = 0$ and g_{sf} varies with the values in the legend. In (b) and (e), $g_{\text{sf}} = 0$ and g_{so} varies with the values in the legend. And at last, in (c) and (f) $g_{\text{sf}} = g_{\text{so}}$ and varies with the legend. The other parameters are $\ell = 10$ nm, $\xi_S = 30$ nm, $\zeta = 2$, $\theta = \pi/2$, $\phi = \pi/2$, $G_\varphi = 4$, $G_{\text{MR}} = 0$, and $T/T_c = 0.02$.

Spin and Charge Supercurrent

The spin- and charge-supercurrent are affected quite differently by the two scatterings, depending on which kind of scattering the system is subject to. In Figure 4.9 we have plotted the supercurrents as function of α for a variety of different scattering strengths. We see that, whereas the spin-flip scattering monotonically decreases both the spin- and the charge-current in (a) and (d), the spin-orbit scattering seems to only destroy the triplet part of the superconductivity in (b) and (e), and in fact enhance the singlet correlations. It seems like the triplet Cooper pairs are converted back into singlet ones giving us an overall enhancement of singlet superconductivity, since the charge-current increases due to spin-orbit scattering. The trend is that we lose the 0-π transition via α, and that the spin-current decreases and goes towards a pure $\sin\theta$ behavior, like in the weak proximity limit. We also notice that the spin-flip scattering destroys the spin-current more rapidly than the spin-orbit coupling does, and that the combination of both destroys the spin-current even faster.

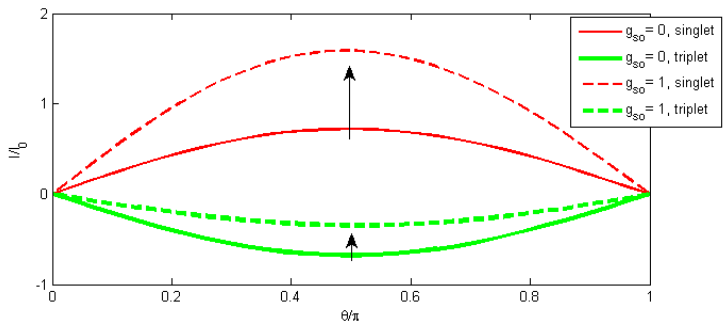

Figure 4.10: The singlet (red) and triplet (green) components of the charge-supercurrent as function of superconducting phase difference θ, with and without spin-orbit coupling. The coupling strength g_{so} is given in the legend. The parameters are $\ell = 15$ nm, $\xi_S = 30$ nm, $G_\varphi = 3$, $\zeta = 3$, $\alpha = 0$, $G_{\text{MR}} = 0$, $\phi = \pi/2$, and $T/T_c = 0.02$.

To study the spin-orbit effect deeper, we have separated the singlet and triplet terms of the charge-current as function of θ, as shown in Figure 4.10. Here we see that when exposed to spin-orbit coupling, the singlet current increases while the triplet current decreases. Interestingly, the magnitude of the changes is not of equal value. In fact the singlet component gain more than the triplet component loses, leading to a total enhancement in this particular case.

In figure 4.11 we show how the charge-current decreases as function of the normal metal length ℓ in the parallel configuration with critical current. We see that we also here access a 0-π transition. This transition cannot originate from

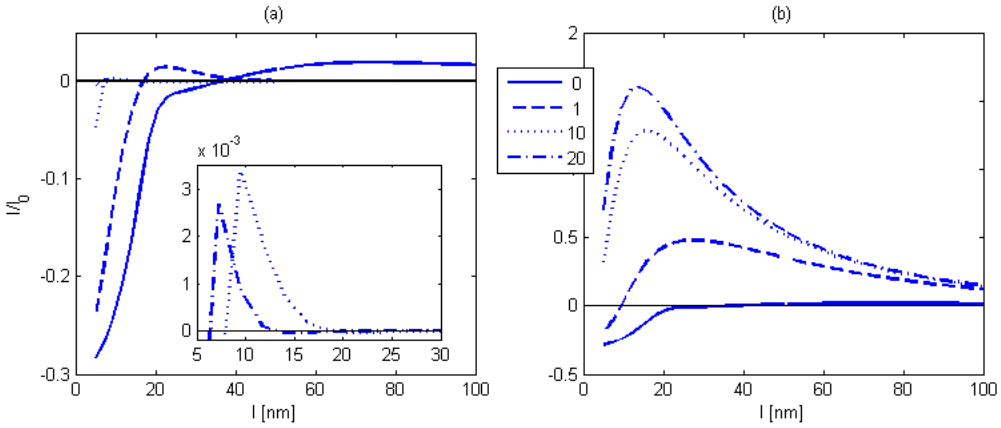

Figure 4.11: Charge-supercurrent as function of the normal metal length ℓ with different contributions of spin-flip and spin-orbit scattering. In (a) $g_{\rm so} = 0$ while $g_{\rm so}$ changes with the values in the shared legend, and the inset shows two of the functions when zoomed in. In (b) $g_{\rm sf} = 0$ while $g_{\rm sf}$ changes with the values in the legend. The parameters are $\xi_S = 30$ nm, $\alpha = 0$, $\theta = \pi/2$ $G_\varphi = 4$, $G_{\rm MR} = 0$, $\zeta = 3$, $\phi = \pi/2$, and $T/T_c = 0.02$.

the energy bands in the normal metal, since there are not any magnetic fields present to split the bands like in a ferromagnet. While a normal SNS junction decays monotonically to zero current from above, we find that the transition in the current length plot comes from the triplet pairing. This transition occurs towards shorter lengths of the normal metal when including spin-flip as in Figure 4.11 (a). It is interesting to notice that the maximum current in Figure 4.11 (b) is not obtained for the shortest length when spin-orbit coupling is included, as for a non-spin-active Josephson junction. The normal metal length that gives the maximum current is probably a compromise resulting in the shortest length possible that has enough scattering to convert all the present triplets. This would explain that this length is shorter for stronger values of $g_{\rm so}$.

In the analytical expressions we found that not only the spin-current but also the charge-current was independent of the position inside the normal metal. In Figure 4.12 we show that this is also the case for the full proximity effect regime, and that the result even holds when spin-orbit and spin-flip scatterings are present. Form conservation of charge, we know that the charge-current in Figure 4.12 (a) has to be independent of x, since this is the only direction current flows in our system. That the spin-current in Figure 4.12 (b) is independent on position in the absence of scattering events, can be understood since there are no mechanism that can destroy the spin once it is inside the normal metal. However, when we include the spin-orbit and spin-flip scatterings the spin-current is still independent

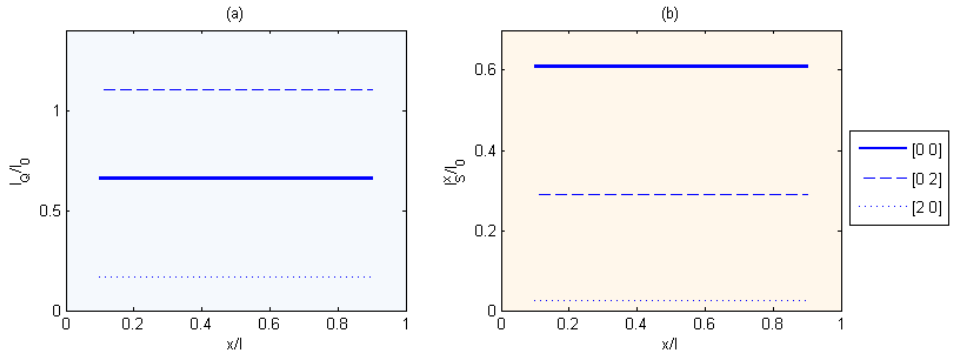

Figure 4.12: Spin- and charge-supercurrent as function of position x inside the normal metal, where $x = 0$ corresponds to the left interface. The scattering strengths are given as $[g_{sf}\ g_{so}]$ in the legend. The other parameters are $\ell = 10$ nm, $\xi_S = 30$ nm, $\alpha = 3\pi/4$, $\theta = \pi/2$ $G_\varphi = 3$, $\zeta = 5$, $\phi = \pi/2$, and $T/T_c = 0.02$.

of position. This is a surprising finding which could warrant further investigation.

Density of States

The density of states confirms the results found from the supercurrents. Figure 4.13 shows how the spin-flip and spin-orbit scattering modifies the density of states from zero scattering to large values of the scattering strength. The spin-flip scattering suppresses all superconductivity and pushes the density of states towards the normal-state value, whereas the spin-orbit coupling turn the low energy enhancement to a clear BCS gap for large values of the coupling strength. This is in accordance with the decay of the triplet current component in Figure 4.9 and the loss of 0-π transition for the total current. The findings also agree with what was found in Ref. [65] for a normal-metal/superconductor junction, where the singlet superconductivity is found to be insensitive to isotropic spin-orbit scattering.

In Figure 4.14 we show how the density of states in the parallel configuration from Figure 4.5 are affected by scattering events. The first row shows spin-orbit coupling and the second row shows spin-flip scattering. In all cases we have used the same strength, and we see that for higher values of the interface parameter G_φ, the junction is less affected by spin-dependent scatterings. This can be understood since the superconductivity is stronger and hence have higher tolerance towards scattering.

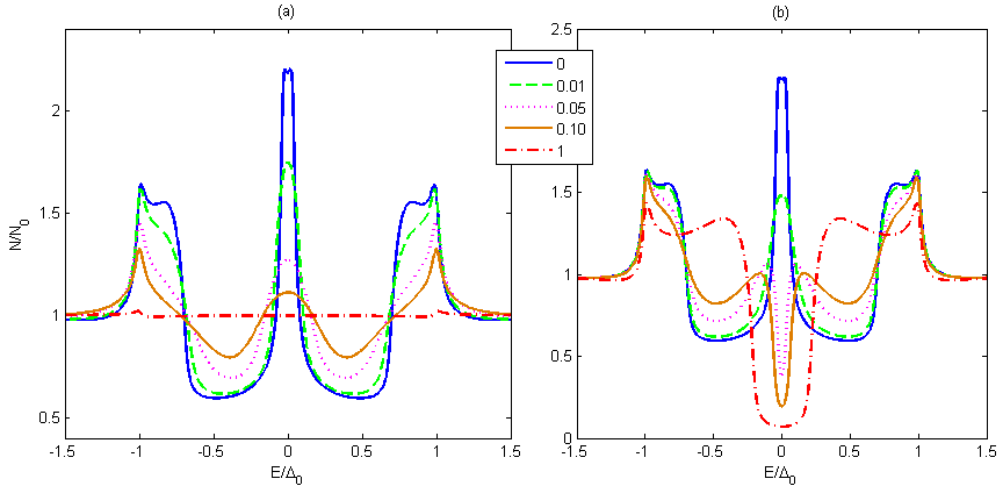

Figure 4.13: Density of states as function of the quasiparticle energy E, with varying contribution of spin-flip scattering in (a) and spin-orbit coupling in (b). the vaulues of $g_{\mathrm{sf,so}}$ are given in the legend. The other parameters are $\ell = 20$ nm, $\xi_S = 30$ nm, $\theta = 0$, $\alpha = 0$, $G_\varphi = 1.1$, $G_{\mathrm{MR}} = 0$, and $\phi = \pi/2$.

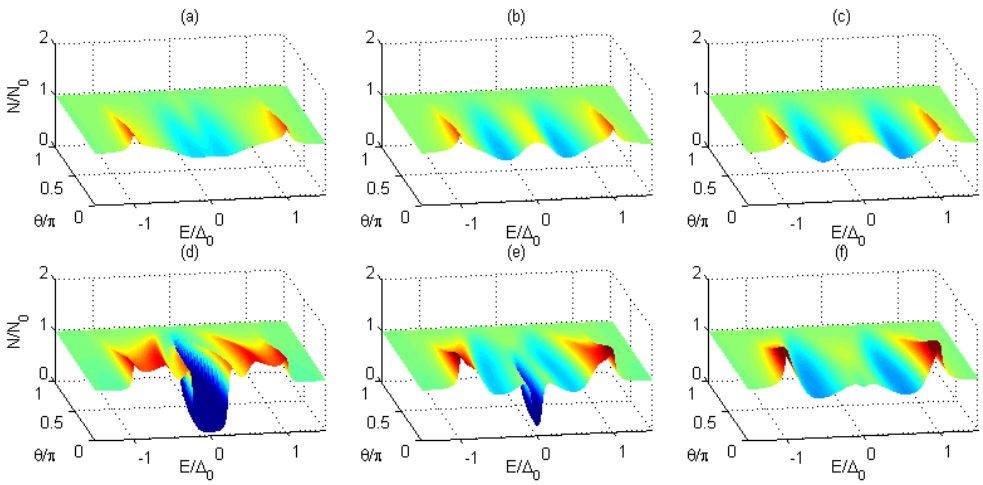

Figure 4.14: Density of states in the plane of quasiparticle energy E and superconducting phase difference θ, with contribution of spin-flip and spin-orbit scattering. In the first row $g_{\mathrm{so}} = 1$ and $g_{\mathrm{sf}} = 0$, and in the second row $g_{\mathrm{so}} = 0$ and $g_{\mathrm{sf}} = 1$. In the first, second, and third column we have the G_φ values 0.5, 1.1 and 1.5 respectivily. We use $\ell = 20$ nm, $\xi_s = 30$ nm, $\alpha = 0$, $\zeta = 4$, $\phi = \pi/2$, and $G_{\mathrm{MR}} = 0$.

4.4 The Inverse Proximity Effect

In real materials, the normal metal properties will to some extent leak into the superconductor, forcing the superconducting correlation to decline near the interface. This correction can be accounted for by solving the Usadel equation not only in the normal metal, but also in the superconductors. Effectively we may consider this scenario as an SS'NS'S junction where the boundary conditions between the S and S' layer are ideal, because they are in fact the same material.

The boundary conditions for ideal interfaces state that the Green function has to be equal at each side of the interface. The Usadel equation will in the superconductors naturally depend on the gap function Δ, and we only use the BCS solution in the uttermost layers and calculate Δ (2.37) in the S' layers. It is important to do this in a self-consistent manner, so that we get the correct solution in the end. We can use the initial guess that Δ equals the BCS solution also in the S' layers and calculate the Green function, which gives us a new Δ. This Δ is used again in the next iteration, until the solution converges. If we for simplicity only want to look at an SN bilayer surrounded by vacuum, we can use the boundary conditions $\partial_x \gamma = 0$ facing the vacuum.

The overall effect of the inverse proximity is that the effective superconducting phase difference θ_{eff}, which is the one measured at the interfaces of the superconductor, is smaller than the actual phase difference θ measured in the bulk of the superconductors [32]. We also get that the magnitude of the superconducting order parameter Δ at the interfaces in the real case is smaller than the bulk magnitude Δ_0, only effecting the results quantitatively and leaving the qualitative findings unaffected.

Chapter 5

Summary and Outlook

We have shown that there exists a dissipationless spin-supercurrent in a spin-active Josephson junction with a normal-metal weak link. This spin-supercurrent is found controllable via the magnetization misalignment angle α of the magnetic insulators, and has a component that is independent of the superconducting phase difference θ. This means that spin-supercurrent is generally present in the absence of phase difference as long as there is a magnetization misalignment. This is in contrast to the charge-supercurrent which is proportional to $\sin\theta$. The charge-current consists of one singlet and one triplet term, and also depend on the relative misalignment angle. The nature of the junction can be controlled both via the misalignment angle and the phase difference externally, showing clear spectroscopic fingerprints for example as a low-energy enhancement in the in the density of state. Changing θ from 0 to π can lead to a change from singlet to triplet proximity effect. Equivalently, the transformation of α from 0 to π leads to a change from triplet to singlet proximity effect.

It has been shown that we can create a 0-π transition by changing the relative magnetization of the two interfaces. This is an effect that is accessible for instance by rotating one layer via a weak applied magnetic field. The transition point is dependent on parameters such as the normal metal length, interface transparency and the spin-dependent interfacial phase shift parameter.

The effect of spin-flip scattering shows a general reduction in the superconducting condensates and thereby the supercurrents, while the effect from spin-orbit coupling destroys the triplet component faster than the singlet, effectively leading to an SNS junction when including strong spin-orbit effects. We shown that the spin-flip scattering reduces the overall supercurrent faster than spin-orbit, and that the spin-current remains independent of position, surprisingly even when including isotropic spin-flip and spin-orbit scattering.

Future Prospects

In this thesis we consider the boundary conditions for weakly polarized interfaces $P_n \ll 1$. However, it would be of great interest to look at the case when having arbitrary polarization. There has recently been developed boundary conditions for exactly this [60], which gives us additional terms to the boundary condition. By extending our calculations, we might get an effect from the polarization in contrast to our findings in this work. It could also be interesting to include more dimensions since we only have solved the Usadel equation in one dimension, while there could be additional transport in other directions too. Then we could look at more complex systems. In addition we could also include the orbital effect from an applied magnetic field since we actually apply weak fields to the spin-active junction in order to control the magnetization directions. Other aspects could be temperature dependence and the effect of an applied bias voltage. It has been predicted that the spin-splitting in the density of state can lead to thermoelectric effect [66, 67].

Bibliography

[1] J. P. Morten, "Spin and Charge Transport in Dirty Superconductors," 2003. Master thesis, NTNU.

[2] G. D. Mahan, *Many-Particle Physics*. Kluwer Academic/Plenum Publishers, 2000.

[3] K. Fossheim and A. Sudbø, *Superconductivity: Physics and Applications*. WILEY, 2004.

[4] J. Linder and J. W. A. Robinson, "Superconducting spintronics," *Nature Physics*, vol. 11, pp. 307–315, 2015.

[5] M. G. Blamire and J. W. A. Robinson, "The interface between superconductivity and magnetism: Understanding and device prospects," *J. Phys. Condens. Matter*, vol. 26, no. 453201, 2014.

[6] F. S. Bergeret, A. F. Volkov, and K. B. Efetov, "Long-range proximity effects in superconductor-ferromagnet structures," *Phys. Rev. Lett.*, vol. 86, no. 18, p. 4096, 2001.

[7] Y. Tanaka and A. A. Golubov, "Theory of the proximity effect in junctions with unconventional superconductors," *Phys. Rev. Lett.*, vol. 98, p. 037003, 2007.

[8] N. Banerjee, C. Smiet, R. Smits, A. Ozaeta, F. Bergeret, M. Blamire, and J. Robinson, "Evidence for spin selectivity of triplet pairs in superconducting spin valves," *Nature Communications*, vol. 5, no. 3048, 2014.

[9] M. Eschrig, "Spin-polarized supercurrents for spintronics," *Physics Today*, vol. 64, no. 1, p. 43, 2011.

[10] F. S. Bergeret, A. F. Volkov, and K. B. Efetov, "Odd triplet superconductivity and related phenomena in superconductor-ferromagnet structures," *Rev. Mod. Phys.*, vol. 77, pp. 1321–1373, 2005.

[11] A. I. Buzdin, "Proximity effects in superconductor-ferromagnet heterostructures," *Rev. Mod. Phys.*, vol. 77, no. 935, 2005.

[12] I. Žutić, J. Fabian, and S. Das Sarma, "Spintronics: Fundamentals and applications," *Rev. Mod. Phys.*, vol. 76, pp. 323–410, 2004.

[13] M. N. Baibich, J. M. Broto, A. Fert, F. N. Van Dau, F. Petroff, P. Eitenne, G. Creuzet, A. Friederich, and J. Chazelas, "Giant magnetoresistance of (001) fe / (001) cr magnetic superlattices," *Phys. Rev. Letters*, vol. 61, no. 21, p. 2472, 1988.

[14] J. Bardeen, L. N. Cooper, and J. R. Schrieffer, "Theory of Superconductivity," *Phys. Rev.*, vol. 108, no. 5, pp. 1175–1204, 1957.

[15] L. N. Cooper, "Bound electron pairs in a degenerate fermi gas," *Phys. Rev.*, vol. 104, pp. 1189–1190, 1956.

[16] W. Meissner and R. Ochsenfeld, "Ein neuer effekt bei eintritt der supraleitfähigkeit," *Die Naturwissenschaften*, vol. 21, no. 44, pp. 787–788, 1933.

[17] S. S. Saxena *et al.*, "Superconductivity at the border of itinerant electron ferromagnetism in uge_2," *Nature (London)*, vol. 406, no. 587, 2000.

[18] D. Aoki and J. Flouquet, "Ferromagnetism and superconductivity in uranium compounds," *J. Phys. Soc. Jpn.*, vol. 81, no. 1, p. 011003, 2012.

[19] P. W. Anderson, "Theory of dirty superconductors," *J. Phys. Chem. Solids*, vol. 11, no. 1-2, pp. 26–30, 1959.

[20] M. Giroud, H. Ciurtois, and K. Hasselbach, "Superconducting proximity effect in a mesoscopic ferromagnetic wire," *Phys. Rev. B*, vol. 58, no. 18, p. 11872, 1998.

[21] V. T. Petrashov, I. A. Sosnin, I. Cox, A. Parsons, and C. Troadec, "Giant mutual proximity effects in ferromagnetic/superconducting nanostructures," *Phys. Rev. Lett.*, vol. 83, pp. 3281–3284, 1999.

[22] R. Keizer, S. Goennenwein, T. Klapwijk, G. Miao, G. Xiao, and A. Gupta, "A spin triplet supercurrent through the half-metallic ferromagnet cro 2," *Nature*, vol. 439, no. 7078, pp. 825–827, 2006.

[23] V. L. Berezinskii, "New model of the anisotropic phase of superfluid He3," *JETP Lett.*, vol. 20, no. 9, pp. 287–289, 1974.

[24] A. A. Golubov, Y. Tanaka, Y. Asano, Y. Tanuma, "Odd-frequency pairing in superconducting heterostructures," *J. Phys. Condens. Matter*, vol. 21, no. 164208, 2009.

[25] J. W. A. Robinson, J. D. S. Witt, and M. G. Blamire, "Controlled injection of spin-triplet supercurrents into a strong ferromagnet," *Science*, vol. 329, no. 59, 2010.

[26] T. Khaire, M. A. Khasawneh, W. P. Pratt Jr., and N. Birge, "Observation of spin-triplet superconductivity in co-based Josephson junctions," *Phys. Rev. Lett.*, vol. 104, no. 137002, 2010.

[27] M. Eschrig, J. Kopu, J. C. Cuevas, and G. Schön, "Theory of half-metal superconductor heterostructures," *Phys. Rev. Lett.*, vol. 90, no. 137003, 2003.

[28] T. Yokoyama, Y. Tanaka, and A. A. Golubov, "Manifestation of the odd-frequency spin-triplet pairing state in diffusive ferromagnet/superconductor junctions," *Phys. Rev. B*, vol. 75, p. 134510.

[29] P. Kostić, B. Veal, A. P. Paulikas, U. Welp, V. R. Todt, C. Gu, U. Geiser, J. M. Williams, K. D. Carlson, and R. A. Klemm, "Paramagnetic meissner effect in nb," *Phys. Rev. B*, vol. 53, pp. 791–801, 1996.

[30] N. Levy, T. Zhang, J. Ha, F. Sharifi, A. A. Talin, Y. Kuk, and J. A. Stroscio, "Experimental evidence for s-wave pairing symmetry in superconducting $\mathrm{cu}_x\mathrm{bi}_2\mathrm{se}_3$ single crystals using a scanning tunneling microscope," *Phys. Rev. Lett.*, vol. 110, p. 117001, 2013.

[31] Meissner, H., "Superconductivity of contacts with interposed barriers," *Phys. Rev.*, vol. 117, pp. 672–680, 1960.

[32] P. G. de Gennes, "Boundary effects in superconductors," *Rev. Mod. Phys.*, vol. 36, no. 225, 1964.

[33] A. F. Andreev, "The thermal conductivity of the intermediate state in superconductors," *Soviet Physics JETP-USSR*, vol. 19, pp. 1228–1231, 1964.

[34] B. D. Josephson, "Possible new effects in superconductive tunnelling," *Physics Letters*, vol. 1, no. 7, pp. 251 – 253, 1962.

[35] B. D. Josephson, "Coupled superconductors," *Rev. Mod. Phys.*, vol. 36, pp. 216–220, 1964.

[36] L. Trifunovic, "Long-range superharmonic Josephson current," *Phys. Rev. Lett.*, vol. 107, no. 047001, 2011.

[37] A. Pal, Z. H. Barber, J. W. A. Robinson, and M. G. Blamire, "Pure second harmonic current-phase relation in spin-filter Josephson junctions," *Nature Communications*, vol. 5, no. 3340, 2014.

[38] H. Sellier, C. Baraduc, F. m. c. Lefloch, and R. Calemczuk, "Half-integer shapiro steps at the 0-π crossover of a ferromagnetic josephson junction," *Phys. Rev. Lett.*, vol. 92, p. 257005, 2004.

[39] H. le Sueur, P. Joyez, H. Pothier, C. Urbina, and D. Esteve, "Phase controlled superconducting proximity effect probed by tunneling spectroscopy," *Phys. Rev. Lett.*, vol. 100, no. 197002, 2008.

[40] B. Li *et al.*, "Superconducting spin switch with infinite magnetoresistance induced by an internal exchange field," *Phys. Rev. Lett.*, vol. 110, no. 097001, 2013.

[41] J. W. Serene and D. Rainer, "The quasiclassical approach to superfluid ^{3}he," *Phys. Rep.*, vol. 101, no. 221, 1983.

[42] J. Rammer and H. Smith, "Quantum field-theoretical methods in transport theory of metals," *Rev. Mod. Phys.*, vol. 58, no. 323, 1986.

[43] V. Chandrasekhar, "An introduction to the quasiclassical theory of superconductivity for diffusive proximity-coupled systems," *arXiv:cond-mat/0312507*, 2008.

[44] P. Dubos, H. Courtois, B. Pannetier, F. K. Wilhelm, A. D. Zaikin, and G. Schön, "Josephson critical current in a long mesoscopic S-N-S junction," *Phys. Rev. B*, vol. 63, p. 064502, 2001.

[45] S. V. Bakurskiy, N. V. Klenov, I. I. Soloviev, V. V. Bol'ginov, V. V. Ryazanov, I. V. Vernik, O. A. Mukhanov, M. Yu. Kupriyanov, and A. A. Golubov, "Theoretical model of superconducting spintronic SIsFS devices," *Appl. Phys. Lett.*, vol. 102, no. 192603, 2013.

[46] G. Eilenberger, "Transformation of Gorkov's equation for type II superconductors into transport-like equations," *Zeitschrift für Physik*, vol. 214, no. 2, pp. 195–213, 1968.

[47] A. I. Larkin and Y. N. Ovchinnikov, "Quasiclssical method in the theory of superconductivity," *Sov. Phys. JETP*, vol. 28, p. 1200, 1968.

[48] K. D. Usadel, "Generalized diffusion equation for superconducting alloys," *Phys. Rev. Lett.*, vol. 25, no. 8, pp. 507–509, 1970.

[49] J. P. Morten and A. Brataas, and W. Belzig, "Spin transport and magnetoresistance in ferromagnet/superconductor/ferromagnet spin valves," *Phys. Rev. B*, vol. 72, no. 014510, 2005.

[50] N. Schopohl and K. Maki, "Quasiparticle spectrum around a vortex line in a d-wave superconductor," *Phys. Rev. B*, vol. 52, no. 1, pp. 490–493, 1995.

[51] N. Schopohl, "Transformation of the Eilenberger Equations of Superconductivity to a Scalar Riccati Equation," *arXiv:cond-mat/9804064*, 1998.

[52] I. Gomperud, "Introduction to odd-frequency superconductivity in Josephson juncions with spin-active interfaces." Project thesis NTNU, fall 2014.

[53] A. Cottet, D. Huertas-Hernando, W. Belzig, and Y. V. Nazarov, "Spin-dependent boundary conditions for isotropic superconducting Green's functions," *Phys. Rev. B*, vol. 80, no. 184511, 2009.

[54] M. Y. Kupriyanov and V. F. Lukichev, "Influence of boundary transparency on the critical current of "dirty" ss's structures," *Sov. Phys. JETP*, vol. 67, pp. 1163–1168, 1988.

[55] Y. V. Nazarov, "Novel circuit theory of Andreev reflection," *Superlatt. Microstruct.*, vol. 25, no. 5, pp. 1221–1231, 1999. cited By 170.

[56] M. S. Kalenkov, A. V. Galaktionov, and A. D. Zaikin, "Josephson current in ballistic heterostructures with spin-active interfaces," *Phys. Rev. B*, vol. 79, no. 014521, 2009.

[57] A. Moor, A. Volkov, and K. B. Efetov, "Spin current in junctions composed of multi-band superconductors with a spin-density wave," *Supercond. Sci. Technol.*, vol. 28, no. 025011, 2015.

[58] E. Kreyszig, *Advanced Engineering Mathematics*. WILEY, 9th ed., 2006.

[59] J. C. Hammer, C. C., F. S. Bergeret, and W. Belzig, "Density of states and supercurrent in diffusive sns junctions: Roles of nonideal interfaces and spin-slip scattering and spin-flip scattering," *Phys. Rev. B*, vol. 76, no. 064514, 2007.

[60] M. Eschrig *et al.*, "General boundary conditions for quasiclassical theory of superconductivity in the diffusive limit: Application to strongly spin-polarized systems," *arXiv:1504.06258*, 2015.

[61] S. Kawabata, Y. Asano, Y. Tanaka, A. A. Golubov, "Robustness of spin-triplet pairing and singlet-triplet pairing crossover in superconductor/ferromagnet hybrids," *J. Phys. Soc. Jpn.*, vol. 82, no. 124702, 2013.

[62] J. Linder, A. Sudbø, T. Yokoyama, R. Grein, and M. Eschrig, "Signature of odd-frequency pairing correlations induced by a magnetic interface," *Phys. Rev. B*, vol. 81, no. 214504, 2010.

[63] J. Linder and T. Yokoyama, "Spin current in generic hybrid structures due to interfacial spin-orbit scattering," *Phys. Rev. Lett.*, vol. 106, no. 237201, 2011.

[64] K. Sun and N. Shah, "General framework for transport in spin-orbit-coupled superconducting heterostructures: Nonuniform spin-orbit coupling and spin-orbit-active interfaces," *Phys. Rev. B*, vol. 91, p. 144508, 2015.

[65] J. Linder, T. Yokoyama, and A. Sudbø, "Role of interface transparency and spin-dependent scattering in diffusive ferromagnet/superconductor heterostructures," *Phys. Rev. B*, vol. 77, no. 174514, 2008.

[66] P. Machon, M. Eschrig, and W. Belzig, "Nonlocal thermoelectric effects and nonlocal onsager relations in a three-terminal proximity-coupled superconductor-ferromagnet device," *Phys. Rev. Lett.*, vol. 110, p. 047002, 2013.

[67] M. S. Kalenkov and A. D. Zaikin, "Electron-hole imbalance and large thermoelectric effect in superconducting hybrids with spin-active interfaces," *Phys. Rev. B*, vol. 90, p. 134502, 2014.

Appendix A

Pauli Matrices

The identity matrix and the 2x2-Pauli matrices are given by

$$\sigma_x = \begin{pmatrix} 0 & 1 \\ 1 & 0 \end{pmatrix}, \quad \sigma_y = \begin{pmatrix} 0 & -i \\ i & 0 \end{pmatrix}, \quad \sigma_z = \begin{pmatrix} 1 & 0 \\ 0 & -1 \end{pmatrix}. \tag{A.1}$$

These are all matrices in spin-space. The Pauli matrices in particle-hole space are denoted ρ_i with $i = 1, 2, 3$, and are defined by:

$$\hat{\rho}_1 = \begin{pmatrix} 0 & \sigma_x \\ \sigma_x & 0 \end{pmatrix}, \quad \hat{\rho}_2 = \begin{pmatrix} 0 & -i\sigma_x \\ i\sigma_x & 0 \end{pmatrix}, \quad \hat{\rho}_3 = \begin{pmatrix} \sigma_0 & 0 \\ 0 & -\sigma_0 \end{pmatrix}. \tag{A.2}$$

We have also used the matrices:

$$\hat{\tau}_i = \begin{pmatrix} \sigma_i \nu & 0 \\ 0 & \sigma_\nu^* \end{pmatrix}, \quad \hat{\boldsymbol{\tau}} = \begin{pmatrix} \boldsymbol{\sigma} & 0 \\ 0 & \boldsymbol{\sigma}^* \end{pmatrix}, \quad \boldsymbol{\sigma} = (\sigma_x, \sigma_y, \sigma_z). \tag{A.3}$$

where we have $\nu = x, y, z$. When matrices of different size are present in the same expression it is implied that the smallest matrix should be expanded on the diagonal, so that $\sigma_\nu \hat{\rho}_i = \mathrm{diag}(\sigma_\nu, \sigma_\nu)\hat{\rho}_i$. This also goes for the adding of a scalar constant to the matrix. Then the constant is regarded as accompanied by a unit vector of the size of the matrix.

When we write $\mathrm{diag}(\cdots)$ it means that these are the elements on the diagonal of an empty matrix, such that $\sigma_z = \mathrm{diag}(1, -1)$, and we also use $\sigma_y = \mathrm{offdiag}(i, -i)$.

Appendix B

Green Functions and Keldysh Formalism

The quasiclassical 8x8-Keldysh Green function is a matrix in spin⊗particle-hole⊗Keldysh-space:

$$\check{g} = \begin{pmatrix} \hat{g}^{\mathrm{R}} & \hat{g}^{\mathrm{K}} \\ 0 & \hat{g}^{\mathrm{A}} \end{pmatrix}. \tag{B.1}$$

The quasiclassical retarded Green function $\hat{g}^{\mathrm{R}}$ originates from the normal retarded Green function

$$\hat{G}^{\mathrm{R}} = -i\Theta(t_1 - t_2) \left\langle [\psi(\boldsymbol{r}_1, t_1), \psi^{\dagger}(\boldsymbol{r}_2, t_2)] \right\rangle, \tag{B.2}$$

where we have $\psi(\boldsymbol{r}, t) = \Big(\psi_{\uparrow}(\boldsymbol{r}, t), \psi_{\downarrow}(\boldsymbol{r}, t), \psi^{\dagger}_{\uparrow}(\boldsymbol{r}, t), \psi^{\dagger}_{\downarrow}(\boldsymbol{r}, t)\Big)^{\mathrm{T}}$. The $\dagger$ means complex conjugate and taking the transvers (T), and is called the Hermitian conjugate. The arrows denote the spin configuration, $\psi_{\uparrow}(\boldsymbol{r}, t)$ is the annihilation operator for spin up and $\psi^{\dagger}_{\uparrow}(\boldsymbol{r}, t)$ is the creation operator for spin up. We use the $\langle \cdots \rangle$ to denote the average value. To get the quasiclassical retarded Green function, we first integrate out the relative oscillations by use of the mixed representation, and then we integrating over the energy $\xi_{\boldsymbol{p}} = \boldsymbol{p}^2/2m$

$$\hat{g}^{\mathrm{R}} = \frac{i}{\pi} \int_{-\infty}^{\infty} \mathrm{d}\xi_{\boldsymbol{p}} \hat{G}^{\mathrm{R}}. \tag{B.3}$$

This approximation is excepted since the Green function mostly has values around the Fermi momentum.

The advanced and Keldysh Green functions can be constructed from the retarded via:

$$\hat{g}^{\mathrm{A}} = -\left[\hat{\rho}_3 \hat{g}^{\mathrm{R}} \hat{\rho}_3\right]^{\dagger}, \quad \hat{g}^{\mathrm{K}} = \hat{g}^{\mathrm{R}} \hat{h} - \hat{h} \hat{g}^{\mathrm{A}} \tag{B.4}$$

and in equilibrium we have that $\hat{h} = \tanh(\beta E/2)$.

When parameterizing the retarded Green function as

$$\hat{g}^{\mathrm{R}} = \begin{pmatrix} g & f \\ -\tilde{f} & -\tilde{g} \end{pmatrix}, \tag{B.5}$$

we get from these definitions that

$$\hat{g}^{\mathrm{A}} = -\begin{pmatrix} g^{\dagger} & \tilde{f}^{\dagger} \\ -f^{\dagger} & -\tilde{g}^{\dagger} \end{pmatrix}, \tag{B.6}$$

$$\hat{g}^{\mathrm{K}} = \begin{pmatrix} g + g^{\dagger} & f + \tilde{f}^{\dagger} \\ -(\tilde{f} + f^{\dagger}) & -(\tilde{g} + \tilde{g}^{\dagger}) \end{pmatrix} \tanh\left(\frac{\beta E}{2}\right). \tag{B.7}$$

Appendix C

MATLAB-script

Here we include some of the MATLAB scripts that are used. These are examples of the ones that include spin-flip and spin-orbit scattering. We can set the scattering strength to zero, if we want to disregard these effects. When actually preforming the simulation it will be time-saving to remove terms that are not in use, such as all terms for G_{MR}, when it is set to zero.

First we present the function that solves the gamma-matrices inside the normal metal. Here we make use of the MATLAB function bcp4c, which is especially useful when solving coupled differential equations with boundary conditions. Note that we have the matrix

$$v = \begin{pmatrix} \gamma \\ \tilde{\gamma} \\ \partial_x \gamma \\ \partial_x \tilde{\gamma} \end{pmatrix} \tag{C.1}$$

but since the program need the result to be on vector form, we define `y=v(:)` which means a vector where the columns are placed after each other.

$$y = (\gamma_{11}, \gamma_{21}, \tilde{\gamma}_{11}, \tilde{\gamma}_{21}, \partial_x\gamma_{11}, \partial_x\gamma_{21}, \partial_x\tilde{\gamma}_{11}, \partial_x\tilde{\gamma}_{21}, \gamma_{12}, \gamma_{22}, \tilde{\gamma}_{12}, \tilde{\gamma}_{22}, \partial_x\gamma_{12}, \partial_x\gamma_{22}, \partial_x\tilde{\gamma}_{12}, \partial_x\tilde{\gamma}_{22}) \tag{C.2}$$

The function myBvpSpinActiveSO

```
% The function myBvpSpinActive solves the Usadel equation in the
% normal metal of a spin-active SNS junction for the gamma-matrices
% given by the Riccati parameterization.

function y=myBvpSpinActive(e,a,d,eT,n,y0,z1,z2,Gp1,Gp2,Gm1,Gm2,so,sf)
% We use global parameters to get the same values in all
% underlying functions
```

```
8
9  global E        % Quasiparticle energy in the Usadel equation
10 global alpha    % Angle from the z-axis of m1 (left)
11 global phase    % Superconducting phase difference
12 global Et       % Thouless energy in the normal metal
13 global N        % Number of evaluated points at the x-axis
14 global yInit    % Previous solution of y
15 global zeta1    % R_Barrier/R_N left interface
16 global zeta2    %       ""
17 global Gphi1    % Relative conductance G_phi1/G_T.
18 global Gphi2    %       ""
19 global Gmr1     % Relative conductance G_mr1/G_T.
20 global Gmr2     %       ""
21 global SO       % Spin-orbit: g_so = 1/8*Delta*tau_so
22 global SF       % Spin-flip:  g_sf = 1/8*Delta*tau_sf
23
24 global Theta    % f_BCS = sinh(Theta)
25 global m1       % Magnetization direction left
26 global m2       %       ""
27
28 %% And here we give the global parameters values from the intake:
29 E     = e;
30 alpha = a;
31 phase = d;
32 Et    = eT;
33 N     = n;
34 yInit = y0;
35 zeta1 = z1;
36 zeta2 = z2;
37 Gphi1 = Gp1;
38 Gphi2 = Gp2;
39 Gmr1  = Gm1;
40 Gmr2  = Gm2;
41 SO    = so;
42 SF    = sf;
43
44 Theta = atanh(1/E);
45 %phi = pi/4;  % We use phi together with the alternative
46               % to m1 below, if we want the azimuth
47               % angle to be different from pi half.
48 m1    = [0 sin(alpha) cos(alpha)]; %...
49               % [sin(alpha)*cos(phi) sin(alpha)*sin(phi) cos(alpha)];
50 m2    = [0 0 1];
51
52 %% Here the main code is given:
53 x = linspace(0,1,N);
54 solinit = bvpinit(x,@myInit);
55 options = bvpset('Stats','{off}','RelTol',1e-6);
56 sol = bvp4c(@myOde,@myBc,solinit,options);
```

```
y = deval(sol,x);

% For these lines to work we need to make three functions within this
% main function. The first solves the ordinary differential eq.,
% the next contains the boundary conditions and the last gives an
% initial guess on the solution.

function dydx = myOde(~,y)
global E
global Et
global SO
global SF

% In accordance with the definition of y we have:
gam   =  [y(1) y(9); y(2) y(10)];
gamt  =  [y(3) y(11); y(4) y(12)];
dgam  =  [y(5) y(13); y(6) y(14)];
dgamt =  [y(7) y(15); y(8) y(16)];

N = (eye(2)/(eye(2)-gam*gamt));
Nt= (eye(2)/(eye(2)-gamt*gam));

% Via the Riccati parameterization we get Green function,
% the anomalous Green function and their tilded versions.
g  = N*(eye(2)+gam*gamt) ;
f  = 2*N*gam;
gt = Nt*(eye(2)+gamt*gam);
ft = 2*Nt*gamt;

% We define the Pauli matrices:
tau1 = [0,1;1,0];
tau2 = [0,-1i;1i,0];
tau3 = [1,0;0,-1];

a = E*eye(2)  + 1i*(SF+SO)*(tau1*g*tau1 + tau2*g*tau2 + tau3*g*tau3);
b =           + 1i*(SF-SO)*(tau1*f*tau1 - tau2*f*tau2 + tau3*f*tau3);
c =           - 1i*(SF-SO)*(tau1*ft*tau1 - tau2*ft*tau2 + tau3*ft*tau3);
d = -E*eye(2) - 1i*(SF+SO)*(tau1*gt*tau1 + tau2*gt*tau2 + tau3*gt*tau3);

% Keep in mind that
% dv/dx = [dx(gamma); dx(gamma-tilde); dx^2(gamma); dx^2(gamme-tilde)]

dvdx = [dgam;
        dgamt;
     -2*dgam*gamt*N*dgam - (1i/Et)*(a*gam - gam*d + gam*c*gam - b);
     -2*dgamt*N*gam*dgamt + (1i/Et)*(d*gamt - gamt*a + gamt*b*gamt - c);];
dydx = dvdx(:);

% Now, we turn to the boundary conditions
```

```
function res = myBc(ya,yb)
global phase
global zeta1
global zeta2
global Gphi1
global Gphi2
global Gmr1
global Gmr2
global Theta
global m1
global m2

% ya equals the solution on the left side (x=0) in the normal metal
% and similarly, yb if the solution on the right side (x = \ell)

agam    = [ya(1), ya(9); ya(2), ya(10)];
agamt   = [ya(3), ya(11); ya(4), ya(12)];
adgam   = [ya(5), ya(13); ya(6), ya(14)];
adgamt  = [ya(7), ya(15); ya(8), ya(16)];

bgam    = [yb(1) yb(9); yb(2) yb(10)];
bgamt   = [yb(3) yb(11); yb(4) yb(12)];
bdgam   = [yb(5) yb(13); yb(6) yb(14)];
bdgamt  = [yb(7) yb(15); yb(8) yb(16)];

Na  = eye(2)/(eye(2)-agam*agamt);
Nb  = eye(2)/(eye(2)-bgam*bgamt);
Nat = eye(2)/(eye(2)-agamt*agam);
Nbt = eye(2)/(eye(2)-bgamt*bgam);

% We define the matrix i*tau_y = itau2
% to make the code easier to read.
itau2 = [0,1;-1,0];

% The solution on the superconducting
% side of the interface is given by:
gBCS    = eye(2)*cosh(Theta);              % Same on R and L.
afBCS   = itau2*sinh(Theta);               % phase_L = 0
bfBCS   = itau2*sinh(Theta)*exp(1i*phase); % phase_R = phase

gBCSt   = eye(2)*cosh(Theta);
afBCSt  = -itau2*sinh(Theta);
bfBCSt  = -itau2*sinh(Theta)*exp(-1i*phase);

ag  = Na*(eye(2)+agam*agamt);
af  = 2*Na*agam;
bg  = Nb*(eye(2)+bgam*bgamt);
bf  = 2*Nb*bgam;
```

```
agt = Nat*(eye(2)+agamt*agam);
aft = 2*Nat*agamt;
bgt = Nbt*(eye(2)+bgamt*bgam);
bft = 2*Nbt*bgamt;

% First we have the normal KL boundary conditions
KLa = (eye(2)-agam*agamt)*(gBCS*af - afBCS*agt - ag*afBCS...
    + af*gBCSt - (gBCS*ag - afBCS*aft - ag*gBCS + af*afBCSt)*agam);
KLb = (eye(2)-bgam*bgamt)*(gBCS*bf - bfBCS*bgt - bg*bfBCS...
    + bf*gBCSt - (gBCS*bg - bfBCS*bft - bg*gBCS + bf*bfBCSt)*bgam);
KLat = (eye(2)-agamt*agam)*(gBCSt*aft - afBCSt*ag - agt*afBCSt...
    + aft*gBCS - (gBCSt*agt - afBCSt*af - agt*gBCSt + aft*afBCS)*agamt);
KLbt = (eye(2)-bgamt*bgam)*(gBCSt*bft - bfBCSt*bg - bgt*bfBCSt...
    + bft*gBCS - (gBCSt*bgt - bfBCSt*bf - bgt*gBCSt + bft*bfBCS)*bgamt);

% Then we have the spin-active boundary conditions where we need
% Ma = (m_vec*tau_vec) for x = 0 and Mb = (m_vec*tau_vec) for x = L
Ma = [m1(3), (m1(1) - 1i*m1(2));(m1(1) + 1i*m1(2)), -m1(3)];
Mb = [m2(3), (m2(1) - 1i*m2(2));(m2(1) + 1i*m2(2)), -m2(3)];

% For the spin-dependent phase shift we have:
PHIa  = 2*1i*Gphi1*(agam*conj(Ma) - Ma*agam);
PHIb  = 2*1i*Gphi2*(bgam*conj(Mb) - Mb*bgam);
PHIat = 2*1i*Gphi1*(agamt*Ma - conj(Ma)*agamt);
PHIbt = 2*1i*Gphi2*(bgamt*Mb - conj(Mb)*bgamt);

% And for the spin polarization we have:
a1 = gBCS*Ma + Ma*gBCS;
b1 = afBCS*conj(Ma) + Ma*afBCS;
c1 = -afBCSt*Ma - conj(Ma)*afBCSt;
d1 = -gBCSt*conj(Ma) - conj(Ma)*gBCSt;

a2 = gBCS*Mb + Mb*gBCS;
b2 = bfBCS*conj(Mb) + Mb*bfBCS;
c2 = -bfBCSt*Mb - conj(Mb)*bfBCSt;
d2 = -gBCSt*conj(Mb) - conj(Mb)*gBCSt;

% where we have defined {diag(Ma,Ma*),g_BCS} = [a1, b1 ;c1, d1].

MRa  = 2*Gmr1*(a1*agam - agam*d1 + agam*c1*agam - b1);
MRb  = 2*Gmr2*(a2*bgam - bgam*d2 + bgam*c2*bgam - b2);
MRat = 2*Gmr1*(d1*agamt - agamt*a1 + agamt*b1*agamt - c1);
MRbt = 2*Gmr2*(d2*bgamt - bgamt*a2 + bgamt*b2*bgamt - c2);

% This function treats the conditions in a vector that should be zero
% and we write the total boundary conditions first as a matrix:
% res = 0
res = [4*zeta1*adgam - KLa + PHIa - MRa;
```

```
        4*zeta2*bdgam + KLb - PHIb + MRb;
        4*zeta1*adgamt - KLat - PHIat + MRat;
        4*zeta2*bdgamt + KLbt + PHIbt - MRbt;];

% and then as a vector:
res = res(:);


% The last initial guess function only takes in a predefined
% number of points along the x-axis, which is the same number
% of x- positions as the initial y-solution gives. Then we only need
% to match the positions x to the rigth y.

function y = myInit(x)
global yInit
global N

xvec = linspace(0,1,N);
for i = 1:N
    if x == xvec(i)
        y = yInit(:,i);
    end
end
```

Now we also include two scripts showing how to obtain the spin-supercurrents and the density of states by using the function above.

Supercurrents

```

Evec = -3:0.001:0;            % Energy/Delta_0 Alternativ 1

%Evec1= -3:0.02:-1.5;
%Evec2= -1.499:0.001:1.499;
%Evec3= 1.5:0.02:3;
%Evec = [Evec1 Evec2 Evec3];  % Alternativ 2

disp('Size of Evec: ')
disp(size(Evec))

d = 2e-2;                   % Inelastic scattering (finite lifetime)
ToverTc = 0.02;             % Temperature in critical temperature
beta = 1.76/ToverTc;        % Delta/(kB*T) = 1.76*Tc/T
aVec = linspace(0,pi,39);   % Angle between m1 og m2 (alpha).
p = pi/2;                   % Phase difference.
xi = 30e-9;                 % Superconducting coherence length (e-9=nm)
L = 10e-9;                  % Length of normal metal (e-9=nm).
eT = (xi/L)^2;              % Thouless energy per Delta: E_T/Delta_0.
```

```
n = 20;                     % Length of x-vector
Gp1 = 4;
Gp2 = 4;
z1 = 5;                     % R_Barrier/R_N (left).
z2 = 5;                     % R_Barrier/R_N (right).
Gm1 = 0;
Gm2 = 0;
soV = [0 1 2 5 10 20];      %i/(8*tau_sf)
sfV = [0 0 0 0 0 0];        %i/(8*tau_so)
for m = 1:length(soV)
 disp(['m = ' num2str(m)])
  so = soV(m);
  sf = sfV(m);
  currQ = zeros(1,length(aVec)); % Charge-supercurrent Iq.
  currX = zeros(1,length(aVec)); % Spin-supercurrent Ix
  currY = zeros(1,length(aVec)); % Spin-supercurrent Iy
  currZ = zeros(1,length(aVec)); % Spin-supercurrent Iz

  currQt = zeros(1,length(aVec));% triplet component of Iq
  currQs = zeros(1,length(aVec));% singlet
  currQu = zeros(1,length(aVec));% up up
  currQd = zeros(1,length(aVec));% down down
  for j = 1:length(aVec)
   a = aVec(j);
   % To monitor our progress, we write.
   disp(['alpha nr. ' num2str(j) '/' num2str(length(aVec))])
   dcurrQ = zeros(1,length(Evec));
   dcurrX = zeros(1,length(Evec));
   dcurrY = zeros(1,length(Evec));
   dcurrZ = zeros(1,length(Evec));

   dcurrQt = zeros(1,length(Evec));
   dcurrQs = zeros(1,length(Evec));
   dcurrQu = zeros(1,length(Evec));
   dcurrQd = zeros(1,length(Evec));
   % For the first energy, we use the trivial
   % zero matrix as the initial solution.
   y = zeros(16,n);
   for i = 1:length(Evec)
    e = Evec(i)+d*1i;
    y = myBvpSpinActive(e,a,p,eT,n,y,z1,z2,Gp1,Gp2,Gm1,Gm2,so,sf);
    s = size(y);
    k = round(s(2)/2);  % Evaluates in the middle of N.

    gam   = [y(1,k) y(9,k); y(2,k) y(10,k)];
    gamt  = [y(3,k) y(11,k); y(4,k) y(12,k)];
    dgam  = [y(5,k) y(13,k); y(6,k) y(14,k)];
    dgamt = [y(7,k) y(15,k); y(8,k) y(16,k)];

```

```
    D  = dgam*gamt + gam*dgamt;
    N  = eye(2)/(eye(2) - gam*gamt);

    g   = N*(eye(2) + gam*gamt);
    dg  = 2*N*D*N;
    f   = 2*N*gam;
    df  = 2*(N*D*N*gam + N*dgam);
    ft  = 2*gamt*N;
    dft = 2*(dgamt*N + gamt*N*D*N);

    % Alternative 1: Integrate from 0 to inf.
    dcurrQ(i) = 4*real(-f(1,1)*dft(1,1) + ft(1,1)*df(1,1)...
     - f(1,2)*dft(2,1) + ft(1,2)*df(2,1) - f(2,1)*dft(1,2)...
     + ft(2,1)*df(1,2) - f(2,2)*dft(2,2)...
     + ft(2,2)*df(2,2) )*tanh(beta*(e-d*1i)/2);

    dcurrX(i) = 4*real(-(f(1,1)+f(2,2))*0.5*(dft(1,2)+dft(2,1))...
     + (ft(1,1)+ft(2,2))*0.5*(df(1,2)+df(2,1))...
     - 0.5*(f(1,2)+f(2,1))*(dft(1,1)+dft(2,2))...
     + 0.5*(ft(1,2)+ft(2,1))*(df(1,1)+df(2,2)))*tanh(beta*(e-d*1i)/2);

    dcurrY(i) = 4*imag((f(1,1)-f(2,2))*0.5*(dft(1,2)+dft(2,1))...
     + (ft(1,1)-ft(2,2))*0.5*(df(1,2)+df(2,1))...
     - 0.5*(f(1,2)+f(2,1))*(dft(1,1)-dft(2,2))...
     - 0.5*(ft(1,2)+ft(2,1))*(df(1,1)-df(2,2)) )*tanh(beta*(e-d*1i)/2);

    dcurrZ(i) = 4*real(- f(1,1)*dft(1,1) + ft(1,1)*df(1,1)...
     + f(2,2)*dft(2,2) - ft(2,2)*df(2,2) )*tanh(beta*(e-d*1i)/2);

    dcurrQt(i) = 4*real(- 0.5*(f(1,2)+f(2,1))*(dft(1,2)+dft(2,1))...
     + 0.5*(ft(1,2)+ft(2,1))*(df(1,2)+df(2,1)))*tanh(beta*(e-d*1i)/2);

    dcurrQs(i) = 4*real( + 0.5*(f(1,2)-f(2,1))*(dft(1,2)-dft(2,1))...
     - 0.5*(ft(1,2)-ft(2,1))*(df(1,2)-df(2,1)) )*tanh(beta*(e-d*1i)/2);

    dcurrQu(i) = 4*real(-f(1,1)*dft(1,1)...
     + ft(1,1)*df(1,1))*tanh(beta*(e-d*1i)/2);

    dcurrQd(i) = 4*real(-f(2,2)*dft(2,2)...
     + ft(2,2)*df(2,2))*tanh(beta*(e-d*1i)/2);

    dcurrX(i)=dcurrX(i) + 4*real((g(1,1)-g(2,2))*(dg(1,2)-dg(2,1))...
     - (g(1,2)-g(2,1))*(dg(1,1)-dg(2,2)))*tanh(beta*(e-d*1i)/2);

    dcurrY(i)=dcurrY(i) - 4*imag((g(1,1)+g(2,2))*(dg(1,2)+dg(2,1))...
     + (g(1,2)+g(2,1))*(dg(1,1)+dg(2,2)))*tanh(beta*(e-d*1i)/2));

    dcurrZ(i) = 8*real(g(1,2)*dg(2,1)...
     -g(2,1)*dg(1,2))*tanh(beta*(e-d*1i)/2);
```

```
    %  Alternativ 2: Integrate from -inf to inf.
%   A =   (g*dg - ctranspose(dg*g)) - (f*dft - ctranspose(df*ft));
%   dcurrQ(i) =  2*real(A(1,1)+A(2,2))*tanh(beta*(e-d*1i)/2);
%   dcurrX(i) =  2*real(A(1,2)+A(2,1))*tanh(beta*(e-d*1i)/2);
%   dcurrY(i) = -2*imag(A(1,2)-A(2,1))*tanh(beta*(e-d*1i)/2);
%   dcurrZ(i) =  2*real(A(1,1)-A(2,2))*tanh(beta*(e-d*1i)/2);
%
%   dcurrQt(i) = 2*real(-0.5*(f(1,2)+f(2,1))*(dft(1,2)+dft(2,1))...
%    + 0.5*(ft(1,2)+ft(2,1))*(df(1,2)+df(2,1)))*tanh(beta*(e-d*1i)/2);
%   dcurrQs(i) = 2*real(0.5*(f(1,2)-f(2,1))*(dft(1,2)-dft(2,1))
%    - 0.5*(ft(1,2)-ft(2,1))*(df(1,2)-df(2,1)) )*tanh(beta*(e-d*1i)/2);
%   dcurrQu(i) = 2*real(-f(1,1)*dft(1,1)...
%    + ft(1,1)*df(1,1))*tanh(beta*(e-d*1i)/2);
%   dcurrQd(i) = 2*real(-f(2,2)*dft(2,2)...
%    + ft(2,2)*df(2,2))*tanh(beta*(e-d*1i)/2);
   end

   % We integrate over energy with the trapeze-method.
   for i = 1:length(Evec)-1
    currQ(j)= currQ(j)...
     + 0.5*(dcurrQ(i) + dcurrQ(i+1))*(Evec(i+1)-Evec(i));
    currX(j) = currX(j)...
     + 0.5*(dcurrX(i) + dcurrX(i+1))*(Evec(i+1)-Evec(i));
    currY(j) = currY(j)...
     + 0.5*(dcurrY(i) + dcurrY(i+1))*(Evec(i+1)-Evec(i));
    currZ(j) = currZ(j)...
     + 0.5*(dcurrZ(i) + dcurrZ(i+1))*(Evec(i+1)-Evec(i));

    currQs(j) = currQs(j)...
     + 0.5*(dcurrQs(i) + dcurrQs(i+1))*(Evec(i+1)-Evec(i));
    currQt(j) = currQt(j)...
     + 0.5*(dcurrQt(i) + dcurrQt(i+1))*(Evec(i+1)-Evec(i));
    currQu(j) = currQu(j)...
     + 0.5*(dcurrQu(i) + dcurrQu(i+1))*(Evec(i+1)-Evec(i));
    currQd(j) = currQd(j)...
     + 0.5*(dcurrQd(i) + dcurrQd(i+1))*(Evec(i+1)-Evec(i));
   end
  end
  % And at last, we plot the results, before it
  % start the next iteration for other
  % scattering strengths
  figure(1)
  plot(aVec,currQ,'b',aVec,currX,'r',aVec,currY,'g',aVec,currZ,'m')
  legend('Iq','Ix','Iy','Iz')
  ylabel('I/I_0, 1/(8*\tau_{so})=[0 1 2 5 10 20], 1/(8*\tau_{sf})=0')
  xlabel('\alpha')
  title(['L = ' num2str(L/1e-9) 'nm, \xi_s = '  num2str(xi/1e-9)...
   'nm, \theta = ' num2str(p/pi) '\pi, G_{\phi}^{1(2)} =' num2str(Gp1)...
```

```
    ', \zeta_{1(2)} = ' num2str(z1) ', \phi = \pi/2, and T/Tc = '...
    num2str(ToverTc) '.' ])
   hold on
   figure(2)
   plot(aVec,currQ,'b',aVec,currQs,'r',...
   aVec,currQt,'g',aVec,currQu,'m',aVec,currQd,'y')
   legend('JQ','JQs','JQt','JQu','JQd')
   ylabel('J/J_0 for 1/(8*\tau_{so})=[0 1 2 5 10 20], 1/(8*\tau_{sf})=0')
   xlabel('\alpha')
   title(['L = ' num2str(L/1e-9) 'nm, \xi_s = '  num2str(xi/1e-9)...
    'nm, \theta = ' num2str(p/pi) '\pi, G_{\phi}^{1(2)} =' num2str(Gp1)...
    ', \zeta_{1(2)} = ' num2str(z1) ', \phi = \pi/2, and T/Tc = '...
    num2str(ToverTc) '.' ])
   hold on

 shg % shows the figures
end
```

Density of States

```
Evec = -1.5:1e-03:-1e-03;  % Energy/Delta_0.
disp(['Size of Evec: ' num2str(size(Evec))])

delta = 2e-2;              % Inelastic scattering.
phaseVec = 0:0.02*pi:0.99*pi; % Phase-difference.
disp(['Size of PhaseVec: ' num2str(size(phaseVec))])

z1 = 5;                     % R_Barrier/R_N.
z2 = 5;                     % R_Barrier/R_N.
a = pi;                     % Angle between m1 og m2 (alpha).
xi = 30e-9;                 % Superconducting coherence length.
L = 20e-9;                  % Length of normal metal (e-9 = nm).
eT = (xi/L)^2;              % Thouless energy.
n = 20;                     % Length of x-vector.
k = round(n/2);             % Where to evaluate at x.
Gp1Vec = [0.5 1.1 1.5];     % Vector of G_phi1.
Gp2Vec = [0.5 1.1 1.5];     % Vector of G_phi2.
so = 2;                     % Spin-orbit strength g_so.
sf = 0;                     % Spin-orbit strength g_sf.
Gm1 = 0;
Gm2 = 0;
% We make m number of plots in the plane
% of sc phase difference and quasiparticle energy.
for m = 1:length(Gp1Vec)
 disp(['m = ' num2str(m)])
 Gp1 = Gp1Vec(m);
 Gp2 = Gp2Vec(m);
 % We now construct the density of state matrix.
```

```
 DOS = zeros(length(phaseVec),length(Evec));
 for j = 1:length(phaseVec)
  p  = phaseVec(j);
  disp(['theta = ' num2str(p)])
  % For the first energy, we use the trivial
  % zero matrix as the initial solution.
  y = zeros(16,n);
  for i = 1:length(Evec)
   e = Evec(i)+deltaE*1i;
   % For all other energies we use the solution
   % form the previous energy.
   y = myBvpSpinActive(e,a,p,eT,n,y,z1,z2,Gp1,Gp2,Gm1,Gm2,so,sf);
   % For the solution, we construct the gamma-matrices.
   gam   = [y(1,k), y(9,k); y(2,k), y(10,k)];
   gamt  = [y(3,k), y(11,k); y(4,k), y(12,k)];
   N  = eye(2)/(eye(2) - gam*gamt);
   g   = N*(eye(2) + gam*gamt);
   % And the density of state at energy (i)
   % and phase (j) becomes:
   DOS(j,i) = 0.5*real(trace(g));
  end
 end
 % Since the conventional density of state is symmetric with
 % respect to energy, we have only solved for half the energies,
 % and flip the solution into the other half-plane.
 dos = [DOS fliplr(DOS)];
 evec = [Evec -fliplr(Evec)];

 figure(m+1)
 surf(evec,phaseVec/pi,dos,'linestyle','none')
 xlabel('E/\Delta_0')
 zlabel(['Density of State, so=' num2str(so/1i) ', sf=' num2str(sf/1i)])
 ylabel('\theta/\pi')
 legend(['L=' num2str(L/1e-9) 'nm, \xi_s=' num2str(xi/1e-9)...
 'nm,  \alpha = ' num2str(a/pi) '\pi, G_\phi^{1(2)}=' num2str(Gp1)...
 ',\zeta_{1(2)}=' num2str(z1) ', deltaE=' num2str(deltaE) '.'])
 shg
end
```

Appendix D

Research Article

We here enclose the paper that is
currently undergoing review at
Physical Review B.

Spin-Supercurrent and Phase-Tunable Triplet Cooper Pairs via Magnetic Insulators

Ingvild Gomperud and Jacob Linder
Department of Physics, Norwegian University of Science and Technology, N-7491 Trondheim, Norway
(Dated: June 10, 2015)

We demonstrate theoretically that a dissipationless spin-current can flow a long distance through a diffusive normal metal by using superconductors interfaced with magnetic insulators. The magnitude of this spin-supercurrent is controlled via the magnetization orientation of the magnetic insulators. The spin-supercurrent obtained in this way is conserved in the normal metal just like the charge-current and interestingly has a term which is independent of the superconducting phase difference. The quantum state of the system can be switched between 0 and π by reversing the insulators from a parallel to antiparallel configuration with an external field. We show that the spin-current is carried through the normal metal by superconducting triplet (odd-frequency) correlations and that the superconducting phase difference can be used to enhance these, leaving clear spectroscopic fingerprints in the density of states.

INTRODUCTION

Using superconductors as active components in spintronics devices is a research field that has attracted increasing activity in recent years [1]. Such a synergy becomes possible both due to the special behavior of spin-polarized quasiparticles in superconductors, featuring extremely long spin lifetimes and spin relaxation lengths [2–4], and because superconducting Cooper pairs can become spin-polarized [5–7]. This type of Cooper pairs occur not only in superconductors with intrinsic triplet pairing, such as UGe_2 [8] and its cousins URhGe and UCoGe [9], but can in fact be artificially engineered in hybrid structures between conventional superconductors and magnetic materials [10, 11]. For samples with substantial impurity scattering, which is the experimentally most common scenario, these triplet Cooper pairs acquire a special property known as odd-frequency symmetry [12] in order to satisfy the Pauli principle. What this means is while the Cooper pair wavefunction is symmetric under both an exchange of space- and spin-coordinates, it is antisymmetric under an exchange of time-coordinates. This property leads to remarkable features such as gapless superconductivity [13], anomalous Meissner effects [14–17], and the possibility to create spin-supercurrents in diffusive ferromagnetic materials [18]. It is worth mentioning that paramagnetic Meissner effects and zero-bias conductance peaks can also originate from other types of effects which are not related to unconventional superconductivity, as shown previously in the context of d-wave superconductivity in the cuprates [19–21] and more recently for topological insulators [22]. The quality of the materials and avoiding crashing the STM tip into the sample are of paramount importance for proper identification of unusual types of superconductivity such as the odd-frequency one mentioned above.

In the context of utilizing superconductors for spintronics purposes, the possibility of spin-supercurrents in ferromagnetic materials [23] has earned the triplet Cooper pairs much attention. It is known that in structures featuring inhomogeneous magnetic order, such as intrinsically textured ferromagnets like Ho [24, 25], or multilayers with several ferromagnets [26], triplet supercurrents can arise even when using conventional s-wave superconductors which feature spinless Cooper pairs. However, spin-currents arising in this way in textured magnetic layers are in general not conserved due to the spatially changing magnetization direction. Moreover, it can be difficult practically to control the magnetization direction of each of the individual layers when using complex structures as in Ref. [26] to create the spin-supercurrent. A large amount of works have studied how triplet supercurrents can arise in various types of structures including both weakly and strongly polarized ferromagnets (see *e.g.* Refs. [27–39]). However, it would be highly desirable to create a spin-supercurrent flowing in a *normal (non-magnetic)* metal with a minimum amount of magnetic elements required due to the ensuing simplification in how to control the existence, and the properties, of the spin-supercurrent.

Now, it was recently experimentally shown in Ref. [40] that by using magnetic insulators (MI) in a superconducting spin-valve setup, it was possible to control the superconducting critical temperature T_c by changing the relative magnetization configuration from parallel (P) to antiparallel (AP) by application of an external field, causing an essentially in-

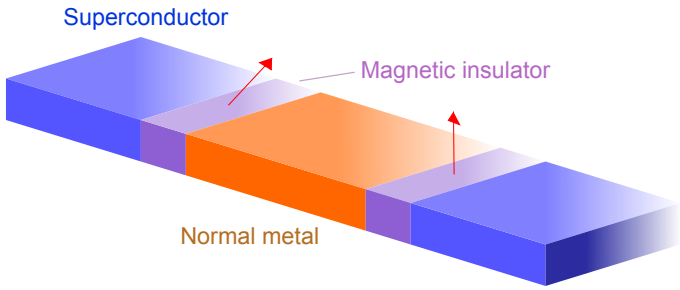

FIG. 1: (Color online) The proposed setup: a Josephson junction with magnetic insulators (MIs) inserted between the superconductors and the normal metal. The magnetic insulators have a magnetization that due to shape anisotropy is expected to be confined to the plane perpendicular to the tunneling direction. The magnetic moments of the MIs on the left and right side of the junction, $\mathbf{m}_L$ and $\mathbf{m}_R$, may be misaligned and an applied superconducting phase difference across the junction drives both a charge and spin supercurrent.

finite magnetoresistance effect. This finding prompted us to pose the question: what happens when magnetic insulators are used in a Josephson junction that has a normal, non-magnetic metal as its weak link? Can this create a spin-polarized dissipationless flow and, if so, can such a spin-supercurrent be controlled externally? We here demonstrate that the presence of magnetic insulators in a Josephson junction offers an interesting way to create a conserved spin-supercurrent in a normal metal (see Fig. 1). This spin-flow is controlled with the relative misalignment angle between the magnetic insulators. A main advantage with this setup, compared to previous proposals using ferromagnets, is that (i) the magnetic configuration is easily tunable since the magnetization of one single very thin (1-2 nm) magnetic insulator needs to be altered and that (ii) the spin-supercurrent is conserved in the normal metal, unlike what happens in textured ferromagnets.

Moreover, the spin-supercurrent is carried by odd-frequency Cooper pairs which leave a clear spectroscopic fingerprint in the density of states. We show that by tuning the superconducting phase difference θ, one can qualitatively change the nature of the proximity effect from a conventional singlet one to a triplet one *in situ*. We also show that the presence of magnetic insulators not only creates a spin-supercurrent, but that it has important consequences for the quantum phase of the system which undergoes a dynamic 0-π transition for a single sample by changing from a P to AP configuration for the insulators.

THEORY

We use the quasiclassical theory of superconductivity [41, 42] in the diffusive limit, where the physics is described by the Green matrix function $\check{g}$ of the system which is an 8×8 matrix in Keldysh-Nambu space. It is defined in terms of the retarded, advanced, and Keldysh part of the Green function: $\check{g} = \begin{pmatrix} g^R & g^K \\ 0 & g^A \end{pmatrix}$. In the absence of non-equilibrium effects, such as applied voltages and temperature-gradients, it is sufficient to consider the retarded part $g^{\mathrm{R}} \equiv g$, which may be parametrized conveniently as follows [43]:

$$g = \begin{pmatrix} \underline{\mathcal{N}}(\underline{1} + \underline{\gamma}\underline{\tilde{\gamma}}) & 2\underline{\mathcal{N}}\underline{\gamma} \\ -2\underline{\tilde{\mathcal{N}}}\underline{\tilde{\gamma}} & -\underline{\tilde{\mathcal{N}}}(\underline{1} + \underline{\tilde{\gamma}}\underline{\gamma}) \end{pmatrix}, g^2 = 1. \quad (1)$$

We have defined $\underline{\mathcal{N}} = (\underline{1} - \underline{\gamma}\underline{\tilde{\gamma}})^{-1}$ for normalization and the $\underline{.}\tilde{.}$ operation means complex conjugation and reversal of quasiparticle energy. The Ricatti-matrices $\{\underline{\gamma}, \underline{\tilde{\gamma}}\}$ are 2×2 matrices in spin space and the Green function g satisfies the Usadel equation [44] in the normal metal

$$D\partial_x(g\partial_x g) + \mathrm{i}[\varepsilon\rho_3, g] = 0. \quad (2)$$

Here, D is the diffusion coefficient of the normal metal, $\rho_3 = \mathrm{diag}(\underline{1}, -\underline{1})$, and ε is the quasiparticle energy measured relative the Fermi level. In order to account for the magnetic insulators at the interfaces, we use spin-dependent boundary conditions discussed in Ref. [45]. The most important effect of the magnetic insulators is the spin-dependent phase-shifts experienced by quasiparticles scattering at the interface, which are described by a parameter G_φ to be defined below. The superconducting regions are described by bulk Green functions which for the left and right side of the junction are denoted g_L and g_R, where

$$\underline{\gamma}_j = \mathrm{i}\underline{\sigma}_y s/(\underline{1} + \underline{1}c)\mathrm{e}^{\mathrm{i}\theta_j},\ \underline{\tilde{\gamma}}_j = -\mathrm{i}\underline{\sigma}_y s/(\underline{1} + \underline{1}c)\mathrm{e}^{-\mathrm{i}\theta_j}, \quad (3)$$

with $j = \{L, R\}$. We have introduced

$$s = \sinh\Theta,\ c = \cosh\Theta, \text{ with } \Theta = \mathrm{atanh}(\Delta_0/\varepsilon), \quad (4)$$

where Δ_0 is the magnitude of the superconducting order parameter. The bulk solution is an excellent approximation for low interface transparencies when using large superconducting reservoirs. We have used the second Pauli matrix $\underline{\sigma}_y$, and the superconducting phase difference across the junction is defined as $\theta \equiv \theta_R - \theta_L$. The boundary conditions read:

$$\begin{aligned} 2d\zeta_L g\partial_x g &= [g_L, g] + \mathrm{i}G^L_\varphi[\mathcal{M}_L, g] \text{ at } x = 0, \\ 2d\zeta_R g\partial_x g &= [g, g_R] - \mathrm{i}G^R_\varphi[\mathcal{M}_R, g] \text{ at } x = d, \end{aligned} \quad (5)$$

where $\zeta_j = R_{B,j}/R_N$ is the ratio between the normal-state barrier resistance on side j and the resistance of the normal metal, and $G^j_\varphi = -\sum_n \mathrm{d}\varphi_n / \sum_n T_n$ where T_n is the transmission probability for channel n and $\mathrm{d}\varphi_n$ are the spin-dependent part of the phase-shifts picked up by particles scattered at the interface. Finally, the matrix $\mathcal{M}_j$ describes the orientation of the magnetic moment of the magnetic insulator on side j, while d is the length of the normal metal. Experimentally, it is likely that the magnetic insulators will have exchange fields lying in the plane perpendicular to the tunneling direction due to shape anisotropy if one uses a layered 'pancake' geometry for the junction. This case, and other configurations, are covered by us setting the right interface to $\mathcal{M}_R = \mathrm{diag}(\underline{\sigma}_z, \underline{\sigma}_z)$ whereas the left interface is allowed to have an arbitrary orientation, i.e. $\mathcal{M}_L = \cos\alpha\mathrm{diag}(\underline{\sigma}_z, \underline{\sigma}_z) + \sin\phi\sin\alpha\mathrm{diag}(\underline{\sigma}_y, -\underline{\sigma}_y) + \cos\phi\sin\alpha\mathrm{diag}(\underline{\sigma}_x, \underline{\sigma}_x)$. Here, ϕ is the azimuthal angle in the xy-plane and α is the angle between the magnetization and the z-axis. For later use, we define the magnetic moments of the insulators on the left and right side as $\mathbf{m}_L$ and $\mathbf{m}_R$.

The boundary conditions used here can also be extended [45] to include a magnetoresistance term G_{MR} which accounts for the different transmission probabilities for spin-$\uparrow$ and spin-$\downarrow$ particles. Inclusion of such a term amounts mainly to an overall reduction of the superconducting proximity effect and we have explicitly verified numerically that the spin-supercurrent exists even in its presence. The magnetic moment associated with each magnetic insulator should be understood as the net average moment of the interface region, since a disordered interface might have an internal magnetic structure. Moreover, interfaces in hybrid structures are intrinsically accompanied by the lack of inversion symmetry. For

this reason, spin-orbit effects could arise at the interface and modify the spin-dependent scattering at the superconducting interface [46–48]. However, it is currently unknown how to incorporate such interfacial spin-orbit scattering in the boundary conditions of quasiclassical theory. Nevertheless, even if such a mechanism existed, the spin-dependent phase-shifts due to the magnetic insulators captured by the parameter G_φ in our work is sufficient to produce triplet Cooper pairs, and so we do not expect that a second mechanism that accomplishes the same thing (due to spin-orbit interaction) would bring about any major changes.

Finally, we will later on include non-ideal effects such as spin-flip scattering due to magnetic impurities and spin-orbit impurity scattering to see how they influence the spin- and charge-flow as well as the density of states in the system. These are accounted for [41, 42] by adding extra self-energy terms in the commutator part of the Usadel equation Eq. (2):

$$\begin{aligned} &\text{Magnetic impurities: } \Sigma_{\text{sf}} = \frac{i}{8\tau_{\text{sf}}}\boldsymbol{\tau} g \boldsymbol{\tau}, \\ &\text{Spin-orbit scattering: } \Sigma_{\text{so}} = \frac{i}{8\tau_{\text{so}}}\boldsymbol{\tau}\rho_3 g \rho_3 \boldsymbol{\tau}, \end{aligned} \tag{6}$$

Here we have defined the matrix vector $\boldsymbol{\tau} = (\tau_x, \tau_y, \tau_z)$, where the components are given by:

$$\tau_\nu = \text{diag}(\underline{\sigma}_\nu, \underline{\sigma}_\nu^*),\ \nu = \{x, y, z\}. \tag{7}$$

For future reference, we introduce the normalized strength of magnetic impurity and spin-orbit scattering as $g_{\text{sf}} = 1/8\Delta_0\tau_{\text{sf}}$ and $g_{\text{so}} = 1/8\Delta_0\tau_{\text{so}}$, where $\tau_{\text{sf/so}}$ are the relaxation times associated with each type of scattering.

RESULTS

Spin-Supercurrent via Magnetic Insulators

We proceed to discuss how the charge- and spin-supercurrents sustained by the system are influenced by the presence of the ferromagnetic insulators. In the quasiclassical framework, these are given by

$$I_Q = \frac{N_0 e D A}{4}\int_{-\infty}^{\infty} \mathrm{d}\varepsilon \mathrm{Tr}\{\rho_3(\check{g}\partial_x\check{g})^{\mathrm{K}}\} \tag{8}$$

and

$$I_S^\nu = \frac{N_0 \hbar D A}{8}\int_{-\infty}^{\infty} \mathrm{d}\varepsilon \mathrm{Tr}\{\rho_3\tau_\nu(\check{g}\partial_x\check{g})^{\mathrm{K}}\}. \tag{9}$$

Here, N_0 is the density of states at the Fermi-level in the normal-state, e is the electric charge, $\hbar$ is the reduced Planck constant, while A is the interface contact area. For future use, we also define the bulk superconducting coherence length $\xi_S = \sqrt{D/\Delta_0}$. In the weak proximity effect regime, we were able to find a general analytical result for the supercurrents of spin and charge (see Appendix for details). We first briefly consider the charge-supercurrent which reads:

$$I_Q = (I_{Q,0} + I_{Q,1}\cos\alpha G_\varphi^L G_\varphi^R)\sin\theta, \tag{10}$$

where the coefficients $I_{Q,0}$ and $I_{Q,1}$ are lengthy expressions that depend on junction parameters such as the width d, misalignment angle α, temperature T, and the interface transparencies $\zeta_{L/R}$. The charge-current is found to be independent of which orientation the magnetic moments have in the xy-plane, ϕ. We see that the presence of magnetic insulators coupled to the superconductors introduces a $\cos\alpha$-dependence on the supercurrent, not only tuning its overall magnitude, but also changing the quantum ground-state of the junction from 0 to π when

$$I_{Q,1}\cos\alpha G_\varphi^L G_\varphi^R = -I_{Q,0}. \tag{11}$$

Thus, 0-π transitions can now occur even with a normal metal interlayer by changing α, a feature which was also reported in the ballistic limit in Ref. [27]. To demonstrate that this is a robust feature, we have computed the charge supercurrent without any assumption of a weak proximity effect, thus using the full Riccati parametrization. This is shown in Fig. 2(d), where the current changes sign at $\alpha \simeq 0.2\pi$ corresponding to the 0-π transition. Further information may be inferred from the analytical expression for the charge-supercurrent in the Appendix, Eq. (18): as the width d of the junction increases, larger values for the spin-dependent phase-shifts G_φ are required in order to make the 0-π transition possible.

Interestingly, there exists not only a superflow of charge in the system, *but also of spin*. The polarization occurs in the direction $\mathbf{m}_L \times \mathbf{m}_R$, and so we find that while $I_S^z = 0$, one has:

$$I_S^x = G_\varphi^L G_\varphi^R \sin\phi\sin\alpha(I_{S,0} + I_{S,1}\cos\theta). \tag{12}$$

Eq. (12) is one of the main results of this work. It is seen that the spin-supercurrent vanishes if one only has one magnetic insulator, in which case G_φ^L or G_φ^R is zero. Moreover, it is proportional to $\sin\alpha$, which shows that it is also absent in the P or AP alignment ($\alpha = 0, \pi$). For other angles α, however, it is in general present. The coefficients $\{I_{S,0}, I_{S,1}\}$ are purely real and vanish in the absence of superconductivity ($\Delta = 0$). There exists a simple relation between the components of the spin-supercurrent in the xy-plane:

$$\frac{I_S^x}{I_S^y} = -\frac{\sin\phi}{\cos\phi}. \tag{13}$$

This spin-supercurrent has several remarkable features: first of all, it is conserved throughout the normal metal just like the charge-current. Secondly, it is long-ranged as it flows through a normal metal without any exchange field. Thirdly, it has one component that is *independent* of the superconducting phase difference θ. The other component goes like $\cos\theta$, meaning that the total spin-supercurrent satisfies $I_S^x(\theta) = I_S^x(-\theta)$. This can be understood physically, since a spin-current is invariant under time-reversal symmetry. The latter operation

transforms $\theta \to (-\theta)$ and causes the charge-supercurrent to change sign. In the Appendix, we give the full expression of the spin-supercurrents including the coefficients and their dependence on the junction parameters. The spin-supercurrent vs. misalignment angle α is shown in Fig. 2(a)-(c) for different junction parameters.

The properties of this spin-supercurrent are such that it resolves two aforementioned challenges: the spin-current is conserved and it is readily controlled with a weak external field coupling to the magnetic insulators. We underline that our structure, unlike previous works, does not include any ferromagnetic metals. In fact, a conceptually similar experimental structure to the one that we propose to use in our manuscript has recently been demonstrated in Ref. [40]. There, the authors investigated a spin-valve structure consisting of a superconductor flanked by two magnetic insulators of slightly different thicknesses (both of order a few nm). Applying an external magnetic field would then control the magnetization orientation of the thinner of these layers. This indicates that our results are of experimental relevance using currently available techniques.

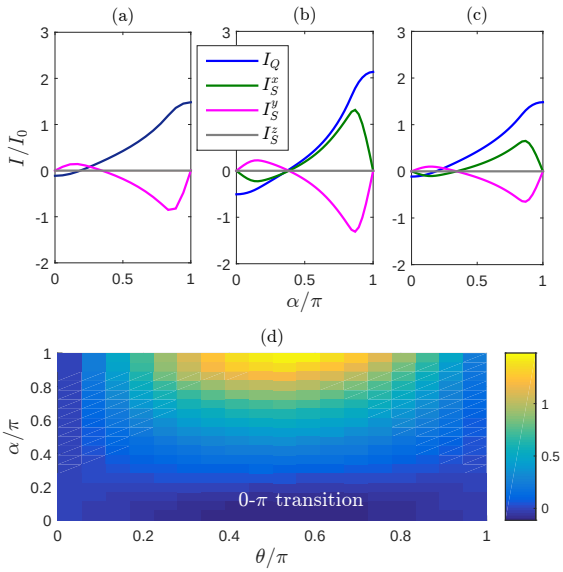

FIG. 2: (Color online) Plot of the spin- and charge-supercurrents in the system. We have used $\xi_S = 30$ nm and the relative temperature $T/T_c = 0.02$. The interface parameters are set to be equal, $G_\varphi = 3$ and $\zeta = 2$, and the phase difference is the one supporting the critical current, $\theta = \pi/2$. In (a), we have set $d = 20$ nm, $\phi = 0$. In (b), we have $d = 5$ nm and $\phi = \pi/4$. In (c), we set $d = 20$ nm and $\phi = \pi/4$. As expected, the components of the spin-supercurrents are mirror-images of each other in (b) and (c) due to the choice of magnetic configuration of the insulators, $\phi = \pi/4$ [see Eq. (13)]. The charge-supercurrent is independent of ϕ. As seen, it changes sign when going from $\alpha = 0$ to $\alpha = \pi$, signalling a 0-π transition. The normalization constant of the charge-current is $I_0 = N_0 eDA/4$ while for the spin-currents it is $I_0 = N_0 \hbar DA/8$. The contour plot in the bottom panel (d) is the charge-supercurrent in the θ-α plane using $d = 20$ nm, showing the occurrence of the 0-π transition around $\alpha \simeq 0.2\pi$.

In an experimental setting, the normal metal sample may well include some degree of magnetic impurities or spin-orbit scattering on impurities. Thus, it is of interest to see how such non-ideal effects influence the predictions made in this paper. Although no tractable analytical expression is accessible in this case, we have computed numerically the charge- and spin-supercurrent in the presence of spin-flip scattering and spin-orbit impurity scattering as described by Eq. (6). Interestingly, the dissipationless flow of charge and spin are affected very differently depending on the type of scattering. Consider first the charge-supercurrent [top row of Fig. 3]. With increasing spin-flip scattering, the current is monotonically suppressed. However, this is not the case for spin-orbit impurity scattering (middle panel). Instead, the 0-π transition point vanishes and the current retains its order of magnitude even for very large values of $g_{\rm so}$. Turning to the spin-supercurrent, we find that both magnetic impurity scattering and spin-orbit impurity scattering suppress the spin-flow monotonically.

The physical origin of the different behavior of the charge- and spin-supercurrents when adding magnetic impurities and spin-orbit scattering can be traced back to how the singlet and triplet superconducting correlations are affected by them [53, 54]. It can be demonstrated analytically that the singlet component is insensitive to spin-orbit impurity scattering in the absence of a magnetic field, as is reasonable since spin-orbit scattering respects time-reversal symmetry. On the other hand, the triplet component is suppressed as the spin-orbit scattering rate increases. Based on this, one can now understand why the charge-supercurrent evolves different with increasing spin-flip and spin-orbit scattering respectively. In the former case, both the singlet and triplet components are

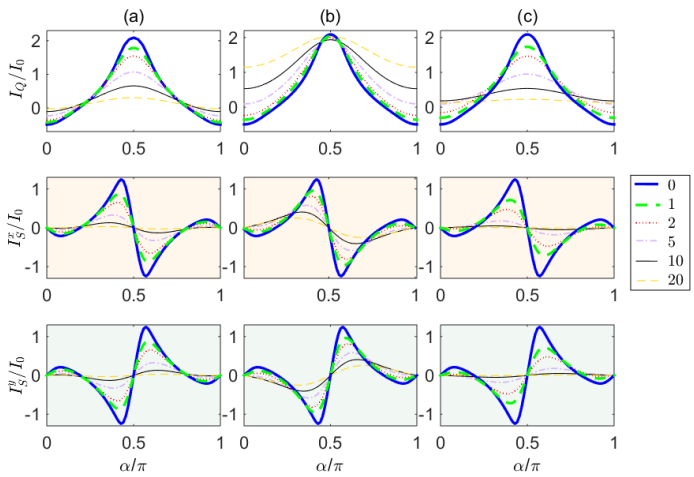

FIG. 3: (Color online) Plot of the charge-supercurrent and the components of the spin-supercurrent in the presence of spin-flip scattering due to magnetic impurities and spin-orbit impurity scattering. Column (a) corresponds to magnetic impurity scattering (lines corresponding to different values of $g_{\rm sf}$), column (b) to spin-orbit scattering ($g_{\rm so}$), and column (c) to both present with equal magnitude. The parameters are set to $d = 5$ nm, $\xi_S = 30$ nm, $G_\varphi = 3$, $\zeta = 2$, $T/T_c = 0.02$, and $\theta = \pi/2$

suppressed, i.e. the total superconducting proximity effect is reduced, and the current simply decays montonically. In the latter case, however, only the triplet part is suppressed. With only the singlet part remaining in the normal metal, there is no mechanism to cause a 0-π transition and the sign of the current remains positive and still of appreciable magnitude.

The same reasoning can be applied to the spin-current. In this case, it is solely the triplet part which is responsible for its existence. Since both magnetic impurities and spin-orbit scattering suppress the triplet Cooper pairs, the spin-supercurrent decays monotonically as the scattering rate increases. It can be seen from Fig. 3 that the dependence of the spin-supercurrent on the misalignment angle α between the magnetic insulator moments goes toward a pure $\sin\alpha$ profile as $g_{\rm so}$ becomes large.

Phase-tunable Triplet Superconductivity

Besides the appearance of this unusual spin-supercurrent, a Josephson junction with magnetic insulator interfaces offers a unique way to control triplet superconductivity as we now demonstrate. It has previously been shown that a crossover from pure conventional even-frequency pairing to odd-frequency pairing is made possible via spin-active interfaces in S|MI|N bilayer junctions [50]. The pivotal parameter is the ratio between the spin-dependent phase-shifts and the normal-state tunnel conductance, in our notation G_φ, which causes a pure odd-frequency proximity pairing state at the Fermi level ($\varepsilon = 0$) when $G_\varphi > 1$ while a pure even-frequency state occurs when $G_\varphi < 1$. Experimentally, this is manifested as a large zero-energy peak in the density of states when the odd-frequency triplets dominate. Conversely, a minigap appears in the spectrum for conventional singlet pairing. To observe such an effect, it would be necessary to fabricate several samples with a varying ratio G_φ. One way to accomplish this could be to vary the width of the MI interlayer in order to tune the tunneling probability.

Instead, we here show that when spin-active interfaces are incorporated in a Josephson junction geometry, the crossover from even- to odd-frequency pairing can now be controlled by the *superconducting phase difference* θ, which in turn is determined by the current flowing through the system. This offers a new way to induce a triplet proximity effect which can be changed *in situ* within a single sample, simply by varying θ. The crossover is manifested by the qualitative nature of the proximity effect, going from a minigap (conventional singlet proximity effect) to an enhanced low-energy peak (odd-frequency triplet proximity effect). In order to probe how the change in pairing symmetry is manifested experimentally, we here compute the density of states in the normal metal region and its phase-dependence numerically which allows us to relax the assumption of a weak proximity effect. The DOS normalized to its normal-state value is obtained from the solution

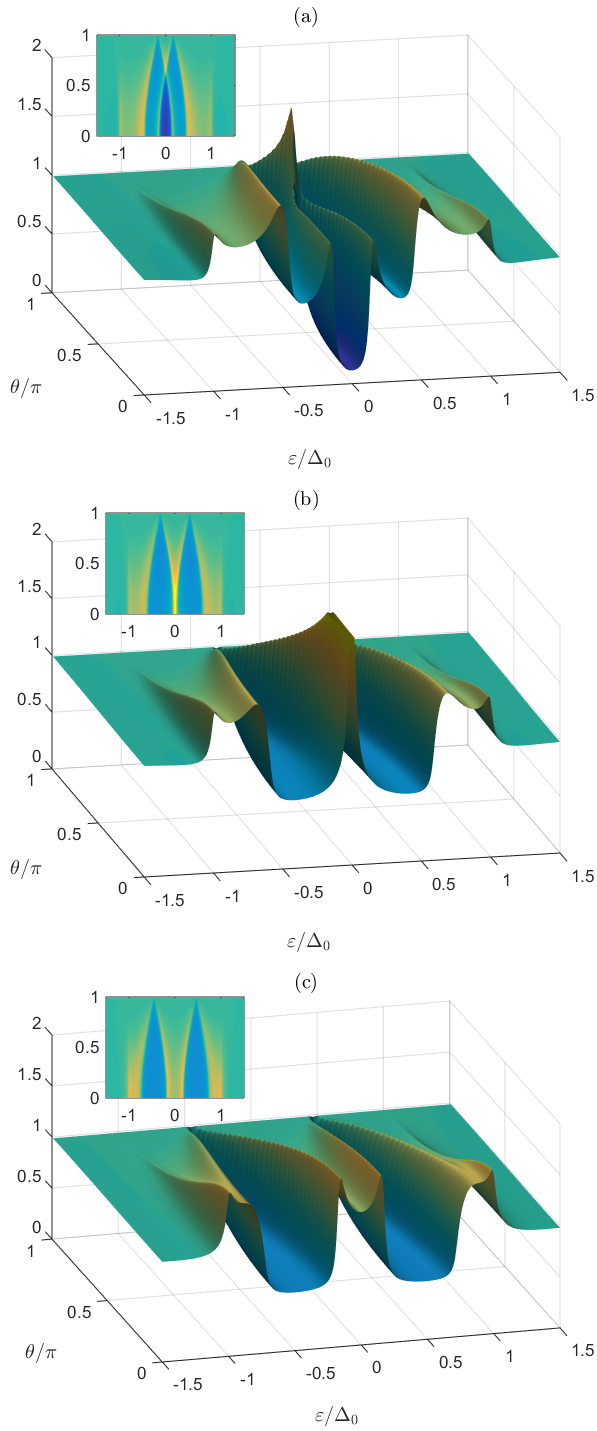

FIG. 4: (Color online) Proximity-induced density of states $N(\varepsilon,\theta)$ (normalized to its normal-state value) in the middle of the normal metal region. In all cases, we are considering the P configuration where both magnetic insulators have moments pointing in the z-direction. The strength of the spin-dependent phase-shifts occuring at the interfaces are given by (a) $G_\varphi = 0.55$, (b) $G_\varphi = 1.05$, and (c) $G_\varphi = 1.55$. We have used the parameters $d = 20$ nm, $\xi_S = 30$ nm, and $\zeta = 5$.

of the Ricatti equations via:

$$N(\varepsilon,\theta) = \mathrm{Re}\{\mathrm{Tr}[\underline{\mathcal{N}}(\underline{1}+\underline{\gamma\tilde{\gamma}})]\}/2. \tag{14}$$

To make better contact with experimental measurements, we have added a small imaginary part to the quasiparticle energies, $\varepsilon \to \varepsilon + \mathrm{i}\delta$ where $\delta/\Delta_0 \ll 1$, which represents inelastic scattering.

We consider the most general case where each superconducting interface contains a magnetic insulator. The results are shown in Fig. 4, where we have focused on the experimentally most accessible configuration with the insulators in the P state. Three choices of the strength of the spin-active scattering at the interfaces are considered in (a)-(c) with $G_\varphi = \{0.55, 1.05, 1.55\}$. It is seen that the nature of the superconducting proximity changes qualitatively due to the presence of the magnetic insulators. It is known that in the absence of magnetic elements ($G_\varphi = 0$), a minigap is induced in the normal metal which is largest for $\theta = 0$ and closes at $\theta = \pi$. In Fig. 4(a), the minigap is prominent at small phase-differences θ. However, instead of monotonically closing the minigap as θ is driven towards π, the density of states becomes strongly enhanced at low energies. This feature arises due to the odd-frequency symmetry of the triplet Cooper pairs in the normal metal [49–51]. When the spin-active scattering, taking place at the insulators, becomes stronger in Fig. 4(b) and (c), the minigap has vanished all-together, leaving behind only a clear zero-energy peak in the density of states.

The qualitative change in the density of states (going from fully suppressed to enhanced at low energies) can be seen clearly also when keeping the superconducting phase difference θ fixed and varying the magnetic configuration α. This is shown in Fig. 5: as one changes from a P to AP configuration (going from $\alpha = 0$ to $\alpha = \pi$), the system makes a transition from hosting proximity-induced triplet superconductivity to singlet superconductivity. Our work thus demonstrates a *conversion between singlet and triplet Cooper pairs in a normal metal by tuning either the superconducting phase difference or the configuration of the magnetic insulators*. This has the important advantage that it can be done *in situ*, as opposed to using ferromagnets where *e.g.* several samples with different widths are created to suppress the singlet component relative the triplet one.

It is interesting to note that the density of states for each electron-spin is highly non-degenerate and tunable, as shown in Fig. 6. This could potentially be utilized in creating large thermoelectric effects based on the idea of Ref. [55] which demonstrated that the spin-splitted density of states arising in superconductor/ferromagnet hybrids could yield a thermoelectric figure of merits far exceeding what is obtained in the non-superconducting phase.

Similarly to our treatment of the spin- and charge-supercurrent, we also investigate the influence of spin-flip and spin-orbit scattering on the density of states. In the left column of Fig. 7, we consider different values for G_φ and the spin-flip scattering rate. Regardless of the value of G_φ, in particular of whether it is smaller than or greater than the critical value $G_{\varphi,c} = 1$, the influence of the superconducting proximity effect on the DOS is diminished. As discussed previously in the context of the charge- and spin-supercurrents, this may be understood physically from the fact that magnetic impurities suppress singlet and triplet components alike, such that the DOS eventually reverts to its normal-state value for any phase-difference and energy. The situation is different when considering spin-orbit impurity scattering, shown in the right column of Fig. 7. Now, the spectroscopic manifestation of the superconducting proximity effect depends on whether we are in the singlet-dominated regime $G_\varphi < 1$ or the triplet-dominated regime $G_\varphi > 1$. For $G_\varphi = 0.55$, the presence of spin-orbit scattering leaves the minigap intact while suppressing the zero-energy peak that emerges as the superconducting phase-difference increases. Hence, the superconducting proximity effect remains clearly visible in the DOS. For $G_\varphi > 1$ shown in (d) and (f), however, increasing the spin-orbit scattering rate causes the low-energy enhancement of the DOS to be absent since the triplet component is suppressed by this type of scattering. When applying even stronger values of

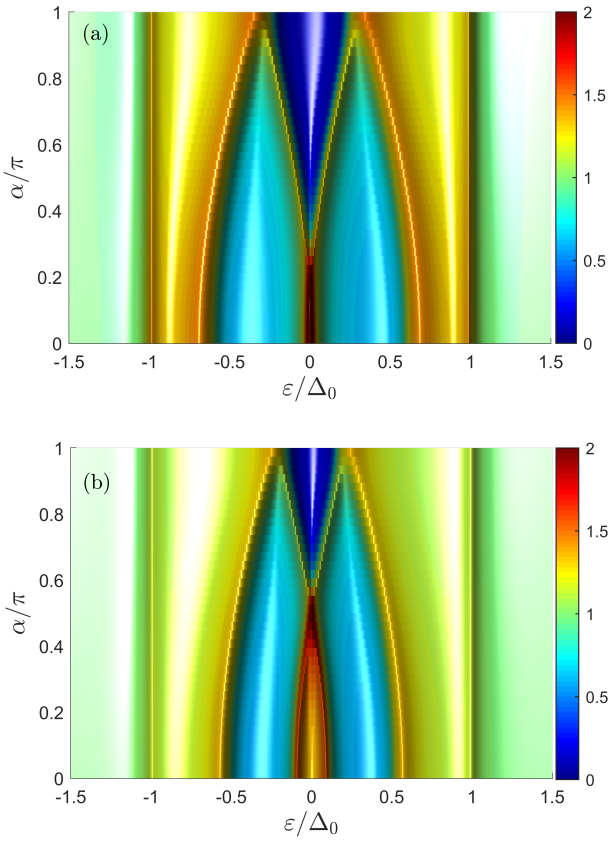

FIG. 5: (Color online) Proximity-induced density of states $N(\varepsilon,\theta)$ (normalized to its normal-state value) in the middle of the normal metal as a function of quasiparticle energy ε and the misalignment angle α of the magnetic insulators. In (a), the superconducting phase bias is set to $\theta = 0$, corresponding to zero current-flow. In (b), we have $\theta = \pi/2$, corresponding to the critical current-flow. The other parameters are set to $d = 20$ nm, $\xi_S = 30$ nm, $G_\varphi = 1.05$, $\zeta = 5$.

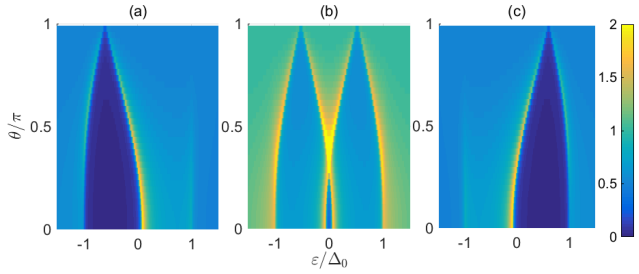

FIG. 6: (Color online) Spin-resolved density of states (normalized to its normal-state value) in the $\varepsilon - \theta$ plane. In (b), the total density of states is shown whereas in (a) and (c) the spin-$\downarrow$ and spin-$\uparrow$ contributions are shown, respectively. The parameters used are $\zeta = 5$, $G_\varphi = 0.9$, $d = 10$ nm, $\xi_S = 30$ nm, and $\alpha = 0$.

spin-orbit scattering, a clear minigap appears for all the values of G_φ. It should also be noted that the spectroscopic fingerprints of the superconducting proximity effect are much more sensitive toward the presence of magnetic impurity and spin-orbit scattering than the charge- and spin-supercurrents, the former being suppressed in magnitude faster compared to the current at a given value of $g_{\text{sf/so}}$.

DISCUSSION AND CONCLUDING REMARKS

We here discuss in more detail how our work is related to previous findings. In the proposal by Houzet and Buzdin [28], a ferromagnetic trilayer was suggested as the minimal structure that would be able to generate a long-ranged triplet supercurrent. In another work by Grein *et al.* [32], strongly polarized ferromagnets with two spin-active interfaces were considered, thus in some sense being similar to the trilayer system of Ref. [28] with the exception that the spin-bands were now assumed to be completely decoupled in the bulk due to the large exchange field. In this case, a spin-supercurrent was shown to also be generated. Shomali *et al.* [31] studied the spin-current in a Josephson junction with a ferromagnetic metal bilayer and it was realized that a long-ranged supercurrent in ferromagnets could in fact be generated with only two ferromagnets [29], albeit only as a higher-order effect. More precisely, there would be a contribution to a long-ranged triplet supercurrent from the second Josephson harmonic $\sin(2\theta)$. This could make experimental detection difficult, since the magnitude of the second harmonic latter is usually much smaller than the first harmonic, and a very specific fine-tuning of the junction parameters would be required to observe the effect. Spin-supercurrents have also been analyzed in other types of superconducting structures, including magnetic textures such as spirals, and also using intrinsically triplet bulk superconductors [58–62]. Very recently [64], spin supercurrents in junctions composed of multiband superconductors coexisting with a spin-density wave state was studied theoretically. Similar dependencies on the superconducting phase difference and magnetic misalignment between the spin-density waves as in our case was shown, even if the system under consideration in this work is physically quite different from Ref. [64].

In contrast, the spin-supercurrent reported in our work occurs in the first harmonic, i.e. it is not a higher-order effect, meaning that it is present without any fine-tuning of parameters in order to suppress the first harmonics in favor of higher ones. Moreover, it occurs *without use of any ferromagnetic metals*: the spin superflow takes place in a non-magnetic normal metal.

There are several different choices for magnetic insulators that can be used in the proposed setup shown in Fig. 1. Previous experiments considering superconducting hybrid structures have utilized magnetic insulators such as EuO [52], EuS [40], and GdN [56]. The particular choice of magnetic insulator also depends on how well it can be grown at the interface between the superconductor and the normal metal. We speculate that suitable material combinations to construct our setup could be Nb and EuO as the superconductor and mag-

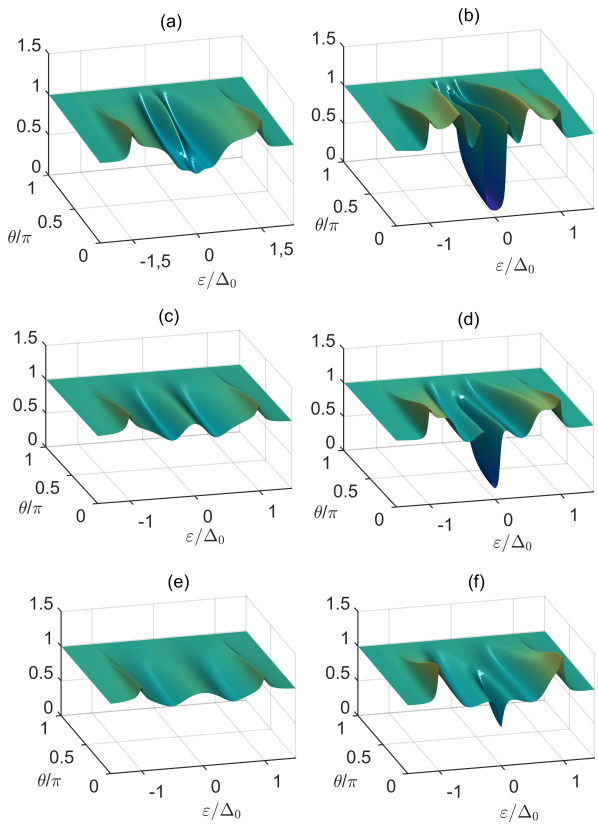

FIG. 7: (Color online) Plot of the density of states $N(\varepsilon, \theta)$ (normalized to its normal-state value) in the energy-superconducting phase difference (ε-θ) plane. The top row illustrates the case where $G_\varphi = 0.55$ and (a) $g_{\text{sf}} = 0.05$, (b) $g_{\text{so}} = 0.05$. The middle row has $G_\varphi = 1.05$ and (c) $g_{\text{sf}} = 0.10$, (d) $g_{\text{so}} = 0.10$. The bottom row shows $G_\varphi = 1.55$ and (e) $g_{\text{sf}} = 0.15$, (f) $g_{\text{so}} = 0.15$. The remaining parameters are set to $d = 20$ nm, $\xi_S = 30$ nm, and $\zeta = 5$, in the P configuration.

netic insulator, or alternatively NbN and GdN. Concerning the phase-dependent density of states in the normal metal, experimental techniques are available for measuring this quantity as demonstrated in Ref. [57] in a conventional SNS Josephson junction. By integrating the junction in a loop geometry, the superconducting phase θ is then tunable via a minute magnetic flux. Using AFM-spectroscopy, a complete mapping of how the density of states evolves spatially through the junction as a function of θ is possible.

We note that very recently, quasiclassical boundary conditions valid for *any* strength of the barrier polarization were derived [63]. This opens the possibility to study theoretically systems with very strongly spin-polarized magnetic insulators and even half-metallic (fully polarized) ferromagnets.

In summary, we have shown that by integrating superconductors with magnetic insulators, one arrives at a unique way to both create and control triplet superconductivity in a well-defined way with the superconducting phase-difference, and to also create a conserved and tunable spin-supercurrent flowing through a normal metal.

Acknowledgments

The authors thank S. Jacobsen, J. A. Ouassou, I. Kulagina, A. Pal, A. di Bernardo, J. Robinson, M. Blamire, and M. Eschrig for many useful discussions. This work was supported by the "Outstanding Academic Fellows" programme at NTNU, the COST Action MP-1201 'Novel Functionalities through Optimized Confinement of Condensate and Fields, and Norwegian Research Council grants no. 205591 and no. 216700.

APPENDIX: DETAILED EXPRESSIONS FOR CHARGE- AND SPIN-SUPERCURRENTS

We here provide comprehensive results for the analytical expressions of the supercurrents of charge and spin supported by the system. In the weak proximity effect, one finds the following completely general expressions:

$$\begin{aligned}
I_Q &= \frac{N_0 eDA}{4}\int_0^\infty \mathrm{d}\varepsilon \tanh\Big(\frac{\beta\varepsilon}{2}\Big) 4\mathrm{Re}\Big\{[2f_s\partial_x\tilde{f}_s - 2f_t\partial_x\tilde{f}_t - f_\uparrow\partial_x\tilde{f}_\uparrow - f_\downarrow\partial_x\tilde{f}_\downarrow] - [\tilde{\cdot\cdot}]\Big\},\\
I_S^x &= \frac{N_0\hbar DA}{8}\int_0^\infty \mathrm{d}\varepsilon \tanh\Big(\frac{\beta\varepsilon}{2}\Big) 4\mathrm{Re}\Big\{[-(f_\uparrow + f_\downarrow)\partial_x\tilde{f}_t - f_t\partial_x(\tilde{f}_\uparrow + \tilde{f}_\downarrow)] - [\tilde{\cdot\cdot}]\Big\},\\
I_S^y &= \frac{N_0\hbar DA}{8}\int_0^\infty \mathrm{d}\varepsilon \tanh\Big(\frac{\beta\varepsilon}{2}\Big) 4\mathrm{Im}\Big\{[(f_\uparrow - f_\downarrow)\partial_x\tilde{f}_t - f_t\partial_x(\tilde{f}_\uparrow - \tilde{f}_\downarrow)] + [\tilde{\cdot\cdot}]\Big\},\\
I_S^z &= \frac{N_0\hbar DA}{8}\int_0^\infty \mathrm{d}\varepsilon \tanh\Big(\frac{\beta\varepsilon}{2}\Big) 4\mathrm{Re}\Big\{[-f_\uparrow\partial_x\tilde{f}_\uparrow + f_\downarrow\partial_x\tilde{f}_\downarrow] - [\tilde{\cdot\cdot}]\Big\}.
\end{aligned} \tag{15}$$

Above, the notation $(\tilde{\cdot\cdot})$ means changing the sign of energy and complex conjugate and we defined the inverse temperature $\beta = 1/(k_B T)$. It is seen that the spinless singlet correlations f_s do not contribute to any of the spin-currents. In the special case of a normal metal separating the superconductors, one can work further with the above expressions by inserting the solutions

$$f_m = A_m \mathrm{e}^{\mathrm{i}kx} + B_m \mathrm{e}^{-\mathrm{i}kx}, m = \{s, t, \uparrow, \downarrow\}. \tag{16}$$

We then get expressions for the supercurrents which is independent of position:

$$\begin{aligned}
I_Q &= N_0 eDA\int_0^\infty \mathrm{d}\varepsilon \tanh\Big(\frac{\beta\varepsilon}{2}\Big)\mathrm{Re}\Big\{2\mathrm{i}k[(A_\uparrow\tilde{A}_\uparrow - B_\uparrow\tilde{B}_\uparrow) + 2(A_t\tilde{A}_t - B_t\tilde{B}_t) - 2(A_s\tilde{A}_s - B_s\tilde{B}_s) + (A_\downarrow\tilde{A}_\downarrow - B_\downarrow\tilde{B}_\downarrow)]\Big\},\\
I_S^x &= \frac{N_0\hbar DA}{2}\int_0^\infty \mathrm{d}\varepsilon \tanh\Big(\frac{\beta\varepsilon}{2}\Big)\mathrm{Re}\Big\{2\mathrm{i}k[(A_\uparrow + A_\downarrow)\tilde{A}_t - (B_\uparrow + B_\downarrow)\tilde{B}_t + (\tilde{A}_\uparrow + \tilde{A}_\downarrow)A_t - (\tilde{B}_\uparrow + \tilde{B}_\downarrow)B_t]\Big\},\\
I_S^y &= \frac{N_0\hbar DA}{2}\int_0^\infty \mathrm{d}\varepsilon \tanh\Big(\frac{\beta\varepsilon}{2}\Big)\mathrm{Re}\Big\{2k[-(A_\uparrow - A_\downarrow)\tilde{A}_t + (B_\uparrow - B_\downarrow)\tilde{B}_t + (\tilde{A}_\uparrow - \tilde{A}_\downarrow)A_t - (\tilde{B}_\uparrow - \tilde{B}_\downarrow)B_t]\Big\},\\
I_S^z &= \frac{N_0\hbar DA}{2}\int_0^\infty \mathrm{d}\varepsilon \tanh\Big(\frac{\beta\varepsilon}{2}\Big)\mathrm{Re}\Big\{2\mathrm{i}k[(A_\uparrow\tilde{A}_\uparrow - B_\uparrow\tilde{B}_\uparrow) - (A_\downarrow\tilde{A}_\downarrow - B_\downarrow\tilde{B}_\downarrow)]\Big\}.
\end{aligned} \tag{17}$$

The coefficients $\{A_m, B_m\}$ for the singlet and each of the triplet components are determined by the boundary conditions. For instance, one finds for the charge-supercurrent that

$$I_Q = N_0 eDA\sin\theta\int_0^\infty \mathrm{d}\varepsilon \tanh\Big(\frac{\beta\varepsilon}{2}\Big)\mathrm{Re}\Big\{4\mathrm{i}k\Gamma^{-1}\sin(kd)\sinh^2\Theta\Big(k^2d^2\zeta_L\zeta_R + G_\varphi^L G_\varphi^R\cos\alpha\Big)\Big\}. \tag{18}$$

upon defining the quantity:

$$\Gamma = \Big(k^2d^2\zeta_R^2 + (G_\varphi^R)^2\Big)\Big(k^2d^2\zeta_L^2 - (G_\varphi^L)^2 + 2(G_\varphi^L)^2\cos^2\alpha\Big)\cos^2(kd) - \Big(k^2d^2\zeta_L\zeta_R - G_\varphi^L G_\varphi^R\cos\alpha\Big)^2, \tag{19}$$

The spin-supercurrent is given by:

$$I_S^x = \frac{N_0 \hbar D A \sin\phi \sin\alpha G_\varphi^L G_\varphi^R}{2} \int_0^\infty \mathrm{d}\varepsilon \tanh\Big(\frac{\beta\varepsilon}{2}\Big) \mathrm{Re}\Big\{4\mathrm{i}k\Gamma^{-2}\sin(kd)\sinh^2\Theta\Big(a_1 + a_2\cos\theta\Big)\Big\}, \tag{20}$$

where we have defined the expressions

$$a_1 = \Big(2(G_\varphi^L)^2\cos^2\alpha - (G_\varphi^L)^2 + k^2d^2(\zeta_L^2+\zeta_R^2) + (G_\varphi^R)^2\Big)\Big(k^2d^2\zeta_L\zeta_R - G_\varphi^L G_\varphi^R\cos\alpha\Big)\cos(kd), \tag{21}$$

$$a_2 = \Big(k^2d^2\zeta_L^2 + 2(G_\varphi^L)^2\cos^2\alpha - (G_\varphi^L)^2\Big)\Big(k^2d^2\zeta_R^2 + (G_\varphi^R)^2\Big)\cos^2(kd) + \Big(k^2d^2\zeta_L\zeta_R - G_\varphi^L G_\varphi^R\cos\alpha\Big)^2. \tag{22}$$

[1] J. Linder and J. W. A. Robinson, Nature Physics **11**, 307-315 (2015).
[2] H. Yang, S.-H. Yang, S. Takahashi, S. Maekawa, and S. S. P. Parkin, Nature Materials **9**, 586 (2010) .
[3] C. H. L. Quay, D. Chevallier, C. Bena & M. Aprili, Nature Physics **9**, 8488 (2013)
[4] F. Hübler, M. J. Wolf, D. Beckmann, and H. v. Löhneysen, Phys. Rev. Lett. 109, 207001 (2012).
[5] F. S. Bergeret, A. F. Volkov, and K. B. Efetov, Phys. Rev. Lett. **86**, 4096 (2001).
[6] A. Kadigrobov, R. I. Shekhter, and M. Jonson, EPL **54**, 394 (2001).
[7] M. Eschrig, J. Kopu, J. C. Cuevas, and G. Schön, Phys. Rev. Lett. **90**, 137003 (2003)
[8] S. S. Saxena *et al.*, Nature (London) **406**, 587 (2000).
[9] D. Aoki and J. Flouquet, J. Phys. Soc. Jpn. **81**, 011003 (2012).
[10] F. S. Bergeret, A. F. Volkov, and K. B. Efetov, Rev. Mod. Phys. **77**, 1321 (2005).
[11] A. I. Buzdin, Rev. Mod. Phys. **77**, 935 (2005).
[12] V. L. Berezinskii, JETP **20**, 287 (1974).
[13] A. Balatsky and E. Abrahams, Phys. Rev. B **45**, 13125(R) (1992); E. Abrahams, A. Balatsky, D. J. Scalapino, and J. R. Schrieffer, Phys. Rev. B 52, 1271 (1995).
[14] Y. Tanaka, Y. Asano, A. A. Golubov, and S. Kashiwaya, Phys. Rev. B **72**, 140503(R) (2005).
[15] T. Yokoyama, Y. Tanaka, and N. Nagaosa, Phys. Rev. Lett. **106**, 246601 (2011).
[16] M. Alidoust, K. Halterman, and J. Linder, Phys. Rev. B **89**, 054508 (2014).
[17] Ya.V. Fominov, Y. Tanaka, Y. Asano, M. Eschrig, arXiv:1503.04773.
[18] M. Eschrig, Physics Today **64**(1), 43 (2011)
[19] P. Kostic *et al.*, Phys. Rev. B. **53**, 701 (1996).
[20] L. Shan *et al.*, Phys. Rev. B **72**, 144506 (2005).
[21] G.-M. Zhao *et al.*, Phys. Rev. B **82**, 012506 (2010).
[22] N. Levy *et al.*, Phys. Rev. Lett. **110**, 117001 (2013).
[23] R. S. Keizer, S. T. B. Goennewein, T. M. Klapwijk, G. Miao, G. Xiao, and A. Gupta, Nature (London) **439**, 825 (2006).
[24] D. Sprungmann, K. Westerholt, H. Zabel, M. Weides, and H. Kohlstedt, Phys. Rev. B **82**, 060505(R) (2010)
[25] J. W. A. Robinson, J. D. S. Witt, M. G. Blamire, Science **329**, 59 (2010).
[26] T. Khaire, M. A. Khasawneh, W. P. Pratt Jr., and N. Birge, Phys. Rev. Lett. **104**, 137002 (2010).
[27] M. S. Kalenkov, A. V. Galaktionov, and A. D. Zaikin, Phys. Rev. B **79**, 014521 (2009).
[28] M. Houzet and A. I. Buzdin, Phys. Rev. B **76**, 060504(R) (2007).
[29] L. Trifunovic, Phys. Rev. Lett. **107**, 047001 (2011).
[30] M. Fogelstrøm, Phys. Rev. B **62**, 11812 (2000).
[31] Z. Shomali, M. Zareyan, and W. Belzig, New J. Phys. **13**, 083033 (2011).
[32] R. Grein, M. Eschrig, G. Metalidis, and Gerd Schön, Phys. Rev. Lett. **102**, 227005 (2009).
[33] M. Alidoust and J. Linder, Phys. Rev. B **82**, 224504 (2010).
[34] I. V. Bobkova and A. M. Bobkov, Phys. Rev. B **82**, 024515 (2010)
[35] J.-F. Liu and K. S. Chan, Phys. Rev. B **82**, 184533 (2010)
[36] J. N. Kupferschmidt and P. W. Brouwer, Phys. Rev. B **83**, 014512 (2011)
[37] A. Iovan, T. Golod, and V. M. Krasnov, Phys. Rev. B **90**, 134514 (2014
[38] C. Klose, T. S. Khaire, Y. Wang, W. P. Pratt, Jr., Norman O. Birge, B. J. McMorran, T. P. Ginley, J. A. Borchers, B. J. Kirby, B. B. Maranville, and J. Unguris Phys. Rev. Lett. 108, 127002 (2012)
[39] J. A. M. van Ostaay, A. R. Akhmerov, and C. W. J. Beenakker, Phys. Rev. B **83**, 195441 (2011)
[40] B. Li *et al.*, Phys. Rev. Lett. **110**, 097001 (2013).
[41] J. Rammer and H. Smith, Rev. Mod. Phys. **58**, 323 (1986).
[42] V. Chandrasekhar, arXiv:cond-mat/0312507.
[43] N. Schopohl and K. Maki, Phys. Rev. B 52, 490 (1995); A. Konstandin, J. Kopu, and M. Eschrig, Phys. Rev. B **72**, 140501(R) (2005).
[44] K. Usadel, Phys. Rev. Lett. 25, 507 (1970)
[45] A. Cottet, D. Huertas-Hernando, W. Belzig, and Y. V. Nazarov, Phys. Rev. B **80**, 184511 (2009)
[46] J. Linder and T. Yokoyama, Phys. Rev. Lett. **106**, 237201 (2011)
[47] X. Liu, J. K. Jain, and C.-X. Liu, Phys. Rev. Lett. **113**, 227002 (2014).
[48] K. Sun and N. Shah, Phys. Rev. B **91**, 144508 (2015)
[49] Y. Tanaka and A. A. Golubov, Phys. Rev. Lett. *98*, 037003 (2007)
[50] J. Linder, A. Sudbø, T. Yokoyama, R. Grein, and M. Eschrig, Phys. Rev. B **81**, 214504 (2010).
[51] S. Kawabata, Y. Asano, Y. Tanaka, A. A. Golubov, J. Phys. Soc. Jpn. **82**, 124702 (2013)
[52] P. M. Tedrow, J. E. Tkaczyk, and A. Kumar, Phys. Rev. Lett. **56**, 1746 (1986)
[53] M. Faure, A. I. Buzdin, A. A. Golubov, and M. Yu. Kupriyanov, Phys. Rev. B **73**, 064505 (2006)
[54] J. Linder, T. Yokoyama, and A. Sudbø, Phys. Rev. B **77**, 174514 (2008)

[55] P. Machon, M. Eschrig, and W. Belzig, Phys. Rev. Lett. **110**, 047002 (2013).
[56] A. Pal, Z. H. Barber, J. W. A. Robinson, and M. G. Blamire, Nature Communications **5**, 3340 (2014).
[57] H. le Sueur, P. Joyez, H. Pothier, C. Urbina, and D. Esteve, Phys. Rev. Lett. **100**, 197002 (2008).
[58] M. S. Grønsleth, J. Linder, J.-M. Børven, and A. Sudbø, Phys. Rev. Lett. **97**, 147002 (2006).
[59] P. M. R. Brydon, Phys. Rev. B **80**, 224520 (2009)
[60] M. L. Kulic and I. M. Kulic, Phys. Rev. B **63**, 104503 (2001)
[61] I. Eremin, F. S. Nogueira, and R.-J. Tarento, Phys. Rev. B **73**, 054507 (2006)
[62] G. Annunziata *et al.*, Phys. Rev. B **83**, 060508(R) (2011)
[63] M. Eschrig *et al.*, arXiv:1504.06258.
[64] A. Moor, A. Volkov, K. B. Efetov, Supercond. Sci. Technol. **28**, 025011 (2015).